Spring 2013

Performance of Concrete Incorporating Colloidal Nano-Silica

Mohamed Sabry Zeidan

PERFORMANCE OF CONCRETE INCORPORATING

COLLOIDAL NANO-SILICA

by

Mohamed Sabry Zeidan

Bachelor of Science

Alexandria University, Egypt

2000

Master of Science

Alexandria University, Egypt

2006

A dissertation submitted in partial fulfillment of the requirements for the

Doctor of Philosophy in Civil Engineering

Department of Civil and Environmental Engineering and Construction

Howard R. Hughes College of Engineering

Graduate College

University of Nevada, Las Vegas

May 2013

THE GRADUATE COLLEGE

We recommend the dissertation prepared under our supervision by

Mohamed Sabry Zeidan

entitled

Performance of Concrete Incorporating Colloidal Nano-Silica

be accepted in partial fulfillment of the requirements for the degree of

Doctor of Philosophy in Civil Engineering
Department of Civil and Environmental Engineering and Construction

Aly M. Said, Ph.D., Committee Chair

Samaan G. Ladkany, Ph.D., Committee Member

Ying Tian, Ph.D., Committee Member

Spencer M. Steinberg, Ph.D., Committee Member

Brendan J. O'Toole, Ph.D., Graduate College Representative

Tom Piechota, Ph.D., Interim Vice President for Research &
Dean of the Graduate College

May 2013

ABSTRACT

Performance of Concrete Incorporating Colloidal Nano-Silica

By

Mohamed Sabry Zeidan

Dr. Aly M. Said, Examination Committee Chair

Associate Professor of Civil Engineering

University of Nevada, Las Vegas

Nanotechnology, as one of the most modern fields of science, has great market potential and economic impact. The need for research in the field of nanotechnology is continuously on the rise. During the last few decades, nanotechnology was developing rapidly into many fields of applied sciences, engineering and industrial applications, especially through studies of physics, chemistry, medicine and fundamental material science. These new developments may be attributed to the fact that material properties and performance can be significantly improved and controlled through nano-scale processes and nano-structures.

This research program aims at 1) further understanding the behavior of cementitious materials when amended on the nano-scale level and 2) exploring the effect of this enhancement on the microstructure of cement matrix. This study may be considered as an important step towards better understanding the use of nano-silica in concrete. The main goal of the study is to investigate the effect of using colloidal nano-silica on properties of

concrete, including mechanical properties, durability, transport properties, and microstructure.

The experimental program that was conducted included a laboratory investigation of concrete mixtures in which nano-silica was added to cement or to a combination of cement and Class F fly ash. Various ratios of nano-silica were used in concrete mixtures to examine the extent and types of improvements that could be imparted to concrete. The conducted experimental program assessed these improvements in terms of reactivity, mechanical properties, and durability of the mixtures under investigation. Advanced testing techniques – including mercury intrusion porosimetry (MIP) and scanning electron microscopy (SEM) – were used to investigate the effect of nano-silica on the microstructure of the tested mixtures. In addition, the effect of nano-silica on the alkali-silica reaction (ASR) was examined using various techniques, including testing of accelerated mortar-bar and strength.

Furthermore, this study investigated the deterioration of concrete caused by salt crystallization in concrete pores. This physical effect of salt on concrete may cause significant damage under certain environmental conditions in regions where soil is laden with large amounts of certain salts. The effect of nano-silica on this special type of environmental attack was explored by means of a new non-standard testing procedure, including the simulation of changing seasons, on concrete specimens partially immersed in salt solution. These concrete specimens represented concrete structures with foundations in salt-rich soils.

ACKNOWLEDGEMENTS

All praise is due to Allah (God), the lord of the worlds. Only with his compassion and mercifulness, this project could be completed.

I would like to express my deep gratitude to my advisor, Dr. Said, for his support and patience to achieve this work and improve it during the last four years. I wish also to sincerely thank Dr. Mohamed Bassuoni at University of Manitoba for his essential contribution to this research.

I want to thank Dr. Barbara Luke and the Applied Geophysics Center (AGC) team for hosting me during most of my stay at UNLV. I would like also to acknowledge the President Research Award which initiated the funding for this research program and Earthquake in Southern Nevada (ESN) project for providing support to this work. In addition, Nevada Department of Transportation (NDOT) had presented valuable assistance to finish this research.

No enough words can express my gratitude to my wife for supporting me during performing this work and for enduring some tough times to finish this project. I cannot also disregard the considerable support of a great group of friends I knew during my stay at Las Vegas.

Finally, I would like to dedicate this work to the soul of my late father, my mother and my wife.

Table of Contents

LIST OF TABLES

x

LIST OF FIGURES

xii

Chapter 1: Introduction and Background

The new technological capabilities made it possible to explore and control new levels of existence which were never known before. Although the nano-sized matter existed as early as the existence of earth, but it was not until early 20th century when the nano-scale science started with the study of the molecular and atomic sized objects. However, the development of methods to control the materials on the nano-scale level was not started until the last few decades (Porro, 2005).

Current global trends are shifting towards a more sustainable construction industry, which has generated new research needs to control and improve concrete performance. The main approach applied to produce sustainable concrete is to reduce consumption of portland cement, while building more durable structures that have longer service life, yet require minimal maintenance. The reduction of portland cement use may be achieved either by decreasing its content in concrete mixtures or through replacing cement with recycled materials, thus reducing the carbon footprint of concrete (Berndt, 2009). Furthermore, using other recycled materials (e.g. recycled concrete or aggregates) in mixtures is considered as one of the sustainable solutions for concrete (Domtoft et al., 2008).

Another significantly important aspect of concrete sustainability is extending concrete structures' service time while reducing maintenance cost. This is mainly depending on enhancing concrete serviceability, long-term durability and resistance to aggressive environmental attacks (Mehta, 2002). This aspect becomes especially critical in case of structure expected to have a long service life in harsh conditions including, but not

1

limited to, highway pavements and bridges, dams and marine structures. In these cases improving durability of concrete may have a significant impact on the life cycle and maintenance plans for these structures. Concrete pavements and dams demonstrated over the last century that adequately designed and maintained concrete can serve for several decades. As an example, the first concrete paved road in the United States constructed in Bellefontaine, Ohio is still in service. Although this 8 ft strip of the street was built more than 120 years ago (in 1891), it is up till now opened for light vehicular traffic (Snell and Snell, 2002).

1.1 Nanotechnology and Concrete

Nanotechnology was earlier defined by Drexler et al. (1991) as "the control of the structure of matter based on molecule-by-molecule control of products and byproducts". Nanotechnology can be considered as the most modern fields of science and technology. Having great market potentials and economical impact, the need for research in field of nanotechnology is increasingly on the rise. These studies aim at further developing the understanding of materials' behavior on the nano-scale level, which can lead to the ability to improve the microstructures of these materials.

During the last few decades, nanotechnology has been expanding rapidly into many fields of applied sciences, engineering and industry, especially in the fields of physics, chemistry, medicine and fundamental material science. These new developments may be attributed to the fact that material properties and performance can be significantly improved and controlled through nano-scale processes and structures (Sobolev et al., 2009). Nanotechnology is now being introduced into various applications and industrial

2

sectors which lead to the need for further research and innovation. This includes biological molecular functionality, nano-wires, magnetic random access memory and carbon nano-tubes, etc. (Gopalakrishnan et al., 2011;Bergemannet al., 1999; Bartos, 2008). Several agencies in the United States of America are supporting nanotechnology research endeavors with more than a billion dollar per year (Balaguru and Chong, 2008). The ability to control the material properties at the nano-level using nanotechnology may lead to the creation of new materials with unique characteristics and behavior. These developments are promising for breakthroughs in materials and construction industries.

Using nanotechnology in the construction industry was considered to be relatively lagging compared to its use in some other fields due to the lack of foresight and good understanding of its capabilities. But recently, the construction industry has realized the potential impact of nanotechnology (Bartos, 2008), leading to many new areas of research in civil engineering.

Concrete which is known to be the most used manmade material is based mainly on the cement industry with total yearly production worldwide exceeding 2600 million tons (USGS, 2010). Also, it should be mentioned here that the cement industry is considered to be one of the most energy consuming industries and one of the highest emissions sources of carbon dioxide (CO_2), the most important greenhouse gas (GHG) suspected of causing climate change. The cement industry is responsible for around 5% of the global man-made CO_2 emissions every year (WBCSD, 2002), in which approximately 50% of this emissions are caused by the chemical processes during manufacturing, while the rest is caused by fuel consumption. Extensive research efforts have been directed to reduce the effect of cement industry on GHG either by improving the manufacturing process

3

efficiency and technologies (Deja et al.,2010 and Barker et al.,2009) or adopting the use of supplementary cementitious materials (SCMs) that may partially or fully replace ordinary cement (Gartner, 2004). Different SCMs have been thoroughly investigated in the literature including fly ash, ground granulated blast furnace slag (GGBFS), natural pozzolans and silica fume. Recent studies (Damtoft et al., 2008) suggested that using new technologies to improve physical and chemical properties of SCMs may lead to industrial breakthroughs in concrete industry. Nanotechnology is one of the most promising research fields that may significantly change this industry due to its unlimited capabilities.

Fly ash is considered to be one of the mostly used alternatives that may partially replace cement in concrete industry due to its efficiency in reducing cost and its great availability. Also, fly ash as a byproduct of coal consumption is much more environmentally friendly compared to cement (Haque et al., 1984). Therefore, U.S. Green Building Council's (USGBC) considered using fly ash in concrete to earn points in the Leadership in Energy and Environmental Design (LEED) program. Besides its economical and environmental benefits, Class F fly ash can also perform better than ordinary portland cement in cases where aggregates have potential alkali silica reactivity (ASR). Several studies indicated that fly ash can significantly reduce the expansion in cement mortar due to ASR (Alasali and Malhotra, 1991). This makes several agencies mandate the use of fly ash in its specification for concrete mixtures in a minimum percentage to eliminate or mitigate the effect of ASR (Malvar et al., 2002). The main concern about fly ash concrete, particularly that containing Class F fly ash, has been its slow rate of strength development compared to normal concrete (Carette et al., 1993 and

4

Naik et al., 1998). Several studies were performed to identify different solutions for this problem (Naik and Ramme, 1989; Shi, 1998). Fly ash concrete is not suitable for some application where early strength is required.

Silica (SiO_2), which is the most abundant minerals on the Earth's crust (Iler, 1979), has been used in concrete industry as a SCM in the form of silica fume (also known as micro-silica). Silica fume is a byproduct of manufacturing of silicon or ferrosilicon alloys. Silica is also found in fly ash as well as natural pozzolans. However, it is also known that silica exists even in most of the aggregates but usually not in a reactive form. Accordingly, the effect of the silica on the cement hydration process depends on the form of the silica and its reactivity rather than its concentration.

Unlike silica fume, nano-silica is a manufactured material composed of silica particles having particle size smaller than 100 nm. Experimental results indicated that the performance of concrete including nano-silica was generally better than that containing micro-silica in terms of mechanical properties and durability (Ghasemi et al., 2010). Furthermore, several studies showed that significant improvements of performance of cement mortars and concrete occur with the addition of nano-silica (Li et al., 2004). It was initially believed that such improvements in performance observed due to addition of nano-silica are attributed only to its filler effect and pozzolanic reaction caused by the nano-silica. However, recent research indicated that the effect of nano-silica is not limited to this mechanism. The small particle sizes of nano-silica provides larger surface area for the reaction so the smaller the particle sizes, the higher the rate of the early cementitious and pozzolanic reaction (Belkowitz and Armentrout, 2009). Other evidence supporting this idea is that some nonreactive nano-materials, which were mainly added for cosmetic

www.manaraa.com

purposes, lead to improvement in the reaction rate of the cementitious materials. For instance, experimental results (Lee et al., 2009) showed that adding nano-titanium dioxide (TiO_2) accelerates the hydration of tricalcium silicate (C_3S) even though TiO_2 does not take part of neither the hydration nor pozzolanic reactions.

Nano-silica is available in two main forms: 1) compacted dry grains and 2) colloidal suspension. The dry grained nano-silica requires special preparation procedure before mixing. The purpose of this procedure is to ensure dispersion of nano-particles in the mixture through water or liquid admixtures so it can uniformly improve the cement matrix. This preparation, which is generally a mechanical dispersion process, may be associated with human exposure to nano-particles, can be hazardous and has time limitation since agglomeration of particles can start immediately after the end of mixing. On the other hand, the colloidal nano-silica which is manufactured as a suspension electrochemically stabilized in a dispersive solution is a form of the nano-silica that is easier to use. Furthermore, adequate dispersion, provided electrochemically, prevents agglomeration of particles and maintains particle size at the nano-level, thus ensuring the full benefit of nano-silica. This is supported by experimental results, which indicate that better behavior was achieved when colloidal nano-silica was added to mortar specimens compared to the dry grained nano-silica (Campillo et al., 2003). Accordingly, electrochemical dispersion is a more stable form of dispersion for nano-particles compared to compacted dry grains where agglomeration can occur. Such better dispersion can lead to a more pronounced nano-particle effect.

6

1.2 Research Significance and Objectives

In this study, different aspects of the effect of the nano-silica on concrete performance were examined. This includes investigating reactivity, mechanical behavior, durability, salt crystallization resistance and ASR mitigation of concrete incorporating colloidal nano-silica. Furthermore, the changes at the microstructure level caused by the addition of nano-silica were carefully investigated. The main aim of the study is to explore the effect of nano-silica on the major characteristics of concrete. The study presents an extensive experimental program aiming at furthering the understanding of the behavior and properties of concrete incorporating nano-sized particles. Additionally, the study explores the mechanisms of the change in concrete behavior in terms of microstructure and porosity.

1.3 Scope and Contents

The study includes a broad experimental program covering different performance characteristics of concrete incorporating colloidal nano-silica. These characteristics include testing fresh properties, reactivity, mechanical properties, durability, microstructure, porosity, sulfate salt crystallization resistance and ASR mitigation. This extensive testing will be presented in this dissertation through eight chapters. Besides this current first chapter, the other 7 chapter may be briefly described as follow:

Chapter 2: This chapter describes in details the used materials in preparing the concrete mixtures and their proportions. These materials include aggregates, binders, admixtures,

7

as well as colloidal nano-silica. Also, in this chapter, the procedures for mixing, curing and preparation of tested specimen are presented.

Chapter 3: In this chapter, the fresh properties of the tested concrete mixtures are discussed including slump, air content, setting time and adiabatic temperature testing. Moreover, the chapter includes test results for the mechanical properties of the investigated mixtures such as compressive strength at different ages, splitting tensile strength, and modulus of rupture.

Chapter 4: This chapter includes the testing procedure and results for the durability study. The tested durability aspects were rapid chloride ion permeability, abrasion resistance and surface scaling due to freezing-thawing cycles.

Chapter 5: In this chapter, the interpretation of the change in concrete performance incorporating colloidal nano-silica is presented in terms of microstructure. This includes studies about the porosity, pore size distribution and microstructure using scanning electron microscopy among other techniques. Also, the chapter involves thermal analysis of concrete to assess the levels of pozzolanic reaction.

Chapter 6: This chapter explores the phenomenon of crystallization of salts in concrete pores. This phenomenon occurs in concrete adjacent to salt-laden soils under certain environmental condition. The chapter discusses the effect of colloidal nano-silica on concrete resistance to this type of attack.

Chapter 7: This chapter presents an investigation of the effect of colloidal nano-silica on ASR. This effect is studied in terms of the expansion and impact on compressive

strength. In this part of the study, colloidal nano-silica is used either solely or combined with other SCMs typically used to mitigate ASR.

Chapter 8: This chapter includes summary of the findings and conclusions of this study. In addition, recommendations and future research suggestions are presented.

Chapter 2: Materials and Procedures

Extensive experimental program is performed to study the performance of concrete incorporating colloidal nano-silica. This chapter describes in detail the materials and mixtures tested within this program. The mixtures and materials described in this chapter were used for all the testing performed in this study except for Chapter 7 which investigates ASR mitigation techniques involving colloidal nano-silica. For Chapter 7, different types of aggregate, cementitious materials and different mixture proportions were used.

Six concrete mixtures with different ratios of colloidal nano-silica and fly ash were investigated. All the mixtures had a constant water-to-cement ratio (w/c) and a constant total cementitious material content. Three of the mixture had 30% of cement replaced by Class F fly ash in which different dosages of nano-silica were used. For the part of the study that investigates ASR mitigation techniques involving nano-silica described in Chapter 7, eight different mixtures of cement mortars, made with reactive aggregate and six concrete mixtures were evaluated.

2.1 Materials

For all of the mixtures, the materials used including cement, fly ash, nano-silica, coarse and fine aggregates were as follows:

Aggregates: Well-graded natural aggregate was used as course aggregate. The aggregate specific weight was 2.79, its absorption was 0.60% and its rodded unit weight was 102 lb/ft^3. As fine aggregate, rounded shaped natural sand was used. The fine aggregate

10

specific weight was 2.78, its absorption was 0.80% and its fineness modulus was 3.00. Figures 1 and 2 show the gradation curves of the coarse and fine aggregates used in this study (except for Chapter 7), respectively. The moisture contents of coarse and fine aggregates were measured each time before mixing and the mixing water was adjusted for these moisture contents. For ASR testing, a different type of natural aggregate, from one source of known reactivity, is used with different sizes as coarse and fine aggregates. For mortar bar testing (ASTM C1260), fine aggregate graded according to the specifications was used to make the mortar. Both fine and coarse aggregates (reactive) were used for testing the change in concrete strength due to ASR as will be described in Chapter 7.

Cement: The used cement is type II/VI portland cement meeting ASTM C150 specifications. The main chemical and physical properties of the used cement are presented in Table 1.

Fly Ash: Class F fly ash was used for concrete and mortar mixtures. Properties of the used fly ash are shown in Table 1.

Nano-Silica: Colloidal nano-silica was used for this study. The nano-silica was a commercial type supplied by a European manufacturer. The product is a milky white odorless aqueous suspended solution. The SiO_2 content of the solution was 50% by weight. According to the data provided by the manufacturer, the density of the solution was 87.4 lb/ft^3, its pH value was 9.5 and the average particle size was 35 nm.

Admixtures: Polycarboxylate based high range water reducing agent (HRWRA) with specific gravity 1.068 and solids content of 40%was used at different dosages to achieve constant level of workability for all mixtures.
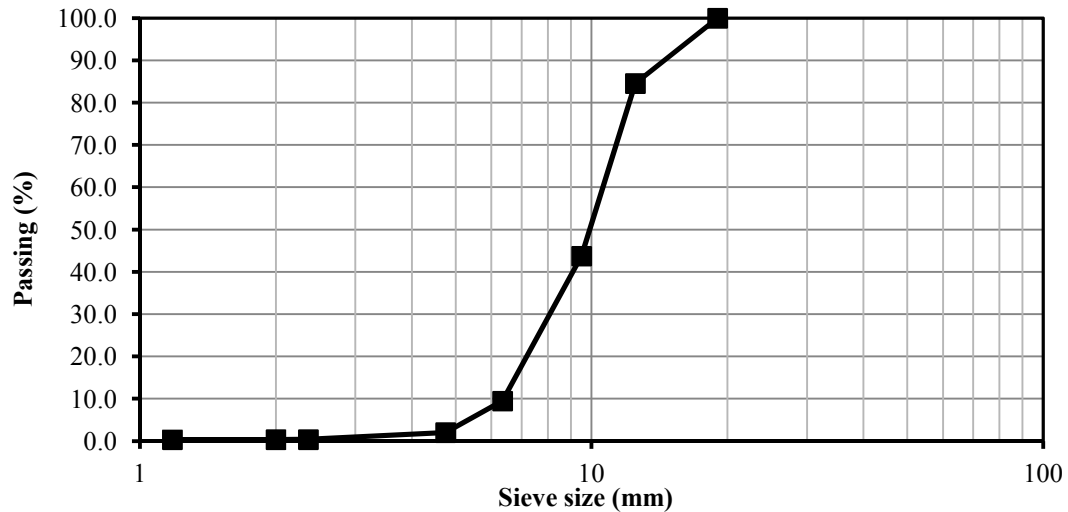
Figure 1 Gradation curve for the coarse aggregate.
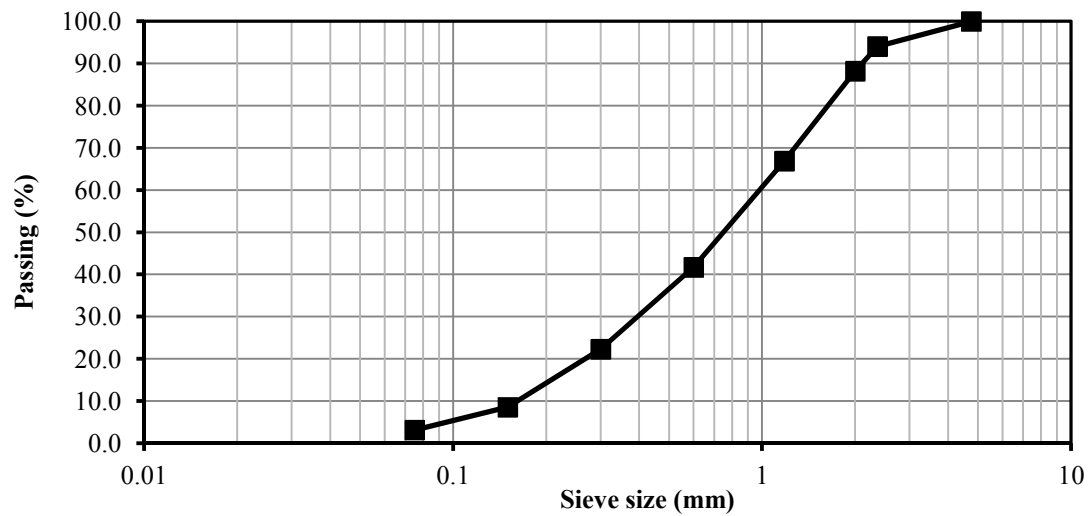
Figure 2 Gradation curve for the fine aggregate.

2.2 Mixing and Curing

The experimental program was designed to investigate the effect of different dosages of nano-silica on the performance of normal and fly ash concretes. To achieve this, the first

12

group of mixtures included only cement as a cementitious material (Group A), while the other group had 30% of the cement replaced by fly ash (Group B). The total cementitious material content and the water to cementitious material ratio were kept constant for all the mixtures as 658 lb/yd^3 (390 kg/m^3) and 0.40, respectively.

Table 1 Properties of cement and fly ash

	Type II/VI Portland Cement	Class F Fly Ash
SiO$_2$ (%)	20.64	58.25
Al$_2$O$_3$ (%)	3.40	16.60
Fe$_2$O$_3$ (%)	3.40	4.63
CaO (%)	63.5	10.23
MgO (%)	4.70	-
SO$_3$ (%)	2.40	0.84
Na$_2$O (%)	0.46	-
Loss on Ignition (%)	1.20	1.52
Specific Gravity	3.15	2.35
Fineness (m^2/kg)	376	290

The ratios of nano-silica used were 0% (as control mixtures), 3% and 6% for each of the two groups of mixtures (A and B). The amount of added mixing water was adjusted for each mixture deducting the amount of water in the nano-silica solution. Also, 6% of micro-silica was used with the two groups. Different amounts of high range water reducing agent (HRWRA) were used for different ratios of nano-silica, in order to keep the same level of workability. The target slump for all mixtures was between 3 to 5 inches. A higher amount of HRWRA (complying with ASTM C494) was needed when a higher amount of nano-silica was added as it has significant effect on workability. This is attributed to the very small particle size of colloidal nano-silica. Table 2 shows the

13

proportions for the six tested mixtures. Mechanical mixing was used to mix the constituent materials according to ASTM C192. These mixtures were used throughout the testing program except for the ASR mitigation study. For ASR testing, different mixture proportions were used and are shown later in this dissertation. All the molded specimens were covered to prevent water loss and were kept in room temperature till de-molding time. The curing of the specimens started after 24 hours of mixing, immediately after removal from molds. The specimens were kept in curing room at a temperature of 73.5 ± 3.5 °F (23 ± 2°C) and relative humidity not less than 95% until testing.

Table 2 Mixtures proportions of tested concrete.

Mixture	Cement lb/yd^3 (kg/m3)	Fly Ash lb/yd^3 (kg/m^3)	Colloidal Nano-SiO$_2$ solution lb/yd^3 (kg/m^3)	Water* lb/yd^3 (kg/m^3)	HRWRA fl oz/100lb of binder (mL/100 kg)	Coarse Aggregate lb/yd^3 (kg/m^3)	Fine Aggregate lb/yd^3 (kg/m^3)
A-0	658 (390)	-	-	263.2 (156)	5 (326)	1996 (1184)	1330 (789)
A-1	658 (390)	-	39.48 (23.4)	243.46 (144.3)	7 (457)	1980 (1175)	1320 (783)
A-2	658 (390)	-	78.96 (46.8)	223.72 (132.6)	14 (914)	1959 (1162)	1305 (774)
B-0	460.6 (273)	197.4 (117)	-	263.2 (156)	4 (261)	1960 (1163)	1306 (775)
B-1	460.6 (273)	197.4 (117)	39.48 (23.4)	243.46 (144.3)	5 (326)	1945 (1154)	1296 (769)
B-2	460.6 (273)	197.4 (117)	78.96 (46.8)	223.72 (132.6)	10 (653)	1927 (1143)	1284 (762)

* The amount of water in the nano-silica solution was subtracted from the total water content.

14

Chapter 3: Fresh Properties, Reactivity and Mechanical Properties

In this chapter, the testing procedure and results of fresh concrete testing are described including slump, air content and setting time tests. Also, in this chapter, the reactivity of concrete mixtures was monitored through adiabatic temperature testing. Moreover, this chapter introduces the results of the mechanical properties testing including the compressive strength at various curing ages, the splitting tensile strength and the modulus of rupture.

3.1 Slump and Air Content

To maintain a consistent level of workability for all mixtures, several trial batches were performed to adjust the dosages of HRWRA. The target slump for all mixtures was between 3 and 5 inches which led to different admixtures dosage as shown in Table 2. Immediately after mixing, slump test was performed on each of the six concrete mixtures investigated in this study according to ASTM C143. The slump values for the different mixtures are shown in Table 3. Also, the actual air content of each mixture was evaluated using the pressure method according to ASTM C231 immediately after mixing. The measured air contents did not vary significantly between different mixtures as all values ranged between1.5% and 2.1% as shown in Table 3.

Table 3 Summary of the fresh properties of the tested mixtures.

Mixture	Slump (in)	Measured Air content (%)
A-0	5.0	1.5%
A-1	4.5	1.4%
A-2	3.0	1.7%
B-0	4.0	2.1%
B-1	3.0	1.8%
B-2	3.5	2.0%

3.2 Setting Time

In order study the impact of nano-silica on the setting time of concrete and mortars, Vicat needle testing was performed according to ASTM C191. Pastes were prepared by mixing 650 grams of cementitious materials with 260 grams of water (w/c=0.40) and mixed as specified in the ASTM standard. Unlike concrete mixtures, no water reducing admixtures were used for any of the pastes as most types of admixtures may affect setting times. The cementitious materials used were selected to represent the same proportions of the concrete mixtures tested during this study (see Table 2). The paste was molded in the standard molds and kept in a moisture closet with temperature of $20 \pm 2°C$ and relative humidity not less than 90%. The penetration of the standard Vicat needle (1 mm in diameter) was recorded every 15 minutes and the molds were kept in the moisture closet between readings. The initial setting time is defined as the time when the needle penetration is equal to 25 mm. This value was determined via interpolation between the two closest readings to 25 mm. On the other hand, final setting time was determined as the time when no penetration could be visually observed. Table 4 shows the tested pastes

16

along with the measured initial and final setting times. Also, Figures 3 and 4 show the measured penetration depths during the testing period for the pastes without fly ash (corresponding to Group A mixtures) and for the pastes incorporating 30% fly ash (corresponding to Group B mixtures), respectively.

Table 4 Summary of Vicat needle testing results.

Cementitious Materials Proportions	Corresponding Concrete Mixture	Initial Setting Time (min)	Final Setting Time (min)
Cement only	A-0	190	245
Cement +3%Nano-Silica	A-1	192	246
Cement +6%Nano-Silica	A-2	145	222
70%Cement+30%Fly Ash	B-0	300	396
70%Cement+30%Fly Ash+3% Nano-Silca	B-1	258	307
70%Cement+30%Fly Ash+6% Nano-Silca	B-2	244	285

Generally, the results of Vicat needle testing indicate that using nano-silica has an impact on shortening of both of the initial and final setting times. For mixtures without fly ash (Group A), adding 6% nano-silica reduced the initial setting time by around 25%, while the final setting time was reduced by around 10%. However, 3% of added nano-silica did not have a considerable effect on setting times in this case. The effect of nano-silica could be more readily observed in case of mixtures incorporating fly ash (Group B). Class F fly ash may generally extend the setting time of cement paste due to the slow hydration process. However, adding 6% of nano-silica to the fly ash concrete reduced the initial and

17

final setting time by around 25%, while this reduction was around 20% in case of adding 3% of nano-silica.
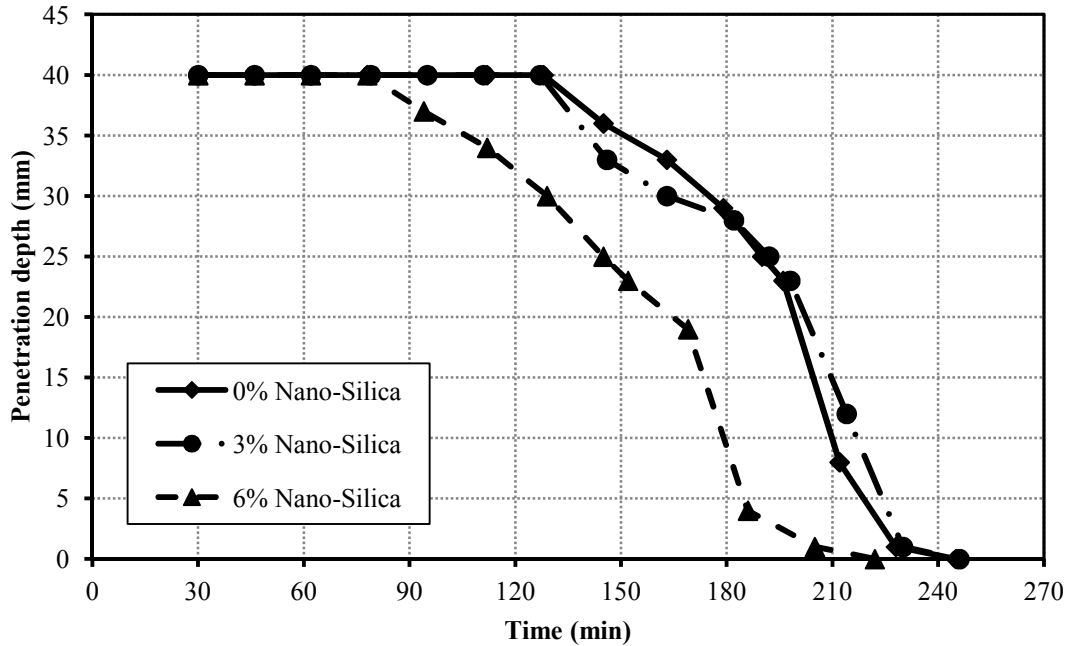
Figure 3 Vicat needle penetration depths for pastes without fly ash.
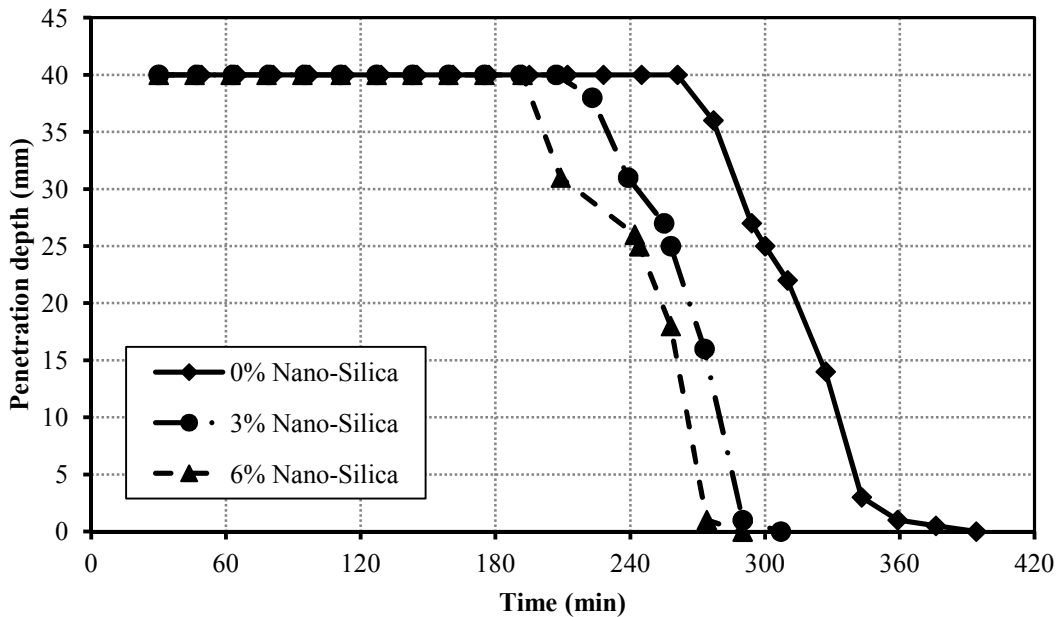
Figure 4 Vicat needle penetration depths for pastes including 30% fly ash.

18

The impact of nano-silica on the fresh properties of concrete was generally significant especially on the workability level in terms of slump values and setting times. This effect was expected due to the very small particle size of nano-silica having significantly larger surface area compared to other concrete components. The large surface area increases the adsorbed water on the surface which impacts the fresh properties of concrete. However, these observations are inconclusive to project an impact of nano-silica on hardened concrete properties. Generally, any fine particles added to concrete, mortar or paste mixtures can impact the workability and sitting time in a similar way. The next sections and chapters of this study discuss the evidence of the effect of nano-silica on hardened concrete performance and cement reactivity.

The previously presented results indicate that the fresh properties of concrete incorporating nano-silica may be a controlling factor for mixture design and proportioning for some application. This is attributed to the significant impact of nano-silica on workability and setting time of concrete.

3.3 Adiabatic Temperature

In order to monitor the change in temperature in the different concrete mixtures during the early hydration period, the adiabatic temperature test was conducted. Immediately after mixing, a 4×8 inches concrete cylinder mold is prepared and a thermocouple is inserted at 4" below of the cylinder top surface (mid hight) in order to measure the temperature of the mixture according to ASTM C1064. The cylinder molds were covered and sealed to prevent moisture loss during the test and were kept in room temperature (73 ± 3°F). The adiabatic temperature of concrete was recorded every 2 minutes using a data

logger for 30 hours after mixing as shown in Figure 5. The temperature recorded over 30 hours was plotted against time as shown in Figures 6 and 7.

For all the mixtures, the temperature increased just after mixing within the acceleration and setting periods until the peak was reached. The increase then was followed by a decrease in temperature during the deceleration period until a relatively constant temperature was recorded. The results indicated that the peak temperature was generally higher for mixtures containing nano-silica. For example, comparing mixtures B-1 and B-2 to mixture B-0 (Figure 7), the peak temperatures were about 20% higher and was reached at a shorter time (4 hours earlier).

Figure 5 Adiabatic temperature test setup.
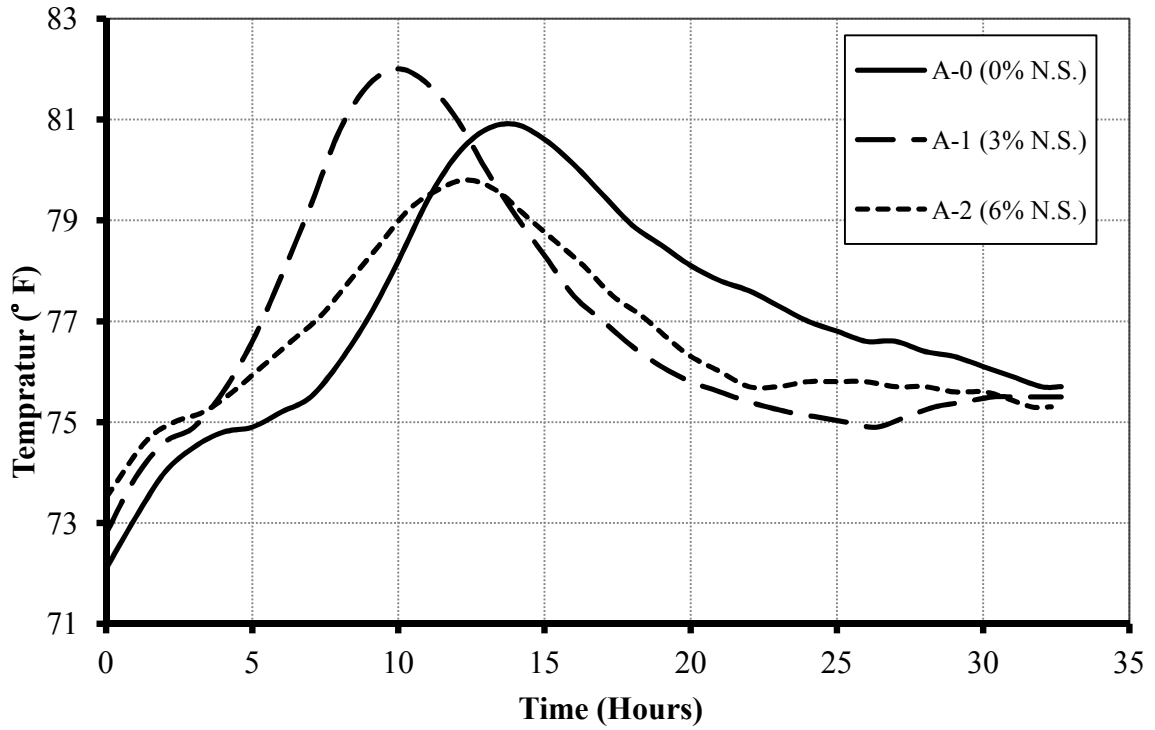
Figure 6 Adiabatic temperature test results for Group A mixtures.
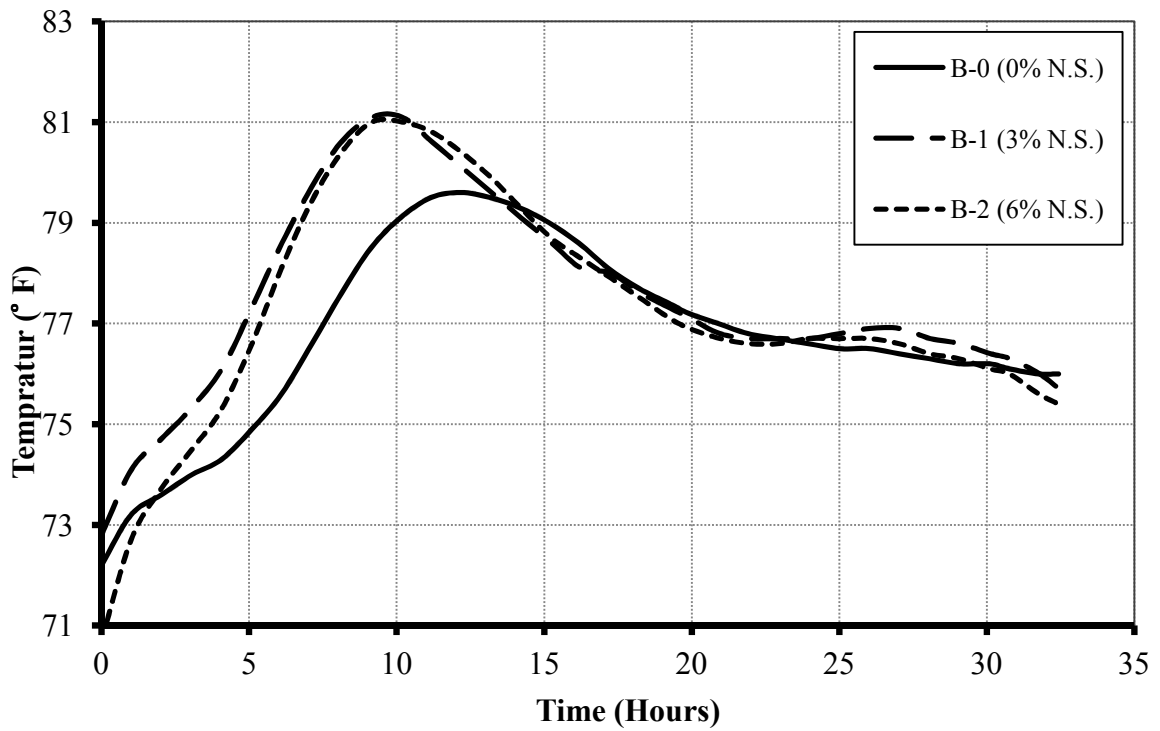
Figure 7 Adiabatic temperature test results for Group B mixtures.

* N.S.: Nano Silica

21

This increase in the peak temperature, within 15 hours after mixing, indicates acceleration in the rate of hydration due the presence of nano-silica. This increase may not be ascribed to the pozzolanic effect of nano-silica as the pozzolanic reaction usually takes place at later time periods after adequate formation of portlandite (Mehta and Monteiro, 2006). Hence, the increase in the peak temperature may be attributed to the very high surface area of nano-silica particles (average particle size of 35 nm) which acted as nucleation sites for the hydration reactions. These results indicate that the role of nano-silica is not limited to pozzolanic or filler effects, but it also speeds up the kinetics of hydration due to its ultrafine nature.

3.4 Mechanical Properties

The compressive strength at different curing ages up to one year was evaluated for the six investigated mixtures. In addition, the splitting tensile strength and modulus of rupture were determined at 28 days. Cylinders of 4 inches diameter and 8 inches height, prepared, molded and compacted according to ASTM C192, were used for evaluation of the compressive and the splitting tensile strengths. The cylinders were unmolded after 24 hours of mixing then cured in a curing room until the time of testing. The compressive strength was measured at ages of 3, 7, 28, 90 and 365 days, with the average of 3 cylinders at least for each age. The splitting tensile test was performed only at the age of 28 days. For evaluation of modulus of rupture, concrete beams 6"×6"×24" (150×150×600 mm) were prepared for the six mixtures. At 28 days, the beams were tested in flexure up to failure.

For the compressive strength testing, steel capping (according to ASTM C1231) was used for the evaluation of the early strengths up to 7 days for all the mixtures. For compressive strength testing at 28 days and beyond, sulfur capping was prepared for the tested cylinders according to ASTM C617. The average compressive strength of the six mixtures at different curing ages is shown in Figure 8. Also, Table 5 shows the early age compressive strength for the six mixtures at 3 and 7 days as these values are not visually clear in Figure 8. The splitting tensile test was performed at 28 days on concrete cylinders according to ASTM C496. The average splitting tensile strength for each of the tested mixtures is presented in Figure 9. For compressive strength and tensile strength testing, at least three cylinders were tested for each mixture at the different testing ages.
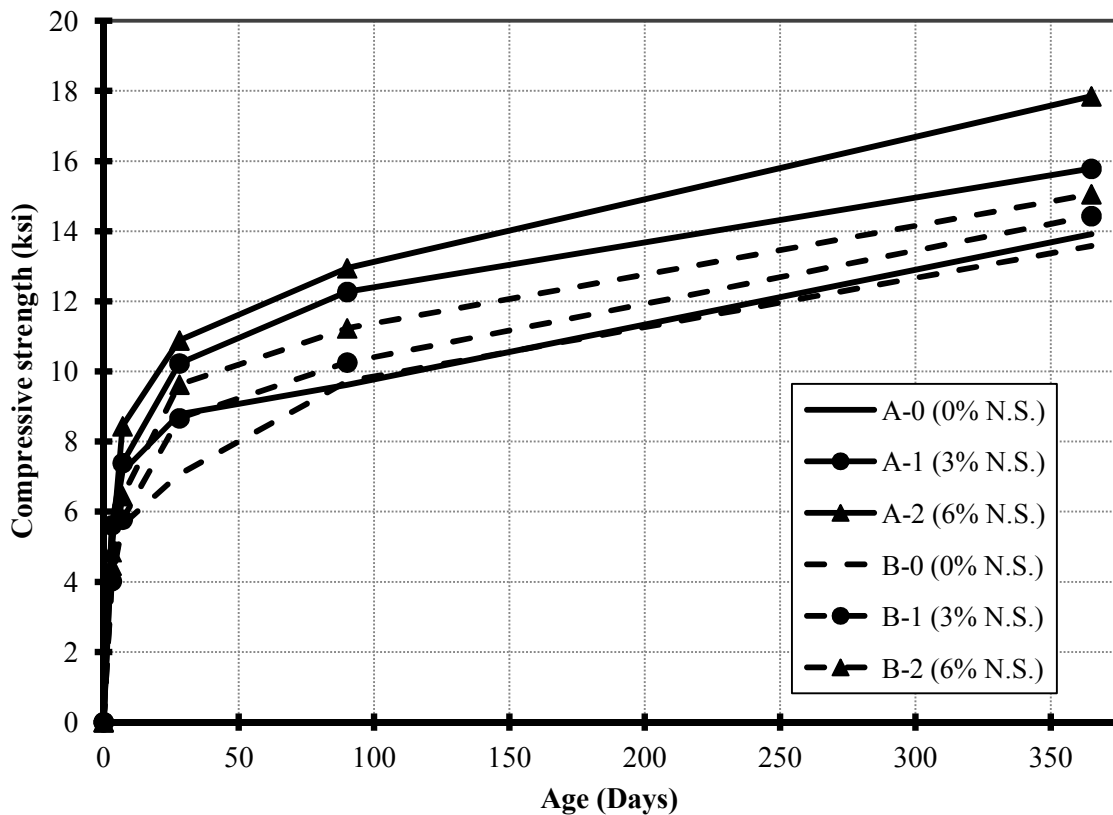
Figure 8 Compressive strength versus curing time.

23

Table 5 Early age compressive strength of concrete mixtures

Mixture	Compressive Strength (ksi)	
	3-days	7-days
A-0	5.25	7.14
A-1	5.61	7.39
A-2	4.85	8.44
B-0	3.97	5.63
B-1	4.02	5.78
B-2	4.47	6.45

For evaluating the modulus of rupture of the tested concrete mixtures, two beams were tested for each mixture according to ASTM C78. The beams were simply supported with two loads applied at one third of the span from each of the two supports. The total span of the tested beams was 18" with 3" overhanging from each side. The modulus of rupture was then calculated for each specimen at failure based on the exact dimensions of the cross section measured at the surface of failure. Figure 10 shows the average measured modulus of rupture for the tested mixtures.

Results generally indicate that the compressive and tensile strength remarkably increased with the addition of nano-silica in both of the mixtures groups. In Table 5, it can be observed that the rate of early age strength gain was improved for mixtures containing nano-silica with or without fly ash. For Group A mixtures, the average (3 and 7 days) early age strength increased by about 18% with increasing the dosage of nano-silica up to 6%. Comparably, for Group B mixtures incorporating Class F fly ash, the average increase in the early age strength was about 14% with increasing the dosage of nano-silica up to 6%. This indicates that low early age strength of concrete incorporating Class F fly ash can be improved by the addition of colloidal nano-silica.

24
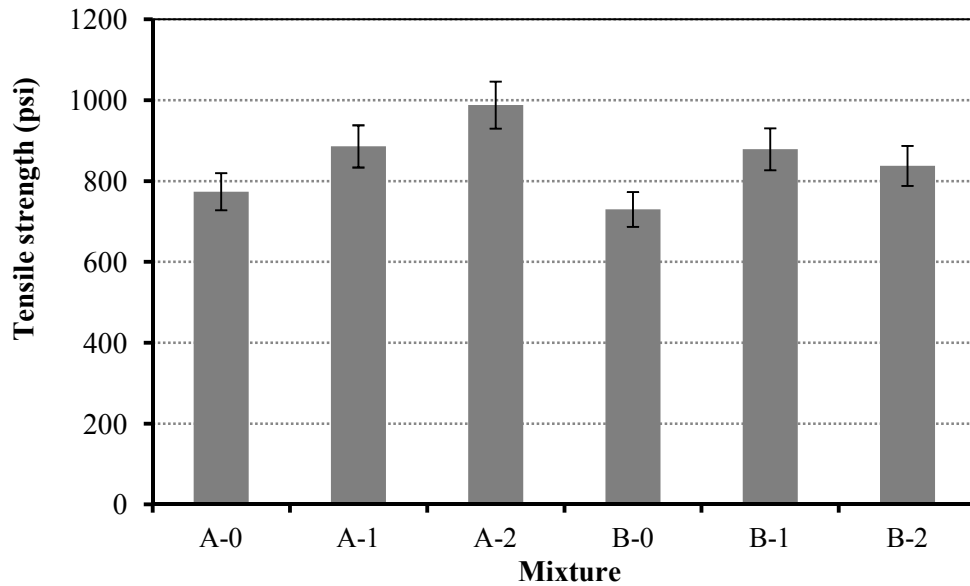
Figure 9 Splitting tensile strength at 28 days for the investigated mixtures.
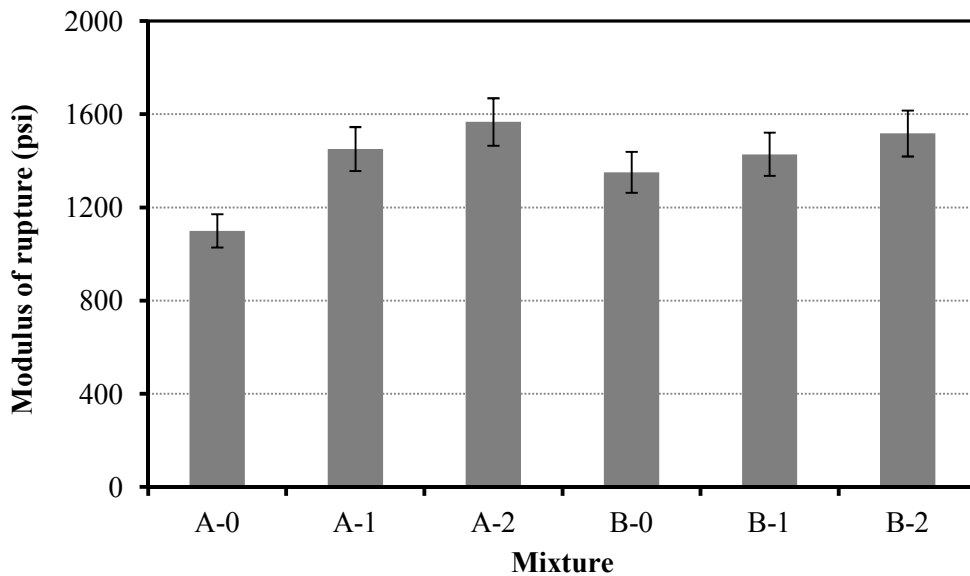
Figure 10 Average modulus of rupture for the tested mixtures.

At 28 days, the compressive strength of mixtures without fly ash (Group A) increased by 17% and 24% for 3% and 6% nano-silica additions, respectively. For mixtures with 30% fly ash (Group B), the 3% and 6% additions of nano-silica increased the strength by 23% and 36%, respectively. The addition of 3% and 6% nano-silica to mixtures with 30% fly

25

ash (mixtures B-1 and B-2, respectively) led to compressive strength that matched or exceeded the strength of the control mixture (A-0) at or before 28 days, while the mixture containing fly ash without nano-silica (B-0) matched the compressive strength of the control mixture (A-0) at around 90 days. For long-term strength, the mixtures containing nano-silica continued gaining strength with a relatively high rate after 28 days.

The compressive strength results were statistically supported by analysis of variance (ANOVA), at a significance level $\alpha = 0.05$. For example, ANOVA for the compressive strength results at 7 and 28 days showed that the increase in the dosage of nano-silica from 0 to 6% had F values of 32.38 and 18.54, respectively which are larger than the corresponding critical F value of 3.89. According to Montgomery (Montgomery, 2001), exceeding the critical value of an F-distribution density function reflects that the tested variable significantly affects the mean of the results.

The results of the modulus of rupture testing were in agreement with the other tested mechanical properties. The addition of nano-silica generally increased the modulus of rupture for the two tested groups (A and B mixtures). This increase was generally proportional to the percentage of the added nano-silica. In general, the improvement in mechanical properties for the mixtures incorporating nano-silica can be attributed to the pozzolanic and filler effects of nano-silica, as indicated by the thermal and micro-structural analyses, which will be discussed later in Chapter 5.

Chapter 4: Durability

The construction industry is taking notable steps towards a more sustainable use of concrete, extending service life of concrete structures as well as minimizing their maintenance costs. The key factor to achieve this goal is to extensively study durability of concrete. Design of mixtures to optimize the performance and economy of concrete to enhance its sustainability is becoming a major interest for agencies and companies. Nanotechnology could be one of the breakthroughs in this field due to its ability to control various characteristics of concrete without increasing its cost or carbon footprint. In this chapter, the effect of nano-silica on some of the main durability aspects of concrete will be investigated. This will include studying this effect on concrete resistance to abrasion, chloride ion permeability and surface scaling due to freeze-thaw action in presence of de-icing salts.

4.1 Abrasion Resistance

Concrete surfaces may deteriorate due to different forms of wear such as cavitation, erosion and abrasion. These types of wear may be caused by friction and scraping of objects or by wind or water currents. For some type of structures, abrasion resistance is an essential characteristic. These structures may include pavements, bridge decks and floors. Generally, concrete resistance to abrasion depends primarily on its mechanical properties. However, other factors may affect the resistance including water-to-cement ratio, type and proportion of aggregates and air entrainment (Laplante et al., 1991 and Naik et al., 1995).

27

Several techniques are used to test the resistance of concrete to abrasion including different methods of mechanical abrasion and sandblasting. In this study, abrasion resistance of the concrete mixtures was tested using sandblasting technique according to ASTM C418. Disk-shaped concrete specimens with diameter of 6" (150 mm) and 3" (75mm) high were used to carry out the abrasion test.

For each mixture, two disks were prepared and cured for 28 days in standard curing tank. The specimens were taken out of the curing tank before testing and surface dried with a damp cloth to obtain saturated surface dry (SSD) condition. Standard sandblasting cabinet equipped with a nozzle that matches the dimensions, air pressure and flow rate specified by ASTM C418. The sand used for testing was natural sand which was selected and graded according to the same ASTM standard. For each specimen, four points were sandblasted for 60 second with the nozzle 3" (75mm) apart from the surface which makes the total tested spots to be eight for each mixture. To measure the abraded volume, oil based clay was used to fill the cavities caused by abrasion as recommended by ASTM standard. The mass of the clay supply was determined before and after filling the cavities and the the volume of the cavities could then be determined as the difference between the two masses divided by the density of the used clay. Figures 11 through 16 show examples of the tested specimens after abrasion and after filling the cavities with clay.
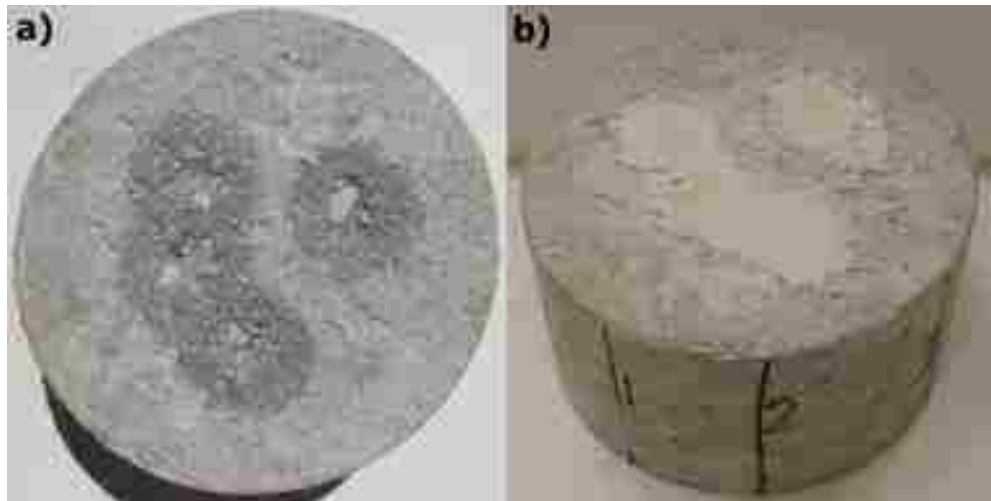
Figure 11 Abrasion specimen A-0 a) after abrasion, b) with clay-filled cavities.
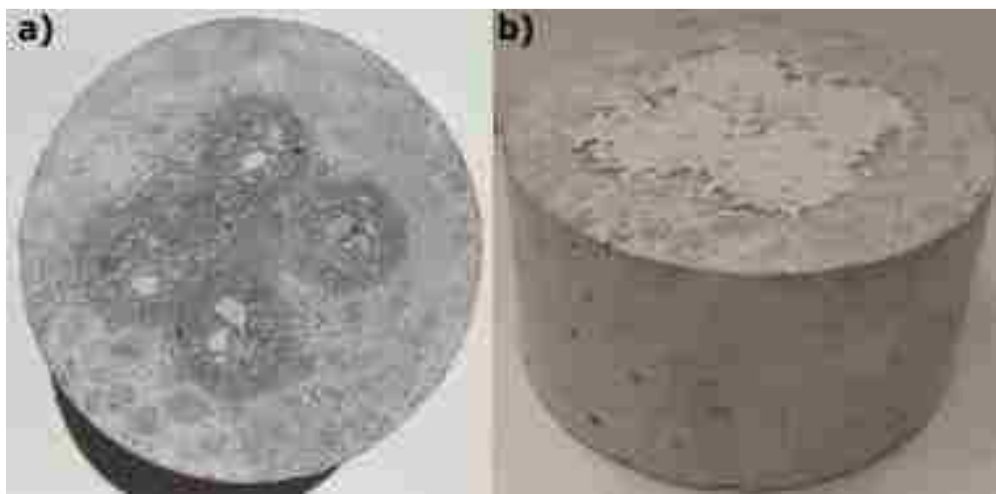
Figure 12 Abrasion specimen A-1 a) after abrasion, b) with clay-filled cavities.
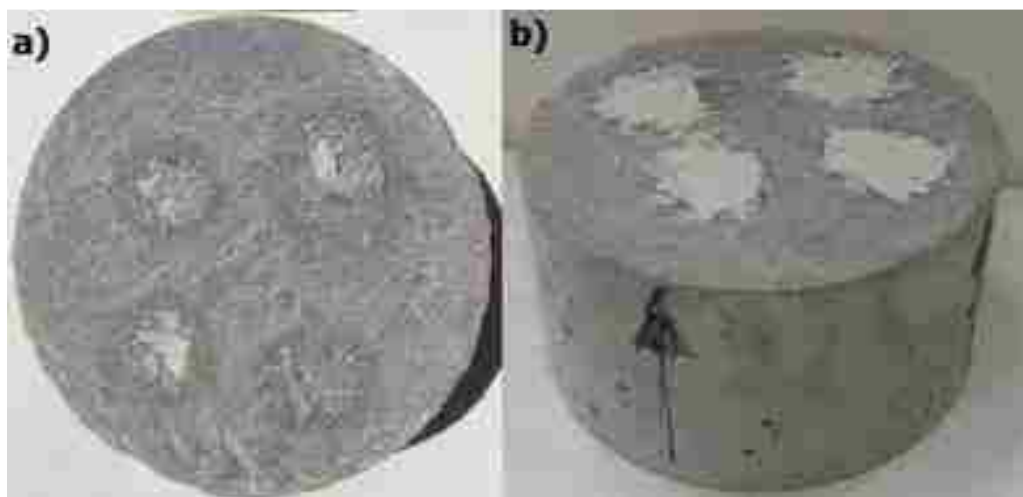
Figure 13 Abrasion specimen A-2 a) after abrasion, b) with clay-filled cavities.

29
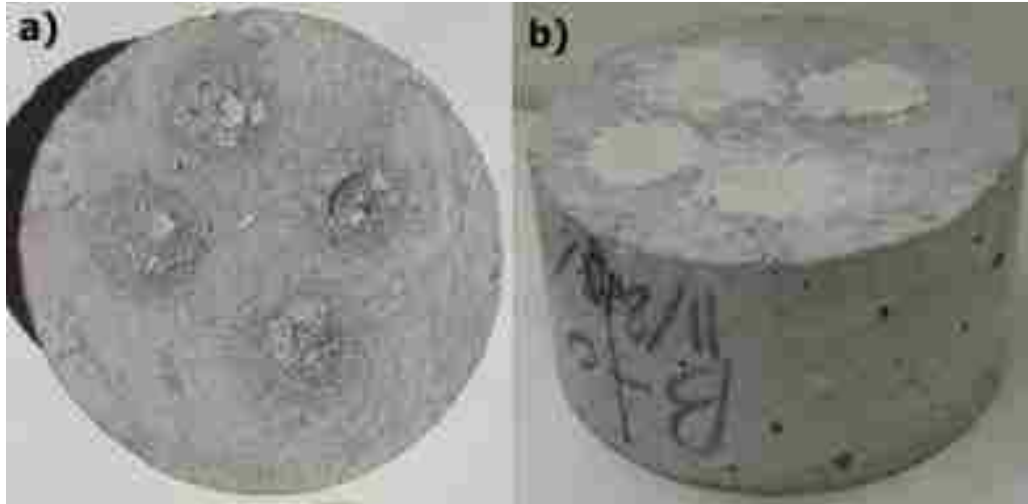
Figure 14 Abrasion specimen B-0 a) after abrasion, b) with clay-filled cavities.
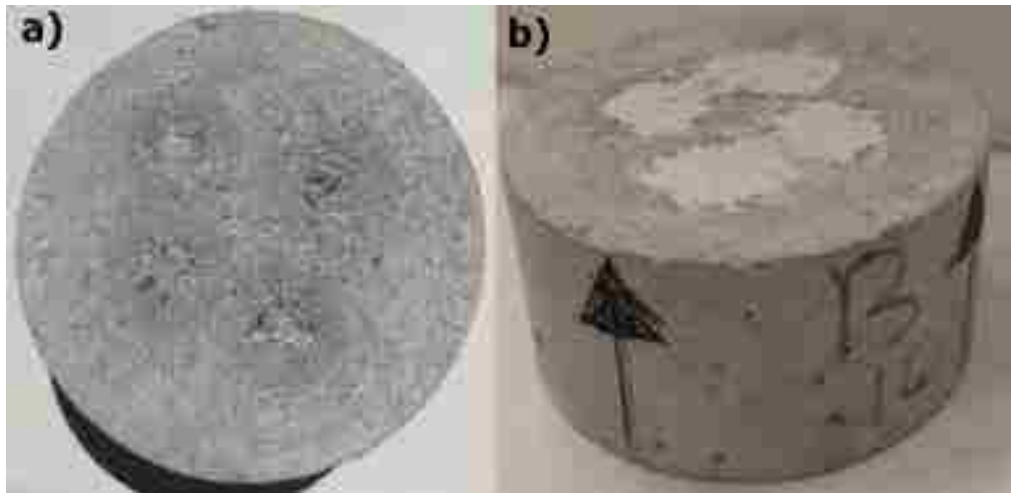
Figure 15 Abrasion specimen B-1 a) after abrasion, b) with clay-filled cavities.
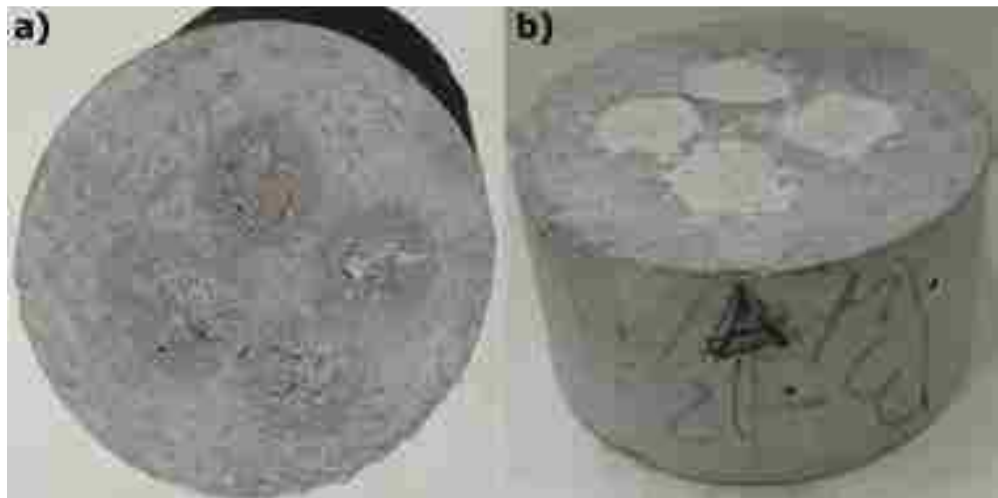
Figure 16 Abrasion specimen B-2 a) after abrasion, b) with clay-filled cavities.

For each of the tested mixtures, the volume of the abrasion cavities was calculated using the loss of clay mass as previously described. The average volume of each cavity was determined by dividing the total abraded volume by number of tested spots as shown in Figure 17. Moreover, the abraded area was measured for each spot and the abrasion coefficients were calculated by dividing the average cavity volume by the mean abraded area of each spot. Table 6 shows the different parameters calculated for the abrasion test results. As indicated in these results, addition of nano-silica has a significant influence on the abrasion resistance of concrete in both of the tested Groups (A and B). The average cavity volume was reduced in approximately linear pattern with the increase of the addition dosage of nano-silica. As expected and previously confirmed in literature (Laplante et al., 1991 and Naik et al., 1995), the abrasion results conform to the mechanical properties results presented in chapter 3. Moreover, these results, along with the mechanical properties, support the conclusion that the addition of nano-silica to concrete significantly enhanced the microstructure of the cement matrix.

4.2 Rapid Chloride Ion Permeability

Chloride salts exist in marine environments as well as soils in some regions, beside that they are commonly used as a deicing agents. However, chlorides are considered to be one of the major contributing factors to reinforcing steel corrosion. Therefore, resistivity of concrete to chloride ion penetration is an important property which correlates to concrete structure durability. Accordingly, rapid chloride ion permeability test (RCPT) is frequently used as a quick assessment for concrete transport properties and consequently its durability. The test is often used because of its relatively simple procedures and short

duration compared to other durability testing. These characteristics make this test very suitable for quality control purposes and for cores assessment.
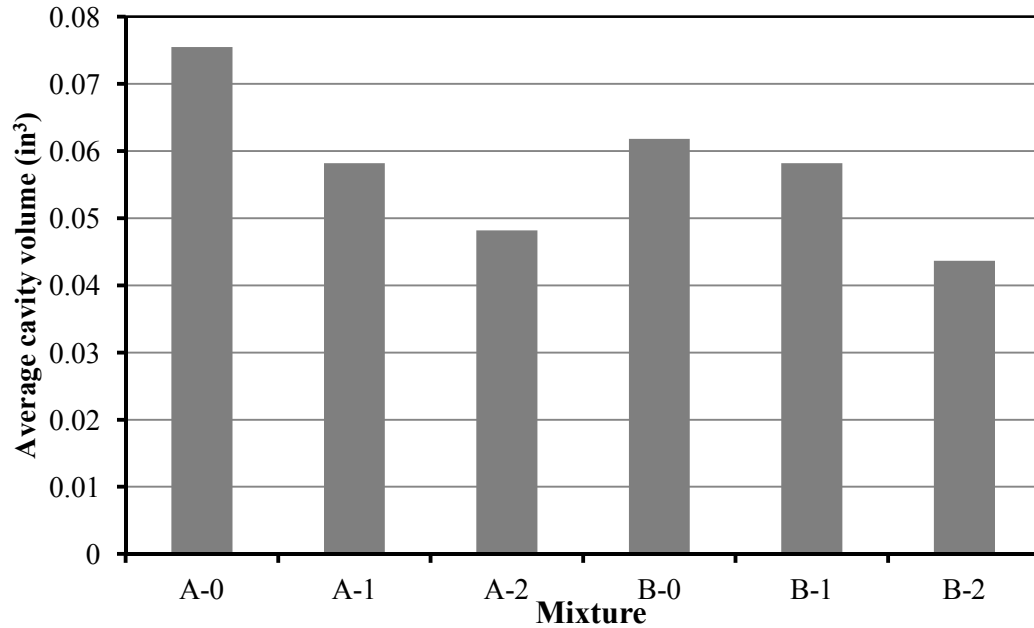
Figure 17 Average abrasion cavity volume for the tested mixtures.

Table 6 Summary of abrasion test results.

Mixture	Average Cavity Volume (in^3)	Average Abraded Area/cavity (in^2)	Abrasion Coefficient (in^3/in^2)
A-0	0.075	1.843	0.041
A-1	0.058	1.838	0.032
A-2	0.048	1.457	0.033
B-0	0.062	1.333	0.046
B-1	0.058	1.361	0.043
B-2	0.044	1.509	0.029

RCPT was conducted for all the mixtures at 28 days according to the procedures specified on ASTM C1202. After curing, the concrete cylinders were cut into 2"discs then conditioned for testing. The conditioning process includes placing the discs in a

32

vacuum desiccators for 3 hours with pressure less than 1 mm Hg (133 Pa), followed by soaking in de-aerated water for 18 ± 2 hours. The specimens then were placed in the testing cell with one side filled with 3.0% sodium chloride (NaCl) solution and the other side filled with 0.3N sodium hydroxide (NaOH) solution. A direct current of voltage of 60 ± 0.1 V is applied between the two sides of the testing cells with the positive terminal connected to the side filled with NaOH solution while the negative terminal is connected to the NaCl side.. The charge passing between the two sides was recorded for 6 hours. Figure 18 shows the test cells and equipments during recording the charge passing through the specimens.

Although RCPT is widely used for concrete durability evaluation, ASTM C1202 states that the results of this test should be used for qualitative purposes rather than comparing the values of the passing charge. To improve the quantitative accuracy of the test, an additional testing procedure was performed at the end of the 6 hour testing period. This procedure involved measuring the physical penetration depth of chloride ions through the disc specimens. To measure this depth, the tested specimens were axially split after testing using an electrical saw. Then the inner face of each half specimen was sprayed with silver nitrate solution which forms a white precipitate of silver chloride after about 15 minutes. The average depth of the white precipitation was calculated by measuring the depth in five different positions along the diameter of each specimen. This average depth was considered to be an indication of the physical ingress of the chloride ion according to the colorimetric method (Bassuoni et al., 2006).

Figure 18 The rapid chloride permeability test setup.

According to ASTM C1202, the charges passed through the concrete disc specimen within 6 hours were recorded. Furthermore, the depth of penetration was measured along the diameter after testing and spraying the split specimens with silver nitrate. The passed charges and the average penetration depths are shown in Table 7, which also includes the qualitative chloride ion penetrability evaluations as specified by ASTM C1202.

The values shown in Table 7 indicate significant improvement in terms of chloride ion penetration resistivity for specimens containing nano-silica. This enhancement could be measured by the reduction of the passing charge and the physical penetration depth. The reduction in the passing charge was more than 50% with the addition of nano-silica for both groups of mixtures (A and B). Also, the penetrability evaluation indicated change the category of the penetrability from low to very low with the addition of nano-silica for Group A specimens. Figures19 and 20 show examples of the physical penetration of the tested specimens with the penetration depth shown with the yellow line. In Figure 19, significant reduction of the penetration depth can be noticed between the specimen

34

without nano-silica (A-0) and the specimen incorporating nano-silica especially for mixture A-1. Moreover, similar observation can be detected in Figure 20 comparing specimen of Group B as significant reduction in penetration depth could be noticed with the addition of nano-silica.

Table 7 Summary of RCPT results.

Mixture	Passed Charge (Coulombs)	Penetrability Evaluation (ASTM C1202)	Average Penetration Depth (in.)
A-0	1837	Low	0.40
A-1	939	Very Low	0.12
A-2	294	Very Low	0.18
B-0	958	Very Low	0.32
B-1	491	Very Low	0.16
B-2	357	Very Low	0.13
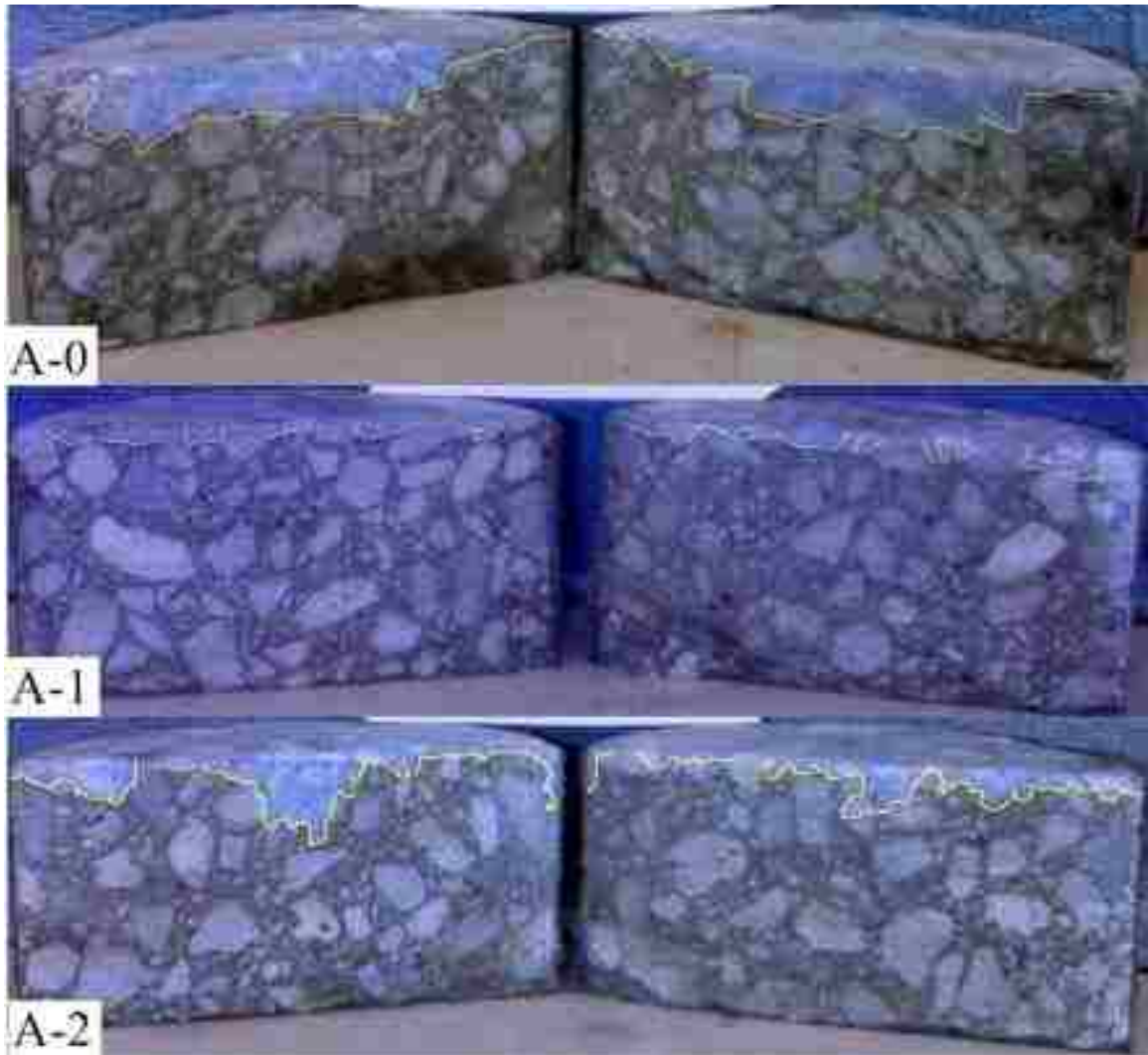
Figure 19 Physical chloride penetration for Group A specimens.

The enhancement imparted through the use of nano-silica indicates that the effect of nano-silica is not limited to its filler action or pozzolanic effect but it may be extended to improving the transport properties of concrete. Moreover, these results suggest considerable improvement in the microstructure and porosity of the cement matrix, which are main factors affecting the transport properties and permeability of concrete.
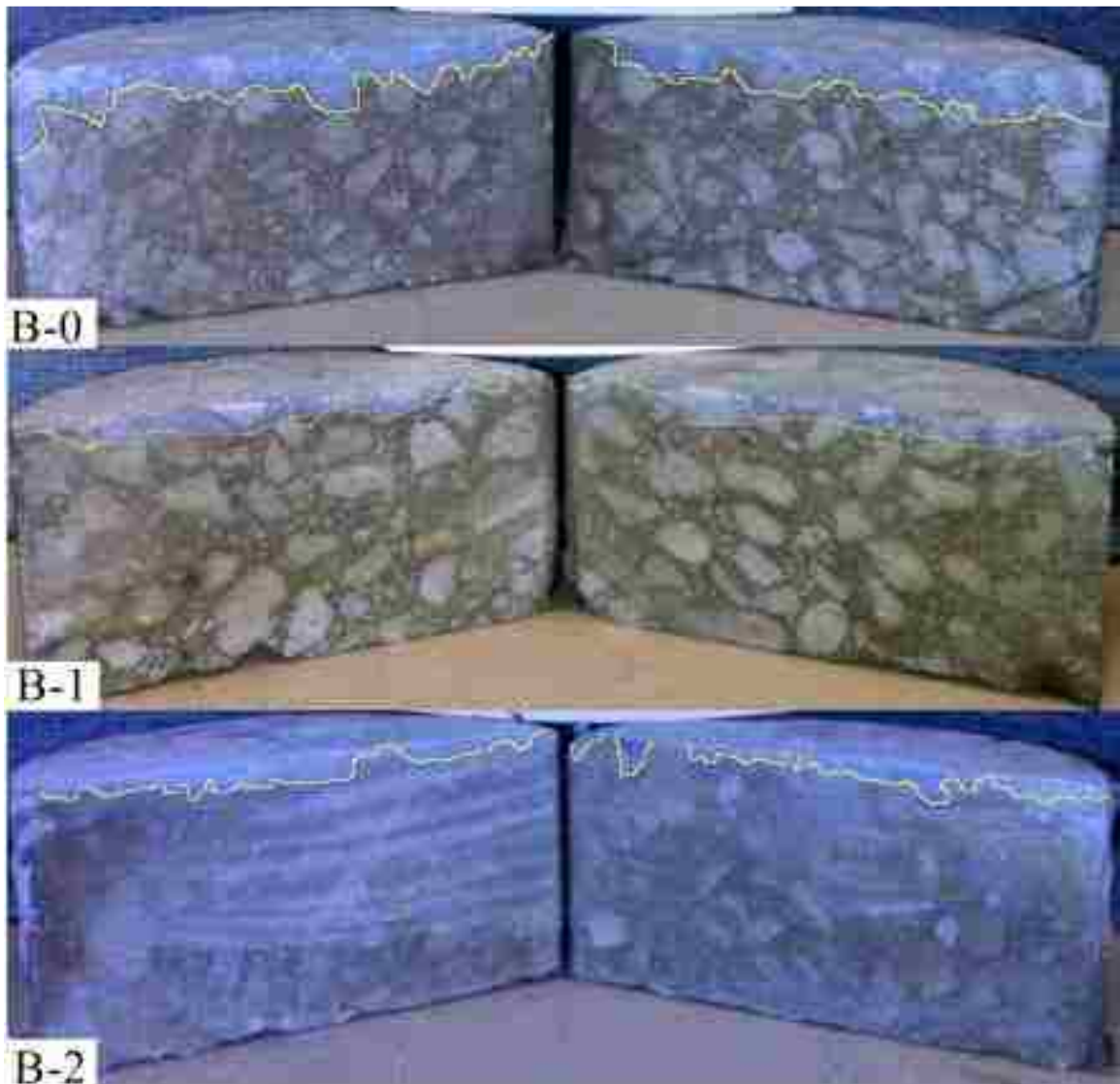
Figure 20 Physical chloride penetration for Group B specimens.

4.3 Surface Scaling

The freeze-thaw cycling action is considered for decades as a major cause of concrete deterioration. As the water in the capillary pores freezes, it starts expanding and driving off the excess water creating hydraulic pressure on the pore walls. Also, the accumulation of the ice in pores builds up additional pressure on the cement paste (Detwiler et al., 1989). In addition to the freeze-thaw action, concrete pavements, sidewalks and bridge

37

decks are subjected also to the effect of de-icing agents which are widely used in some regions. The combined effect of freeze-thaw action and the high concentrations of de-icing chemical may accelerate the deterioration of the surface of concrete in contact with these chemicals (Şahinet al., 2010).

The resistance of the six tested mixtures for freeze-thaw and de-icing salt was investigated according to ASTM C672. Concrete slabs 9"×9"×3" (225×225×75 mm) were prepared as two replicates for each mixture. The specimens were moist cured for 14 days after mixing in the standard curing tank followed by 14 days of air curing in lab conditions (temperature of $20 \pm 2°C$ and relative humidity of 50 ± 5 %). On the surface of each specimen a pond of salt solution was created to simulate the effect of the de-icing chemicals. To keep around ¼" (6 mm) of solution on top of the surface all the time, a dike of height ½" (12 mm) and width ¾" (18 mm) was shaped in the concrete mold. Figure 21shows the surface scaling slab specimens with the solution on top of them during testing. Although ASTM standard adopts using calcium chloride ($CaCl_2$) solution, for this study,4% sodium chloride (NaCl) solution was used instead as it is proved to be more aggressive and it is a more commonly used de-icing salt (Sahin et al., 2010). The specimens were subjected to 24 hour freeze-thaw cycles as they were placed for 16-18 hours inside the freezer at $-18 \pm 3°C$ followed by 6-8 hours in lab ambient conditions ($20 \pm 2°C$ and relative humidity of 50 ± 5 %).

The surfaces of the specimens were flushed and the solution was replaced every 7-10 days. The cycles continued until at least 60 cycles were completed as recommended by ASTM standard. Every two weeks, the surface was visually inspected and the debris was collected from the surface on a sieve #200 and then weighed. The scaling level is visually

rated according to ASTM C672. The rating system is based on a scale of 0 to 5 with 0 means no scaling and 5 having the most severe scaling.

Figure 21 Surface scaling specimens during testing.

Table 8 presents the average cumulative debris mass and the visual rating of the surface of the tested specimens after 30 cycles of exposure and at the end of the experiment. Also, Figure 22 shows the average debris mass at the end of the exposure period. Figure 23 shows the scaling on the surfaces of one set of specimens after 60 cycles of exposure. It might be noticed in the photos that white paste was used at some locations on the dikes of the specimen. This paste was a silicon-based sealant used on some specimens to prevent leakage of the solution through the dikes during the thawing period and to repair the deteriorated dikes.

www.manaraa.com

Table 8 Avegrag debris mass and visual rating of speciemns.

Mixture	After 30 cycles of exposure		After 60 cycles of exposure	
	Cumulative Collected Debris Mass (g/specimen)	Visual Rating (ASTM C672)	Cumulative Collected Debris Mass (g/specimen)	Visual Rating (ASTM C672)
A-0	14.3	1	20.4	1
A-1	6.2	1	15.4	2
A-2	16.6	2	25.5	4
B-0	31.3	3	46.8	4
B-1	46.5	4	68.3	5
B-2	23.0	3	34.7	4
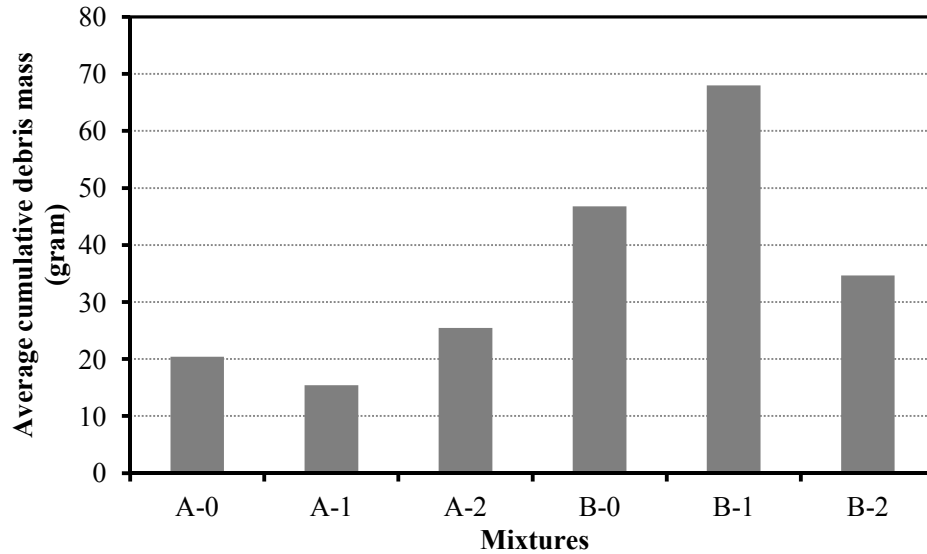
Figure 22 Average total debris mass after 60 cycles of exposure.

At the end of the 60 cycles, most of the specimens experienced significant surface scaling. Generally, mixtures containing fly ash (Group B) suffered of significantly higher levels of scaling at different times of exposure. Furthermore, the mass of the debris in this group was considerably higher. This may be attributed to the increase in percentage of small pores as is discussed later in Chapter 5. The effect of nano-silica was not very significant on the scaling level in case of Group B specimens as the severe surface

40

damage may affect the accuracy of this method. The severe damage causes aggregate to represent most of the surface exposed to the salt solution (see specimen B-1 in Figure 23). On the other hand, for Group A specimens, the addition of nano-silica resulted on higher levels of damage. Linking these results to the porosity results presented in chapter 5, the addition of nano-silica increased the percentage of the micro-pores (less than 0.1 µm in diameter). Generally, it may be observed that the level of scaling in the different mixtures had a good agreement with the results of the porosity testing presented in Chapter 5. For instance, the highest level of damage was observed in mixture B-1 which had the highest percentage of micro-pores (79.7% of total pores). This reduction in pore diameters might have led to higher ice crystallization pressure (Scherer, 1999) as this may prevent the pressure relief to the larger pores or air voids.

Figure 23 Scaling on the surface of the specimens after 60 cycles of exposure.

Chapter 5: Microstructure, Porosity and Thermal Analysis

5.1 Mercury Intrusion Porosimetry

Mercury Intrusion Porosimetry (MIP) was used to assess the pore size distribution and the total porosity of the mixtures. Small chunks obtained from the concrete cylinders after 28 days were used as test samples for MIP (Kumar and Bhattacharjee, 2003). These chunks were around 3 to 10 mm in size and were carefully extracted to avoid the inclusion of large aggregates. The samples were oven dried for 72 hours at temperature of $60 \pm 2°C$, then they were kept in a desiccator containing silica gel until the time of testing. This method of drying (lower temperature for longer period) was adopted to avoid the formation of micro-cracks, which may occur at high temperatures. The contact angle and the mercury surface tension were taken as 130° and 485 dynes/cm, respectively (Shi and Winslow, 1985).

The trends of MIP for Group A and Group B mixtures are shown in Figures 24 and 25, respectively. Also, the apparent total porosities, threshold pore diameters and percentage volume of micro pores (less than 0.1 μm) for the six mixtures are shown in Table 9. The threshold diameters for the six mixtures are also shown in the same table. These diameters represent the pore size where the pressure was enough to let the mercury intrude most of the inaccessible larger pores inside the bulk specimen.

In compliance to the mechanical and durability properties, it can be noted that the total porosity was significantly decreased with the addition of nano-silica (Table 9). In

addition, the threshold pore diameters of mixtures containing nano-silica were significantly less than those of the control mixtures without nano-silica (A-0 and B-0). Further pore structure refinement was achieved with increasing the dosage of nano-silica (Figures 24 and 25 and Table 9). For example, mixtures B-1 (3% nano-silica) and B-2 (6% nano-silica) yielded threshold pore diameters of 36% and 48%, respectively less than that of mixture B-0 (0% nano-silica), which was 0.144 μm. Correspondingly, the percentage volume of micro pores for those mixtures were 8.5% and 5.4%, respectively, larger than that of the reference mixture B-0, which was 73.41%. Again, this trend is ascribed to the pozzolanic and filler effects of nano-silica; however, the contribution of each effect to the refinement of pore structure could not be readily differentiated by the MIP results.

Table 9 Summary of MIP results.

Mixture	Apparent total porosity (%)	Threshold pore Diameter (μm)	Percentage of small pores (<0.1μm) (%)
A-0	10.13	0.10	69.3%
A-1	6.91	0.075	75.4%
A-2	6.44	0.060	72.2%
B-0	12.56	0.144	73.4%
B-1	9.30	0.092	79.7%
B-2	8.21	0.075	77.3%

44
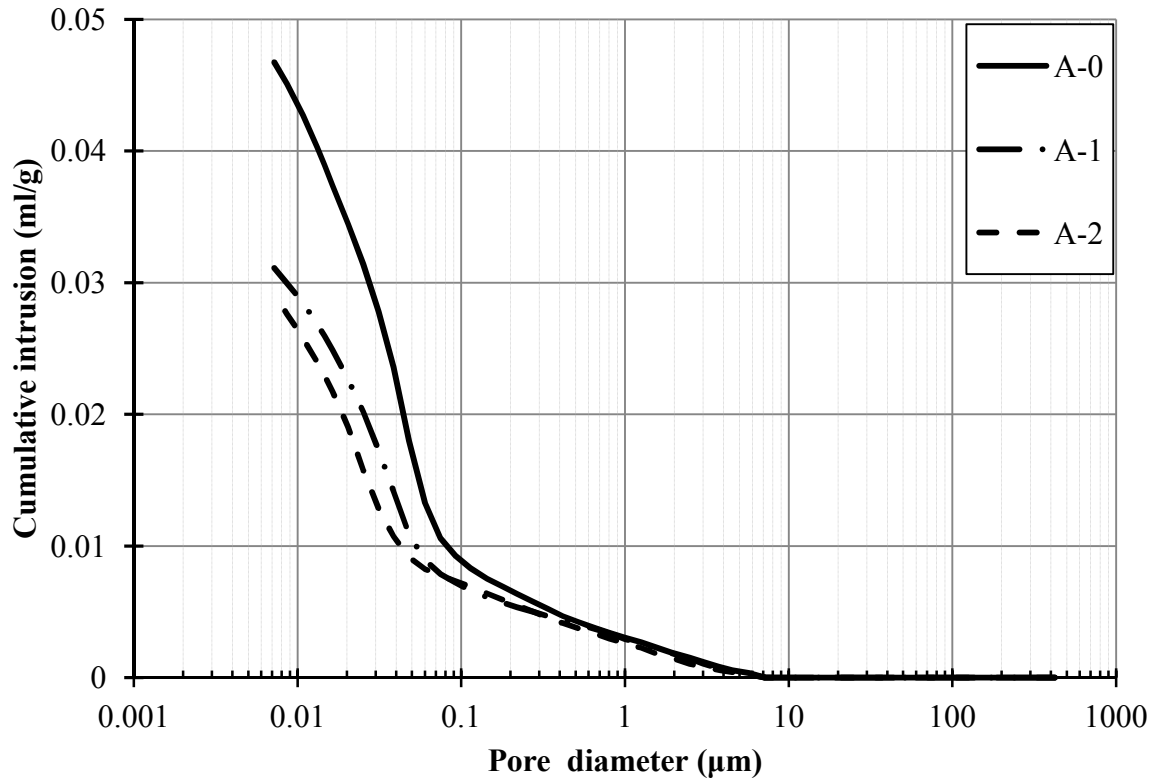
Figure 24 Pore size distribution for mixtures without fly ash (Group A).
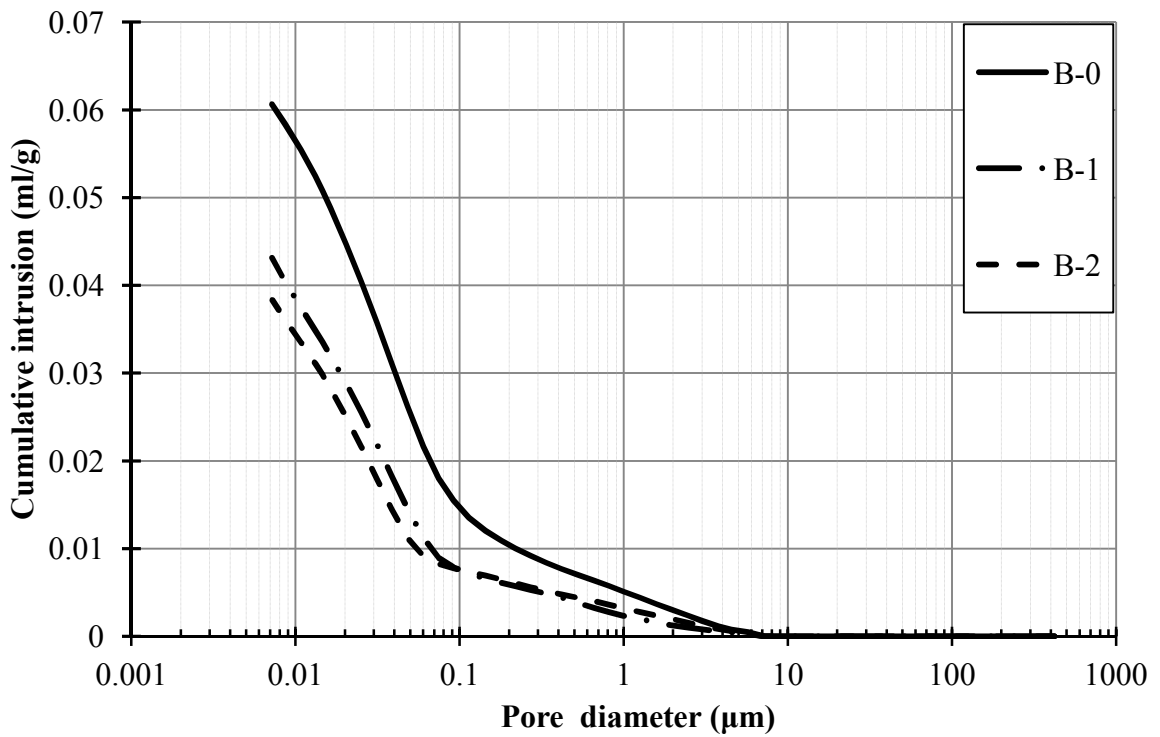
Figure 25 Pore size distribution for mixtures with fly ash (Group B).

45

5.2 Thermogravimetry

The effect of nano-silica on the hydration and pozzolanic reactions was assessed by determining the quantity of portlandite (calcium hydroxide) in the matrix after 28 days. Thermogravimetry (TG) at a heating rate of 10°C/min was used for this purpose. After 28 days, chunks were obtained from crushed concrete cylinders. For the TG tests, the chunks were ground to powder, passing a #200 sieve (75 μm). The content of portlandite was calculated by determining the drop in the percentage mass of TG curves at a temperature range of 420-450ºC (chemically bound water in portlandite) and multiplying it by 4.11 (ratio of the molecular mass of portlandite to that of water).

The thermogravimetry (TG) results are shown in Figure 26. Compared to the control mixtures without nano-silica, the addition of nano-silica in Mixtures A-1, A-2, B-1 and B-2 led to considerable consumption of portlandite (CH) in the cementitious matrix. This can be attributed to the effect of the pozzolanic reaction, which partially led to the pore structure refinement observed in the MIP results (Table 9). However, increasing the nano-silica dosage from 3% to 6% did not seem to have a pronounced effect on the depletion of CH (Figure 26). For example, Mixtures B-1 (3% nano-silica) and B-2 (6% nano-silica) had comparable CH contents of 2.69% and 2.66%, respectively. These mixtures had threshold diameters of 0.092 and 0.075 μm, respectively (Table 9). This may suggest that the general improvement in the mechanical and durability properties and also in pore structure refinement associated with the increase in the nano-silica addition from 3% to 6% may be mainly attributed to the physical filler effect of incorporating a larger volume of ultrafine particles in the cementitious matrix. This

46

statement must be substantiated by further testing in future research by combining nano-silica with other types of inert nano particles.
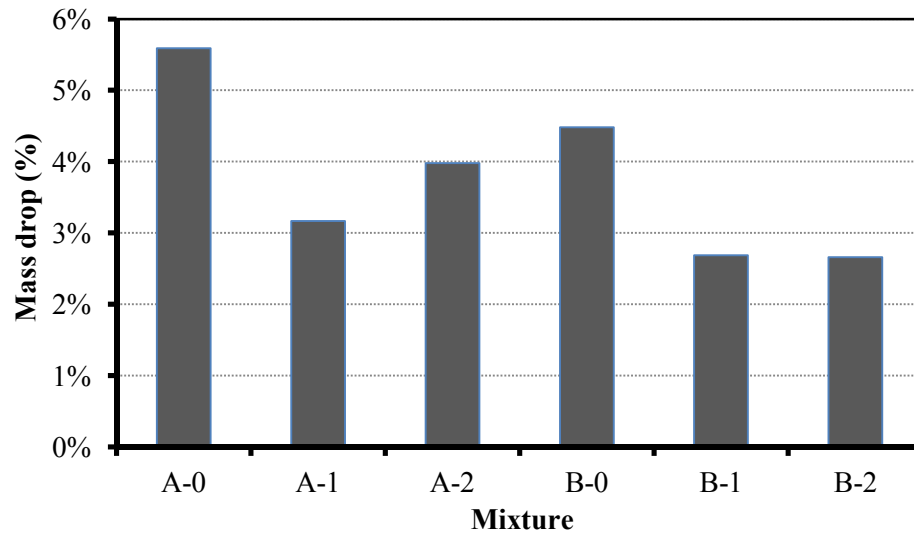
Figure 26 Thermogravimetry (TG) results for portlandite (CH) peaks at about 450 °C.

5.3 Scanning Electron Microscopy

Backscattered scanning electron microscopy (BSEM) was used on polished thin section to compliment the findings of the MIP and TG. Polished thin sections were prepared by cutting 1"× 2" (25×50 mm) specimens from the concrete cylinders after 28 days. Subsequently, they were impregnated by low-viscosity epoxy resin under pressure and polished using diamond surface-grinding equipment.

In general, BSEM observations conformed to the strength, durability, MIP and TG results. For Group A mixtures (without fly ash), significant densification was observed in the matrix at the interfacial transition zone (ITZ) for specimens containing nano-silica. For instance, Figures 27a-b show the ITZ (as indicated by the arrows) for specimens A-0 (0% nano-silica) and A-2 (6% nano-silica). It can be observed that the ITZ for specimen

47

A-0 (Figure 27a) is full of voids and micro-cracks due to the wall effect between aggregates and the cementitious matrix. On the contrary, the ITZ in the section prepared from mixture A-2 (Figure 27b) appears to be densified/refined owing to the chemical (pozzolanic reaction) and physical (filler action) effects induced by nano-silica particles. This conforms to the strength, durability, MIP and TG results. For Group B specimens containing 30% Class F fly ash, a more porous structure was observed in the control specimen (B-0) at 28 days. For example, Figures 28a-b show the BSEM images for specimen B-0 and B-2, respectively. For specimen B-0, without nano-silica, the micrograph (Figure 28a) shows a coarse microstructure for the cementitious matrix incorporating 30% fly ash. Considering that Class F fly was used, the microstructure reflects insufficient degree of hydration of the matrix at this age, which links to the lower strength results shown in Figure 8 and Table 5. Also, this observation conforms to the MIP pore size distribution curve of this mixture (Figure 25), which had higher total porosity, threshold pore diameter and volume percentage of pores larger than 0.1 μm (Table 9). Conversely, for specimen B-2, which incorporated 6% nano-silica with 30% fly ash, the BSEM micrographs (Figure 28b) showed higher degree of hydration as depicted by the refined/denser microstructure and ITZ. Hence, it appears that the addition of a small dosage of well-dispersed colloidal nano-silica efficiently catalyzed the kinetics of Class F fly ash reaction in the cementitious matrix. This suggests that the delay in strength gain, microstructure development and improvement in durability of concretes comprising Class F fly ash can be mitigated by the addition of small dosages of nano-silica.
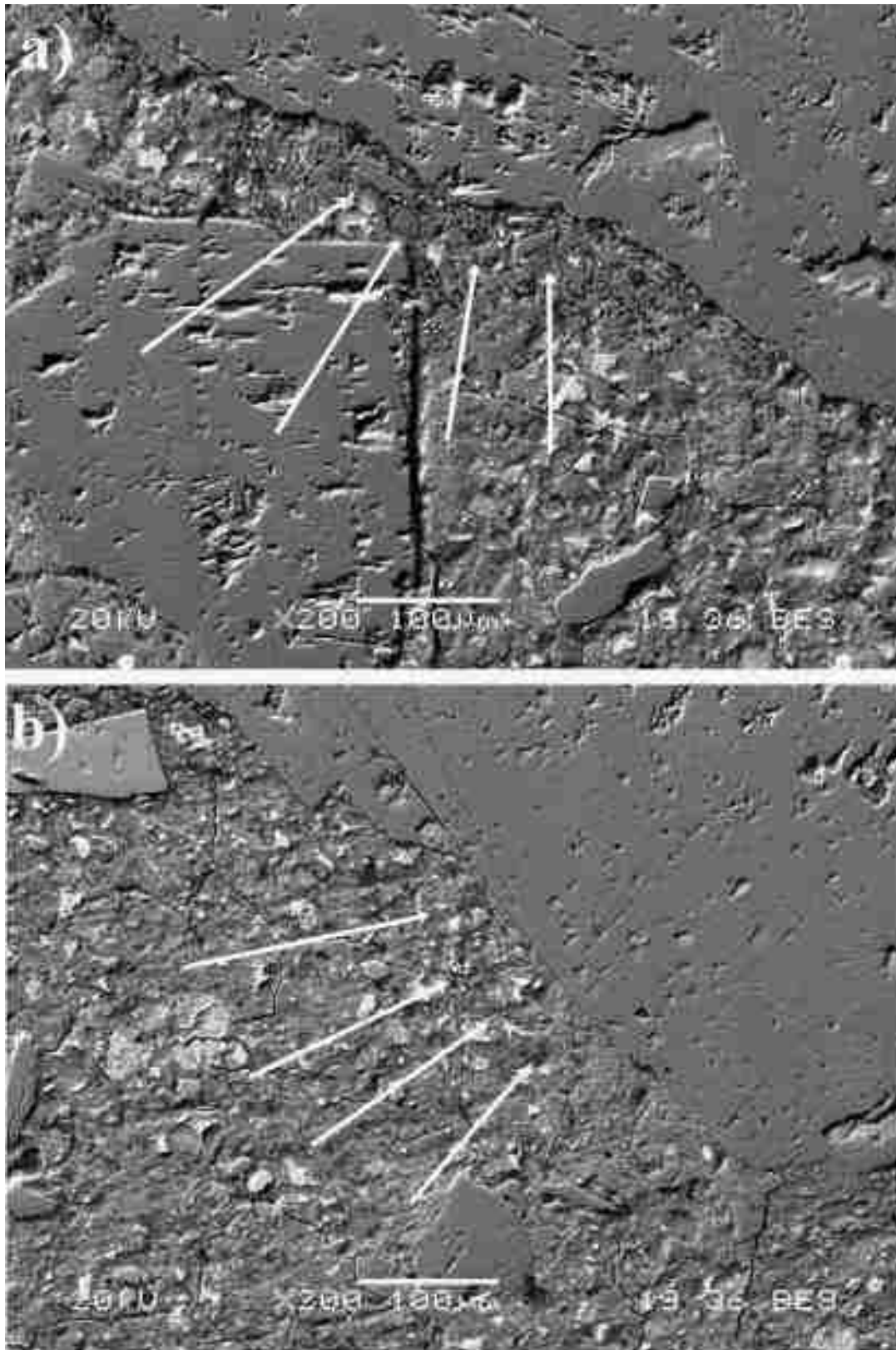
Figure 27 BSEM Images for: a) Specimen A-0 b) Specimen A-2.
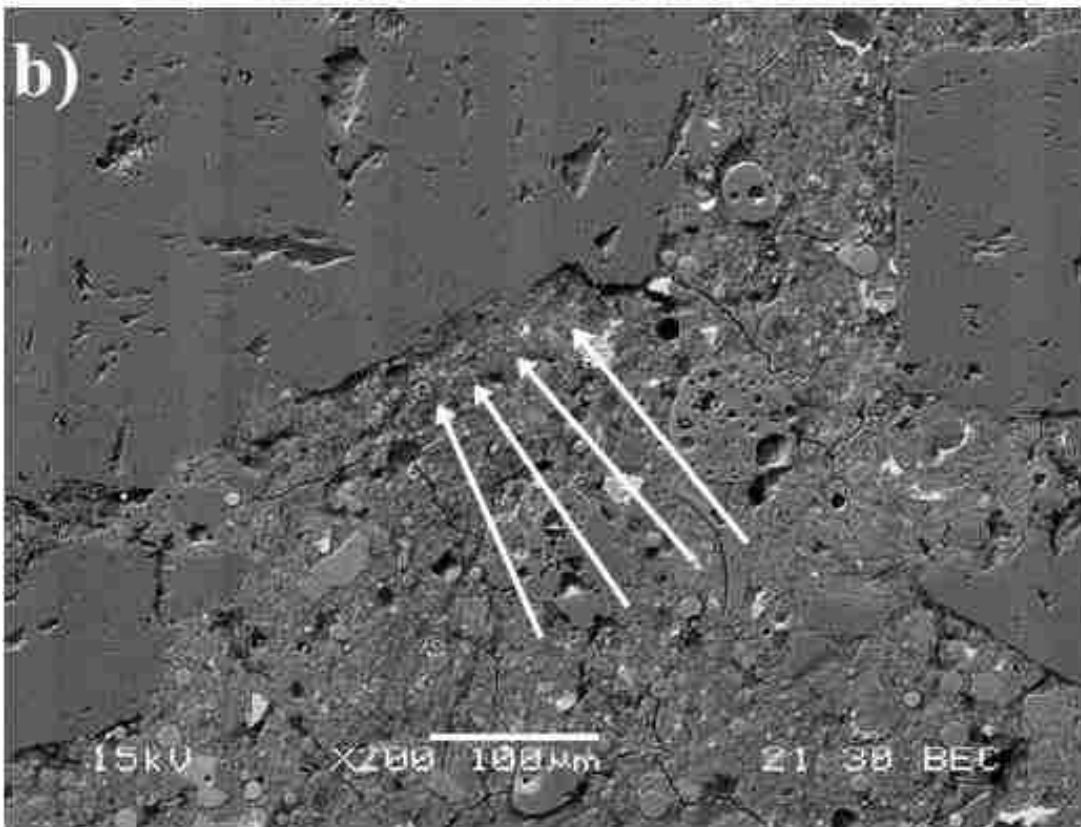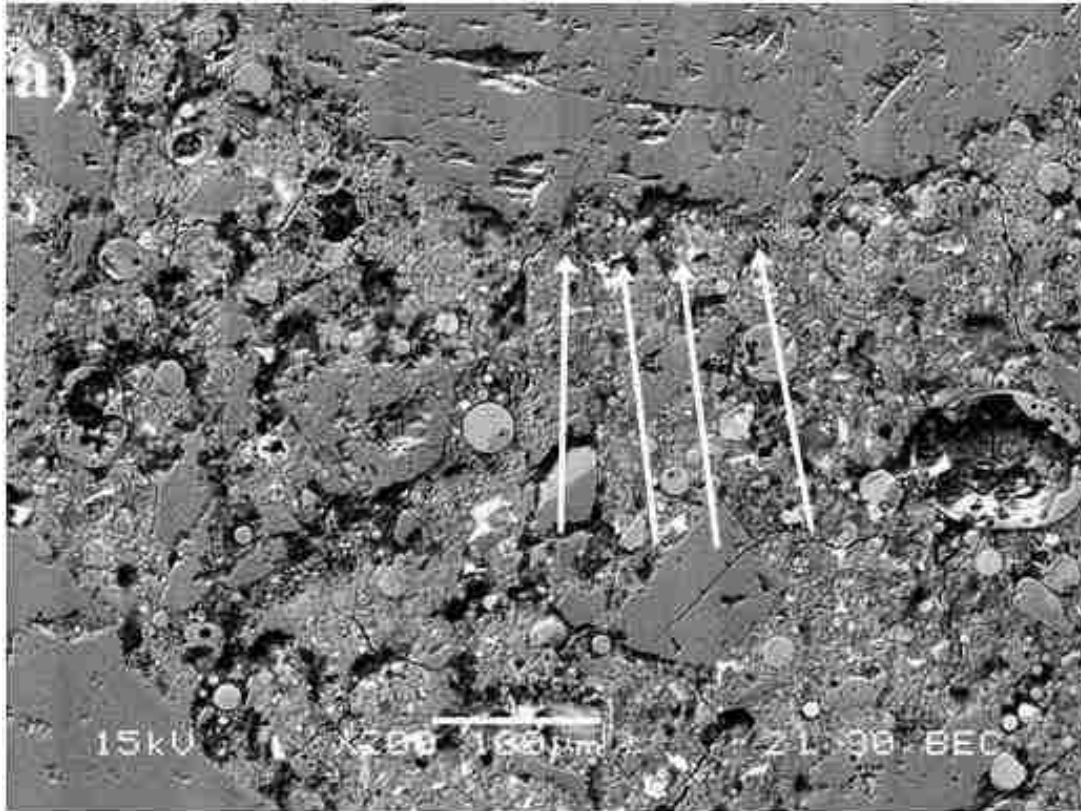
Figure 28 BSEM Images for: a) Specimen B-0 b) Specimen B-2.

Chapter 6: Physical Salt Attack

6.1 Introduction and Background

Salt crystallization was widely studied in natural rocks as one of the main mechanisms of rock breakdown. This type of damage (also known as salt weathering) was considered as a potential risk for many ancient monuments in various location including Mediterranean coast and Middle East, even that Herodotus had referred to this phenomenon in the Nile Valley more than 3400 years ago (Goudie and Viles, 1997). This mechanical disintegration caused by crystal growth of salts in pores was observed not only on Earth but on Mars rocks as well (Malin, 1974). Geologists have investigated damage of natural rock due to salt crystallization; however the mechanism of the distress is not totally explained (Goudie and Viles, 1997; Sperling and Cooke, 1985). Furthermore, the deterioration caused by salt crystallization in building materials including stones and bricks has been investigated (Flatt, 2002; Rodriguez-Navarro et al., 2000).

In areas with high concentration of soil salts, it was believed, by most engineers, that chemical attack was the major cause of reported concrete damage. In soils containing sulfate salts, this damage was mostly identified as sulfate attack which involves chemical interaction between sulfate ions in the soil and the hydrated cement generating products like ettringite and gypsum which may lead to concrete deterioration (Mehta and Monteiro 2006). The mechanism of the sulfate attack in concrete was not fully understood and it has been always a controversial issue among researchers (Cohen and Mather 1991). Also, this chemical effect of sulfates on concrete structures may be overlooked by various

51

studies because proper analytical tools were not used to identify this damage. To verify the damage caused by chemical attack of sulfate salts, advanced analysis should be performed including optical microscopy, scanning electron microscopy (SEM), and X-ray diffraction analysis (XRD) (Haynes et al. 2008).

Only during the last few decades, the damage caused by salt crystallization on concrete structure had caught researchers' interest (Reading, 1982; Haynes et al., 1996; Mehta, 2000; Hime et al., 2001). The physical salt attack (PSA) is not limited to the sulfate salts but it may also occur in concrete exposed to carbonates and chlorides salts with lower aggressive way (Haynes et al., 2010; Haynes and Bassuoni, 2011). Before the recent studies, engineers had usually misidentified the damage caused by crystallization of salts as chemical attack. However, the damage due to salt weathering is associated with surface scaling which appears like that caused by freeze-thaw damage (Haynes et al., 1996).

Salt crystallization in porous concrete can occur under certain environmental condition in presence of high salt concentrations in soil. The main source of these salts is the ancient marine soils containing chloride and sulfate salts from sea water. These salts are usually accumulated in certain regions according to the topography, groundwater flow, surface runoff and proximity to oceans. The porous concrete in contact with these soils may absorb the salt solution which consequently elevates by means of capillarity to the evaporation surfaces of the structure. Repeated cycles of low followed by higher relative humidity increase the concentration of the salts in the pores at and close to the evaporation surface. Crystallization of the salts due to the supersaturated solution may be observed on the concrete surfaces. This surface crystallization, usually known as

efflorescence, has very limited effect on concrete. However, the salt crystallization taking place below the surface (subflorescence) may cause significant scaling in the concrete surface. This subflorescence is formed when the rate of evaporation from the concrete surface exceeds the rate of flow of the solution through capillarity.

The mechanisms of distress caused by PSA were discussed in several studies either in natural rock or concrete (Goudie and Viles, 1997; Scherer, 1999; Thaulow and Sahu, 2004; Chatterji, 2005). Some of these mechanisms are based on the solid volume change during transformation between phases of hydrous and anhydrous minerals. One example of this mechanisms is the transformation of anhydrous form of sodium sulfate (thenardite) (Na_2SO_4) to the hydrous form (mirabilite) ($Na_2SO_4 \cdot 10H_2O$) which is associated with increase in solid volume of around 315%. Other studies suggest that the distress may be caused by moisture absorption of anhydrous salts undergoing solid-state hydration. This hydration generates pressure inside concrete pores causing microstructure disintegration and distress. Another mechanism for concrete damage by PSA was presented by Haynes (2006) which involves the increase in volume of solutions in pores due to crystallization of mirabilite. According to Correns equation (Correns, 1949), the crystallization pressure of salts in the pores of the cement matrix (p) may be quantified as:

$$p = \frac{RT}{V_s} \ln \left(\frac{C}{C_s} \right)$$

where, (R) is the gas constant, (V_s) is the molar volume of the solid salt, (C) is the solute concentration, (C_s) is the saturations concentration at temperature (T). Generally, this equation shows that the crystallization pressure inside the pores increases as the

53

concentration of the salt rises in the pore solution causing progressive damage during exposure.

As a natural phenomenon, the damage caused by salt crystallization is a long-term action that may take decades or even centuries as in case of natural rocks. In case of concrete, the time of exposure causing PSA damage, reported in few available cases, varied depending on the quality of concrete and the location (Haynes, 2002). Lacking a standard testing procedure, several exposure regimes were suggested to simulate the ambient conditions accelerating PSA in laboratory. In several studies, it was found that the highest levels of damage in lab specimens were observed when the specimens where partially immersed in the salt solutions while exposing significant portion of the specimen as an evaporation surface (Reading, 1982; Haynes et al., 2008; Bassuoni and Nehdi, 2009; Hartell et al., 2011)

A recent study investigating the physical effect of sodium sulfate salt (Haynes et al., 2008) employed five different environmental exposures for more than 18 months. In this study, it was found that the most severe damage was observed when the ambient conditions cycled between temperature of 20°C with 82% relative humidity and 40°C with 31% relative humidity. This exposure regime coincides with the cycling between the thenardite and mirabilite phases of sodium sulfate as shown in Figure 29. Another study on the physical effect of sodium carbonate (Haynes et al., 2010) found similar results for the most accelerated ambient cycles. The previously described cycles provided alteration between different phases of sodium carbonate salt as shown in Figure 30. These phases include natron ($Na_2CO_3 \cdot 10H_2O$), hepatahydrate ($Na_2CO_3 \cdot 7H_2O$), and thermonatrite ($Na_2CO_3 \cdot H_2O$).

54
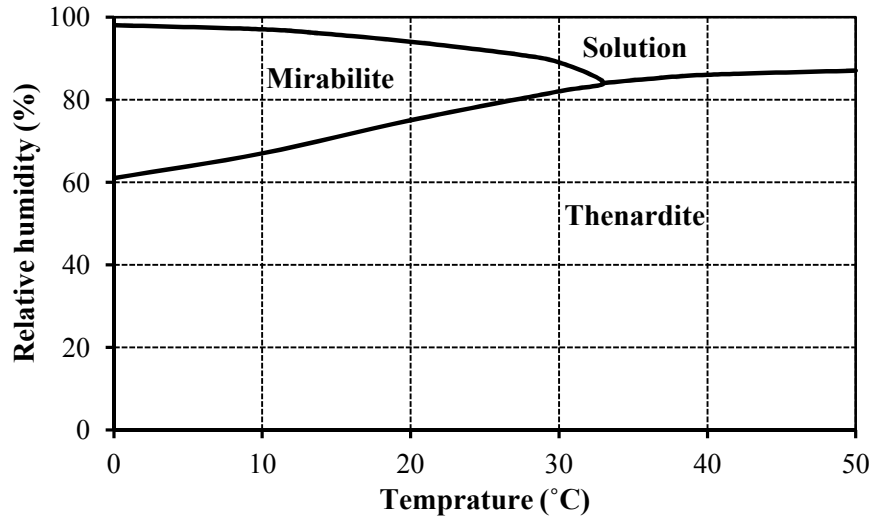
Figure 29 Phase diagram for sodium sulfate (Flatt 2002).
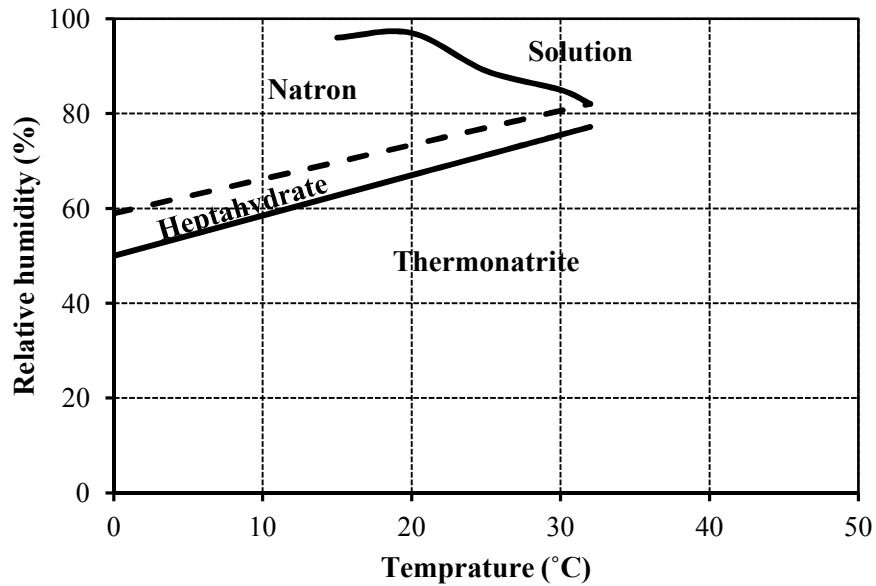
Figure 30 Phase diagram of sodium carbonate (Goudie and Viles 1997).

In this study, the effect of using nano-silica on PSA resistance will be investigated. Six different concrete mixtures with different combinations of cement fly ash and nano-silica will be tested using the most aggressive and accelerated procedure. Based on previous studies, sodium sulfate solution will be used to study the damage caused by salt

55

crystallization of in concrete pores as it represents the most severe form of PSA (Haynes et al., 2008; Haynes et al.,2010; Haynes and Bassuoni, 2011).

6.2 Experimental Program

6.2.1 Specimens and procedures

The test program involved partially immersing 12 concrete cylinders in sodium sulfate solution (two replicates of each of the six tested concrete mixtures). The tested cylinders with aspect ratio of 3 had diameter of 2.0 in. (50 mm) and height of 6.0 in. (150 mm). These non-standard and relatively small specimens' dimensions were selected mainly obtain a high surface-to-volume ratio to accelerate the kinetics of damage due to PSA. Moreover, since the damage caused by PSA starts at the surface of concrete as previously described, the size of the specimen may considerably affect the rate of damage, as reported for several durability tests (Cohen and Mather, 1991; Haynes, 2009). In addition, the aspect ratio was set to be 3.0 to be within the recommended range by ASTM C215 for best results of dynamic modulus of elasticity (DME).

Following a standard moist curing period of 28 days, the cylinders were air dried for 48 hours before measuring the initial weights and DME. The laboratory simulation of the ambient conditions accelerating PSA includes partial immersion of the concrete cylinders (one third of the total height) in salt solution while temperature and relative humidity are changed in repetitive cycles. To achieve the partial immersion and to prevent excessive evaporation of the solution, a separate plastic container was used for each specimen with an air-tight lid. The led had an opening with a diameter approximately equal to the diameter of the specimen to prevent excessive evaporation through the solution surface.

56

The setting of the specimens and the containers including the solution during testing are shown in Figure 31. The containers and the specimens were then placed inside a programmable environmental chamber in which temperature and relative humidity can be controlled.

The solution used in this study was 10% sodium sulfate prepared using USP grade reagent. This concentration may be significantly higher than the concentrations naturally occurring in soil or ground water. However, this relatively high concentration was selected to accelerate the damage caused by PSA. Noteworthy, the actual concentration increased during the testing period due to absorption and evaporation through the specimens. In order to limit the variation in this concentration, the solution was continuously topped off in all containers every 4 to 8 cycles of exposure and it was totally replaced by fresh solution every 12 to 16 cycles.

Figure 31 Specimens partially immersed at the early cycles of testing.

57

The range of change in temperature and humidity in the generated cycles was selected to simulate the natural change in ambient occurring in some regions in the US and worldwide (e.g. southern Nevada, California, Arizona, North Africa and Australia). Based on the published literature, this temperature and humidity range also covers alternation between the two different phases of sodium sulfate as presented in Figure 29. The full cycle was designed to alternate between two ambient conditions in which the first simulate a moderate humid season while the other represents the hot dry one. The ambient cycled between $20 \pm 1°C$ with 80 ± 2 % relative humidity(moderate/humid) and $45 \pm 1°C$ with 15 ± 2 % relative humidity(hot/dry). The exposure was divided into two successive phases. Phase I which was implemented during the first 50 cycles involved running two cycles every week. This was achieved by programming each cycle to be 84 hours of total duration as 42 hours for each of the two ambient conditions. In order to accelerate the surface distress, the cycles were subsequently sped up in phase II so 4 cycles were ran every week. This accelerated cycles involved 21 hours for each ambient period generating a 42 hours total cycle.

6.2.2 Testing and measurements

During the exposures, the physico-mechanical properties of the specimens were monitored at regular time intervals. To achieve this, every 4 to 8 cycles, the specimens were taken out of the environmental chamber after the hot/dry exposure period, then the salt efflorescence and debris were removed using a nylon brush. The specimens were left to dry in lab ambient conditions for 30 minutes to achieve saturated surface dry (SSD) state. The mass of each specimen was then measured to the nearest 0.1 g and the specimens were visually inspected and photographed. In order to monitor the soundness

58

of the specimens, the longitudinal DME was measured for each specimen using impact resonance apparatus according to ASTM C215. For each specimen, at least 3 measurements of the resonance frequency (to calculate DME) were taken in each direction (3 values with impact on the dry end and 3 with impact on immersed end). Monitoring the change of DME during the exposure period can give an idea about the continuity and the soundness of the specimens. Furthermore, this data can give indications about inner micro-cracking occurring in the specimens and indirectly the change in strength.

The DME was evaluated continuously based on measuring the average fundamental resonance frequency of each specimen. Change in the DME usually indicates the change of specimen's stiffness or change in its continuity (e.g. presence of inner cracking). The equation used to calculate the longitudinal DME is a function of the specimen mass and dimensions besides the fundamental frequency as follows:

$$DME = 5.093 \ \frac{L}{d^2} Mn^2$$

where,

DME = longitudinal dynamic modulus of elasticity (N/m^2)

L = specimen length (m)

d = specimen diameter (m)

M = specimen mass (kg)

n = fundamental longitudinal frequency (Hz)

To neutralize the effect of the change in mass on DME, relative dynamic modulus of elasticity (RDME) was calculated as the ratio between the squared fundamental longitudinal frequency and the squared initial fundamental longitudinal frequency. Using this procedure allows the values of RDME to represent only the change in soundness of

the specimens ignoring the effect of change of mass on the DME. Moreover, at the end of exposure, the specimens were tested to evaluate their splitting tensile strength (according to ASTM C496) and compared to the strength of cylinders with the same dimension kept in the standard curing tank and tested at the same time.

6.2.3 Water absorption

Since PSA is related to the absorption and capillarity of concrete (Bassuoni and Nehdi, 2009), the rate of absorption was evaluated for the six tested mixtures to explore the relationship between PSA and the capillary rise in concrete. The test was conducted according to ASTM C 1585 with modifications to the sample conditioning process to match the environmental cycles used during PSA testing. The test specimens were concrete discs of diameter 4" and height of 2". The discs were cut from standard 4"×8" cylinders cured in standard curing tank for 28 days. For each of the six tested mixtures, two disc specimens were cut from two different cylinders and prepared to be tested.

A modified conditioning process involved keeping the discs in an environmental chamber at temperature of $45 \pm 1°C$ and relative humidity equals to 15 ± 2 % which is similar to the hot/dry period of the PSA exposure cycle. The mass of the specimens were measured daily till the change in mass was less than 0.10% between two successive measurements (about 2 weeks). The testing procedures were then carried out according to ASTM standard. The specimens' sides were sealed using aluminum tape to prevent moisture loss during absorption of water through the bottom surface. Also, the top surfaces of the specimens were sealed with loosely attached plastic sheets as recommended by the ASTM standard. The initial mass of the specimens was then determined (including the

60

sides and top seals) to the nearest 0.01g and they were placed in a pan filled with tap water. The water level was kept at 1 to 3 mm above the bottom exposed surface during the eight days test duration. Figure 32 shows some of the specimens during the test procedure. During the test, the increase in mass of the specimens was monitored at specific times up to 8 days according to ASTM C1585. The absorption, I (mm), was calculated as the mass change in each specimen divided by the product of the cross section and the density of water. As specified by ASTM C1585, the absorption values were then plotted against the square root of the time in seconds.

Figure 32 Speciemns during absorption testing.

6.2.4 X-ray diffraction and SEM imaging

To analyze the reaction products and salt crystallization within the cementitious matrix, powder samples were taken from the surface of the PSA specimen at locations having the most severe damage (1" to 2" above the solution surface). Other samples were taken from the bottom of the specimens permanently submerged in the solution. These samples were ground to fine powder size (passing sieve no. 200) and they were used for XRD testing. Rietveld quantitative analysis was performed on the obtained XRD results to

61

quantitatively evaluate the percentages of the minerals detected in each sample. In this method, relative weight fractions for each crystalline phase in the tested sample can be calculated using scale factors of the respective calculated intensities of each crystal phase. With proper correction, performed using highly advanced computer software, the Rietveld method can give considerably accurate quantitative results (Liu and Kuo, 1996).

At the end of exposure and after the specimen were tested (splitting tensile test), concrete chunks were taken to be investigated using SEM. These chunks were selected to represent the cross section of the specimen starting from the outer surface to the center of the specimen. Two fractured samples were taken from each specimen, one representing the immersed portion of the specimen, while the other was selected from the portion above the solution. The surfaces of the samples were then carbon coated and examined using secondary electron imaging (SEI) technique. In addition, energy-dispersive X-ray spectroscopy (EDX) was also used during investigating the sample to recognize the chemical characterization of the identified crystals.

6.3 Results and Discussion

6.3.1 Visual inspection and mass loss

Specimens partially immersed in sodium solution were monitored for over 100 cycles (approximately 10 months) of exposure. Excessive efflorescence of salts was progressively deposited on the evaporation surfaces of the specimen especially during the hot/dry period of the exposure cycles. Figure 33, displaying the efflorescence on the surface of specimens at the end of the hot/dry ambient period, shows that the efflorescence accumulated to cover the whole specimen at the end of the period between

readings and efflorescence removal. During the exposure, considerably high rate of solution evaporation was observed even with tight lids that act as vapor barrier. This was observed through the rapid reduction of the solution level in the containers during the periods between specimen's inspection and solution top off as shown in Figure 33.
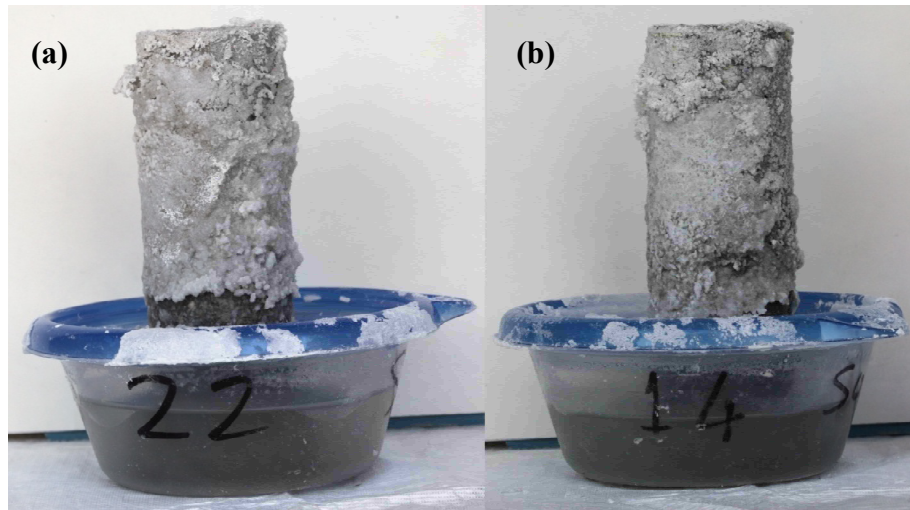
Figure 33 Effloresence in specimens (a) B-2 and (b) B-0.

Figures 34 through 39 show typical examples of the surface damage occurred in the tested specimens at different exposure ages. Inspection of the specimens after 112 cycles of exposure indicated remarkable visual deterioration on the surface of the specimens above the solution level. For all specimens, most of the scaling/flaking took place on the mid-third of the specimens (within approximately 2" above the solution). However, at the end of exposure, some signs of less severe deterioration could be detected at the immersed portions of the specimens. In specimens with severe damage, transverse or slightly inclined surface cracks could be noticed at the end of the exposure. However, these cracks did not seem to continue through the whole cross section as the specimens remained sound and rigid. The most severe scaling was observed in specimens from mixture A-0 from Group A and all of Group B specimen. Scaling started to be visually

www.manaraa.com

noticeable on the surface of some specimens after 8 to 16 cycles. In some specimens, the coarse aggregates became visible on the surface above the solution after around 20 cycles of exposure (for instance, see Figures 34, 37, and 39)

The average mass loss recorded over the exposure period for specimens from Groups A and B are shown in Figures 40 and 41, respectively. The figures indicate faster rate of mass loss in some mixtures (especially for Group B specimens) during the first 25 to 30 cycles, followed by lower rates after that. For instance, specimens B-0 experienced considerable mass loss during the first few cycles of exposure which may be attributed to the insufficient degree of hydration of the matrix at the beginning of exposure (28 days after mixing).

Generally, the mass loss values complied with the visual inspection the surface damage as the highest mass loss (approximately 11 to 12.35 g) were noticed in Group B specimens and mixture A-0 (12 g) having the most severe observed damage. For Group A specimens, Figure 40 indicates notable reduction in mass loss associated with increasing the dosage of nano-silica from 0 to 6%. On the other hand, for Group B mixtures (Figure 41), the effect of nano-silica addition was less significant in terms of mass loss reduction as the variation in mass loss values between the three mixtures was considerably low.
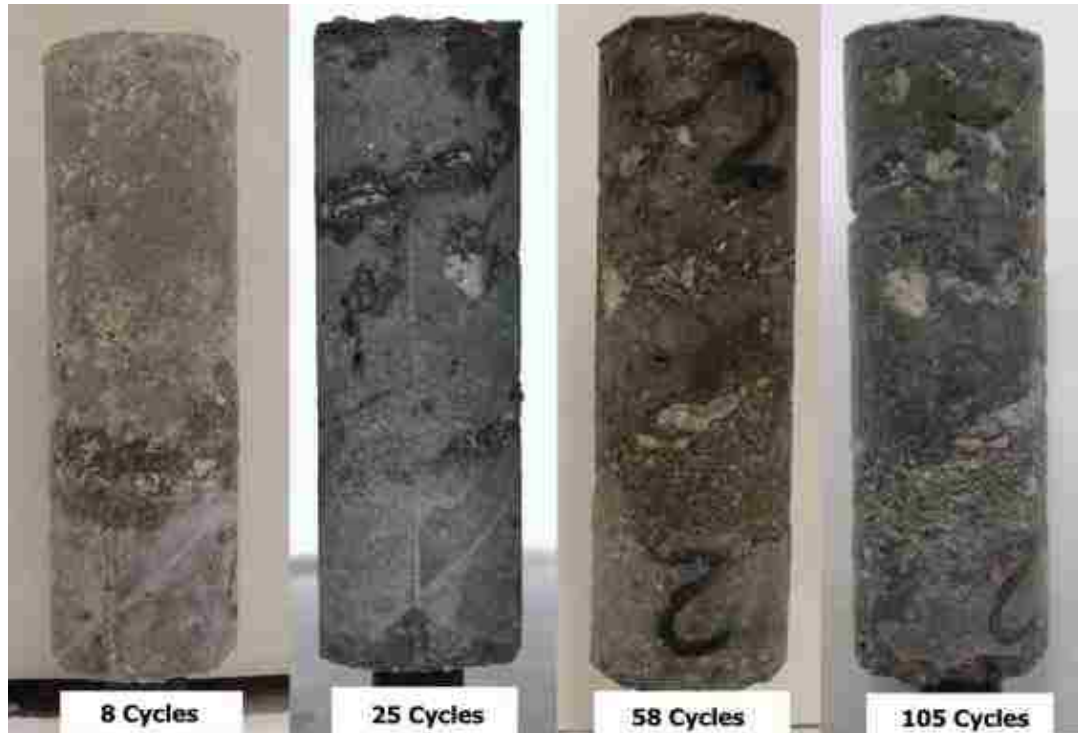
Figure 34 Damage in A-0 specimen at different ages of exposure.

Figure 35 Damage in A-1 specimen at different ages of exposure.

65

Figure 36 Damage in A-2 specimen at different ages of exposure.

Figure 37 Damage in B-0 specimen at different ages of exposure.

Figure 38 Damage in B-1 specimen at different ages of exposure.

Figure 39 Damage in B-2 specimen at different ages of exposure.
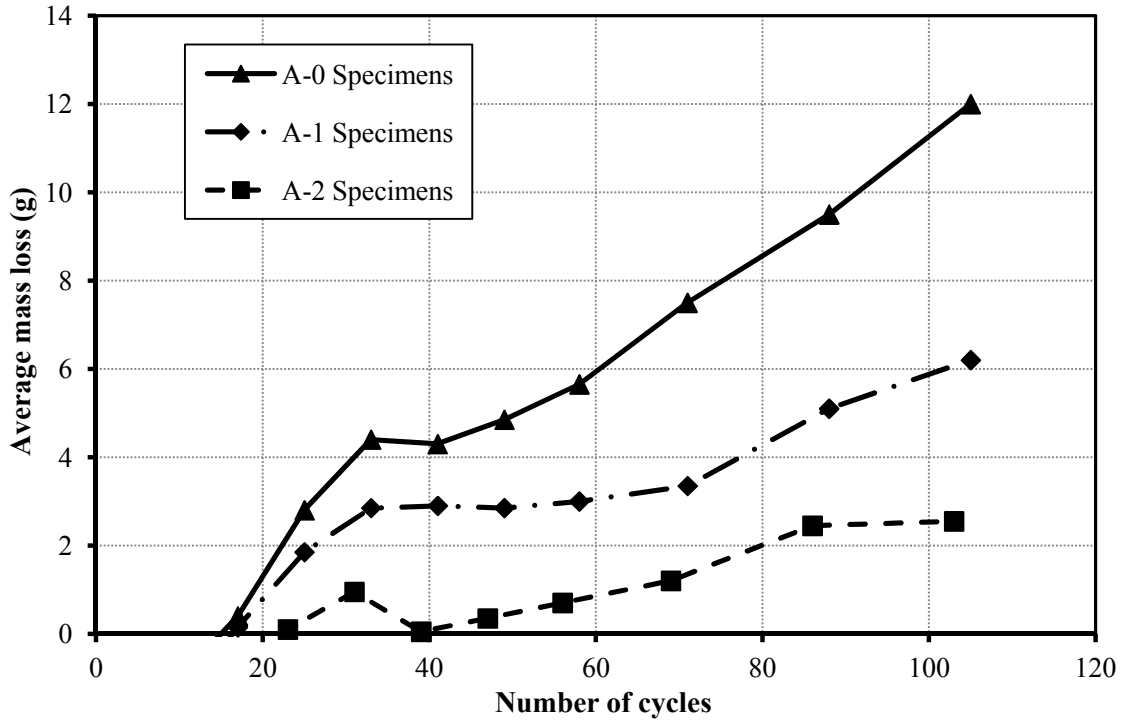
Figure 40 Average mass loss in Group A specimens partially immersed in sodium sulfate.
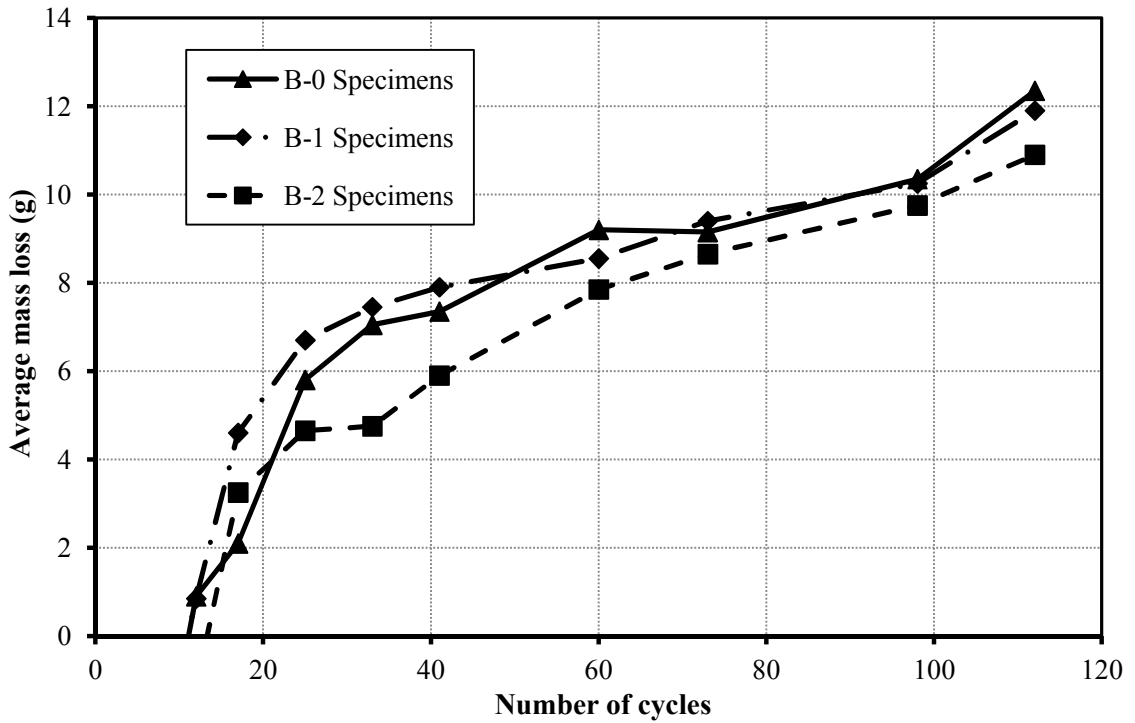
Figure 41 Average mass loss in Group B specimens partially immersed in sodium sulfate.

68

www.manaraa.com

In linking the damage caused by PSA to the pore structure of the cement matrix discussed in Chapter 5, the total cumulative mass loss at the end of exposure was compared to the different parameters determined by MIP testing (Table 9). This comparison indicates that the degree of damage caused by PSA expressed in terms of mass loss can be generally related to the total porosity of the specimens. For Group A mixtures, this trend is very clear as mixtures A-1 and A-2 having the lowest apparent total porosity (see Table 9) experienced the least visual damage and mass loss due to PSA. Moreover, for Group B specimens B-0, experiencing the highest cumulative mass loss (12.35 g), had the largest total porosity (12.56%). This could be attributed partially to slow microstructural development and hydration of this mixture during the initial few weeks of exposure, besides its pore microstructure and relatively low strength (compressive and tensile) compared to the remaining mixtures (Table 5 and Figures 8 and 9). Furthermore, BSEM micrograph (Figure 28a) illustrates the coarse microstructure and insufficient hydration of this mixture incorporating 30% Class F fly ash. However, mixtures B-1 and B-2 experienced considerably high mass loss due to PSA despite of their relatively low total porosity (9.3% and 8.21%, respectively). This may be explained by the excessive pore size refinement as these mixtures had the largest percentage of micro-pores (less than 0.1 µm in diameter). This large proportion of micro-pores was vulnerable to considerable damage by crystallization pressure.

The relationships between the cumulative mass loss at the end of exposure and different pore structure parameters (Table 9) were plotted for the six mixtures tested. Figures 42 and 43 show the total mass loss versus the apparent total porosity and threshold pore diameter, respectively. Micro-porosity was calculated as the product of the total porosity

and the proportion of micro-pores (less than 0.1 μm in diameter) and plotted against the total mass loss (Figure 44). An exponential relationship may be recognized as a general trend for the three previously described relationships with different correlation factors.

Figure 44 may emphasize the combined effect of total porosity and pore size on the damage caused by PSA. For instance, mixtures A-1 and A-2 experienced the lowest mass loss for all the tested mixtures although they had relatively high percentage of micro-pores (75% and72%). However, taking into account their micro-porosity percentages (4.98% and 4.65%), they are considered as the lowest which conforms with the mass loss results. Moreover, mixture B-0 having the highest micro-porosity percentage (9.22%) experienced the highest level of damage in terms of mass loss.
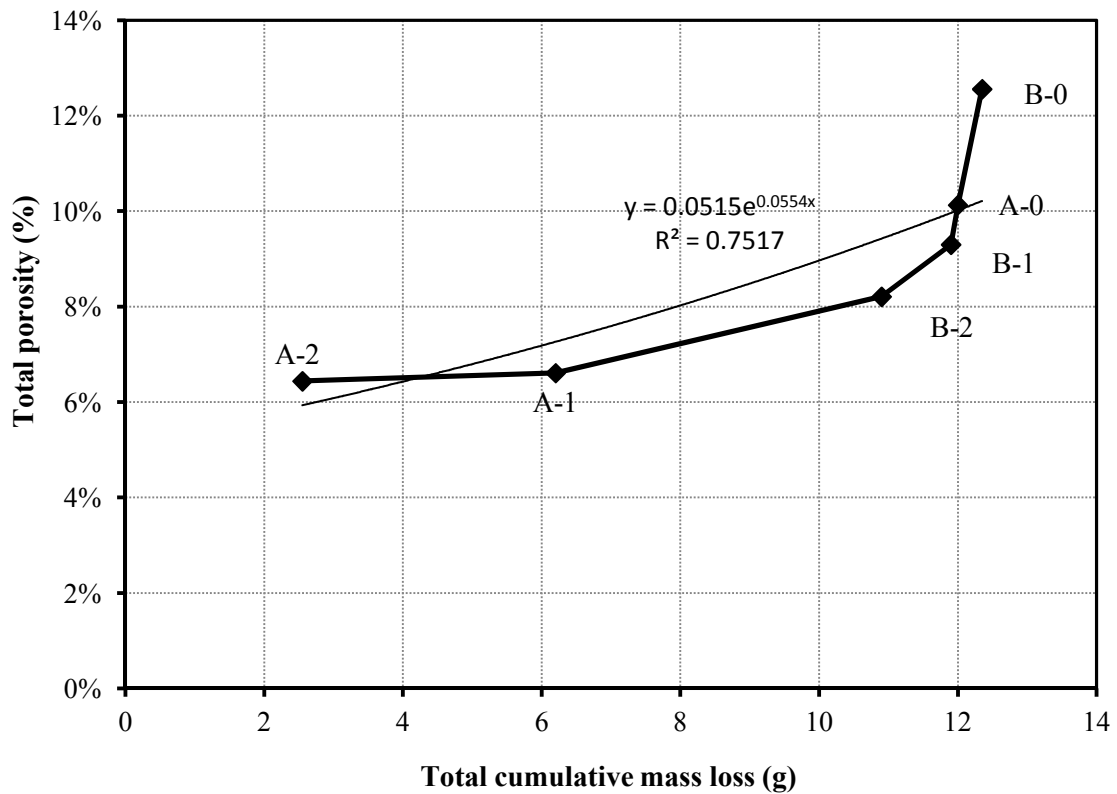
Figure 42 Relationship between total porosity and mass loss caused by PSA.
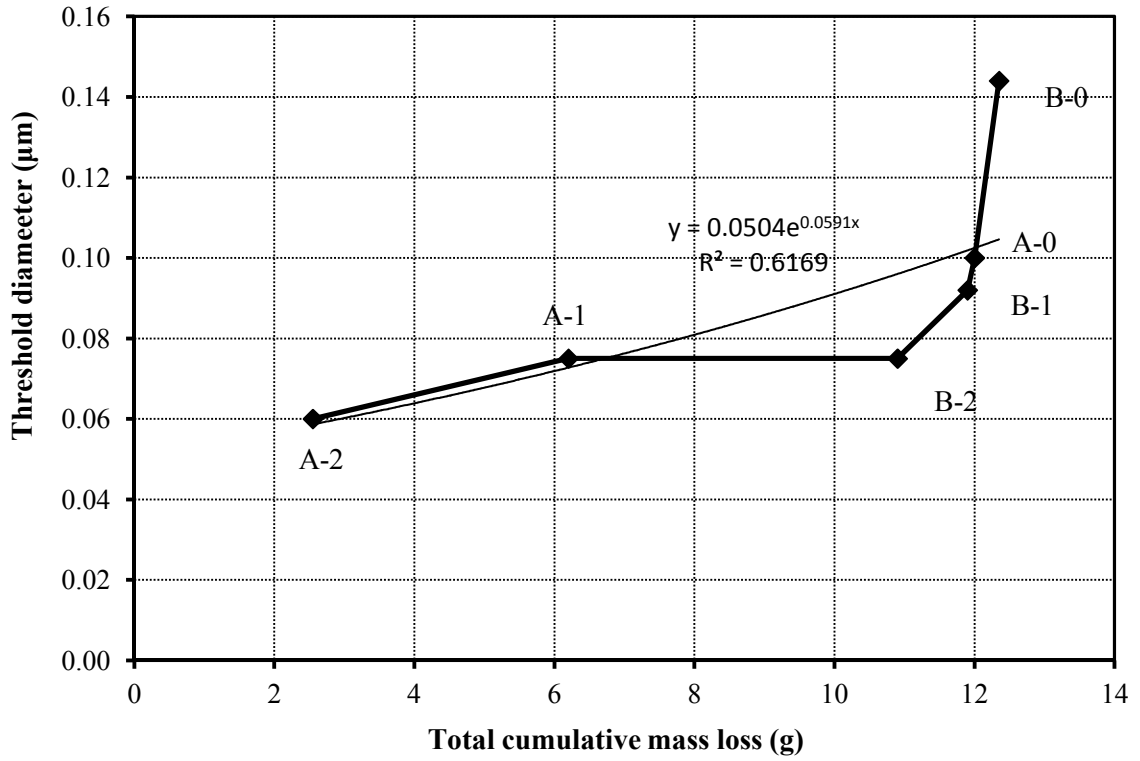
Figure 43 Relationship between threshold diameter and mass loss caused by PSA.
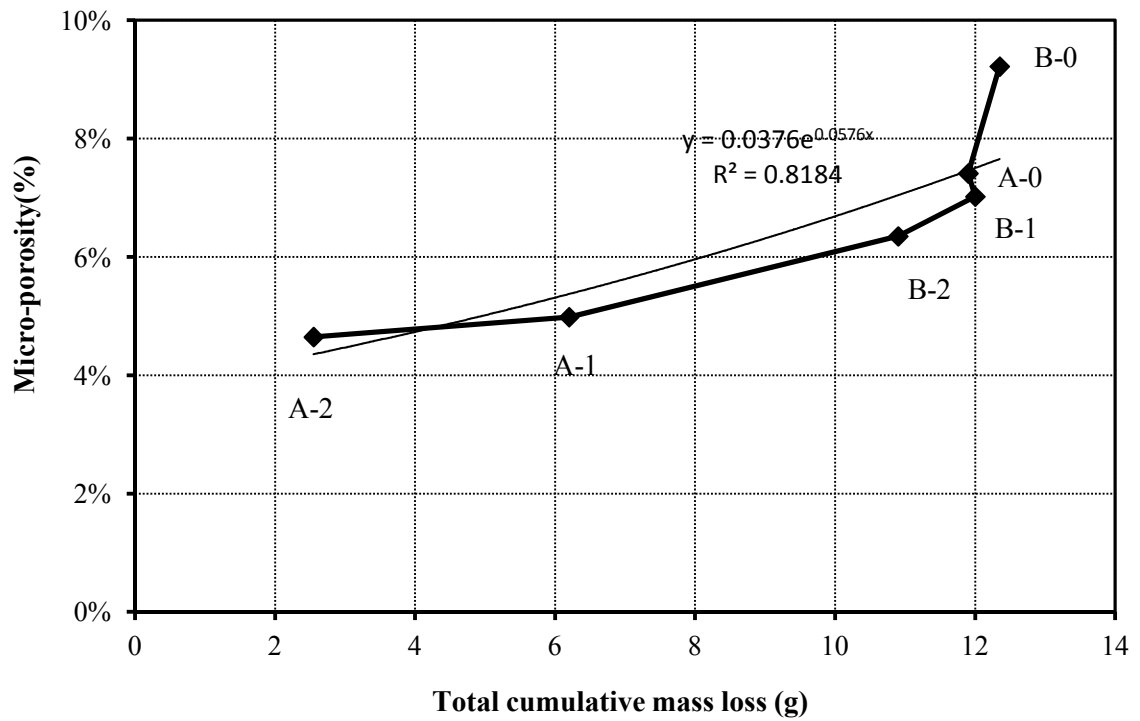
Figure 44 Relationship between micro-porosity and mass loss caused by PSA.

71

6.3.2 Absorption test results

The absorption values (I) were calculated, as previously described, and plotted against the square root of time in seconds for Groups A and B as shown in Figures 45 and 46, respectively. The initial and secondary rates of water absorption (mm/sec$^{1/2}$) were then evaluated as defined by the ASTM standard. The initial rate is determined as the slope of the best fitting line for the previously described plot during the first 6 hours of testing, while the secondary rate is the slope of the line that best fit the data points between 1-8 days. Table 10 presents the calculated rates of absorption for each of the tested mixtures, considering that all the correlation coefficients for the best fitting lines were more than 0.98 as specified by ASTM C1585.

Table 10 Absorption rates for the tested mixtures.

Mixture	Initial absorption rate (mm/sec$^{1/2}$)	Secondary absorption rate (mm/sec$^{1/2}$)
A-0	0.0069	0.0013
A-1	0.0066	0.0008
A-2	0.0047	0.0006
B-0	0.0072	0.0006
B-1	0.0067	0.0009
B-2	0.0071	0.0007

Generally, the absorption test results indicate that the addition of nano-silica resulted in a reduction of the rates of absorption as well as the total absorption, especially for Group A mixtures. This may be attributed to the refinement of the pore structure and the reduction of the total porosity associated with nano-silica addition as described in Chapter 5 (see Figure 24 and Table 9). Although this reduction in pore diameter should lead to higher capillary action and consequently more absorption, these results indicate that the pore

72

refinement was associated with reduction in capillary pores continuity and concrete penetrability. This observation may also be confirmed by the results of RCPT testing presented in Chapter 4 (Table 7) which indicates significant reduction of permeability for concrete incorporating nano-silica.

Figure 47 shows the relationship of the total absorption against the cumulative mass loses at the end of PSA exposure for the six tested mixtures. Generally, linear trends can be observed for both of the tested groups. For instance, for Groups A and B mixtures, the mass loss values at the end of exposure correlated to the total absorption with coefficient of correlation exceeding 0.99 and 0.94, respectively. These correlations indicate that the increase of absorbed solution during PSA exposure led to larger amounts of salt subflorescence which caused more damage at the specimens' surface above the solution for each of the studied groups of mixtures. Moreover, the relationship between the total mass loss caused by PSA and the initial and secondary absorption rates were also examined as shown in Figures 48 and 49, respectively. Realizing that the secondary absorption rate represents the relatively long term absorption behavior, it should be expected that this values should be related to the PSA damage. For Group A mixtures, the secondary absorption rates strongly correlate to the total mass loss (coefficient of correlation of 0.99). The initial absorption rates follow the same nearly linear trend, but at a lower correlation coefficient (0.86). Nevertheless, this correlation did not apply for Group B specimens as no obvious linear trend could be observed for those mixtures.
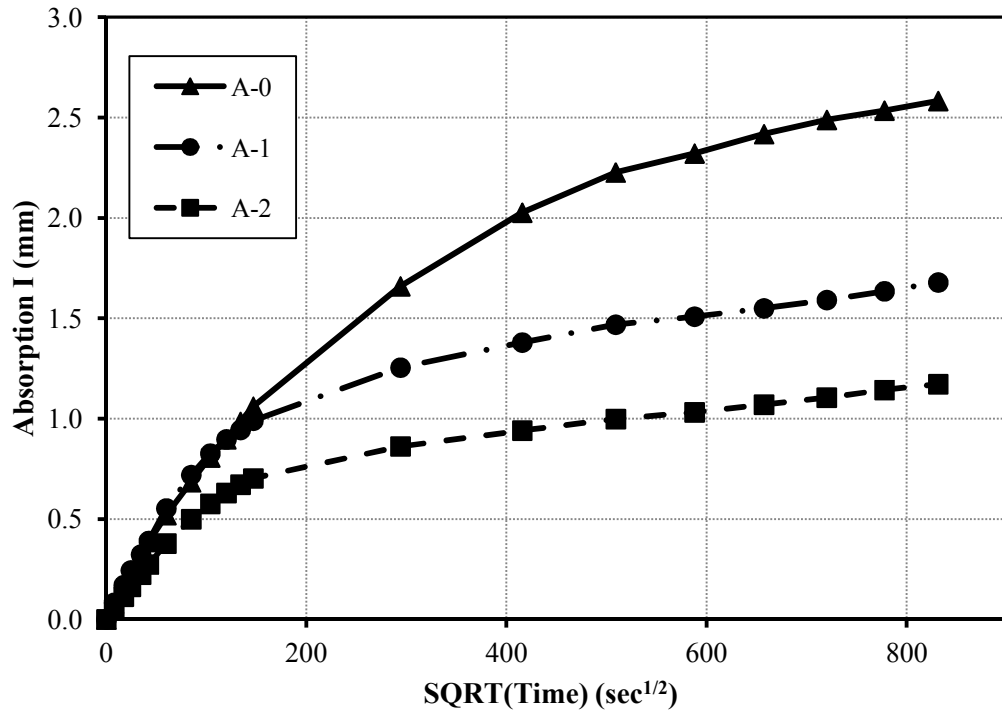
Figure 45 Absorption-time relationships for Group A specimens.
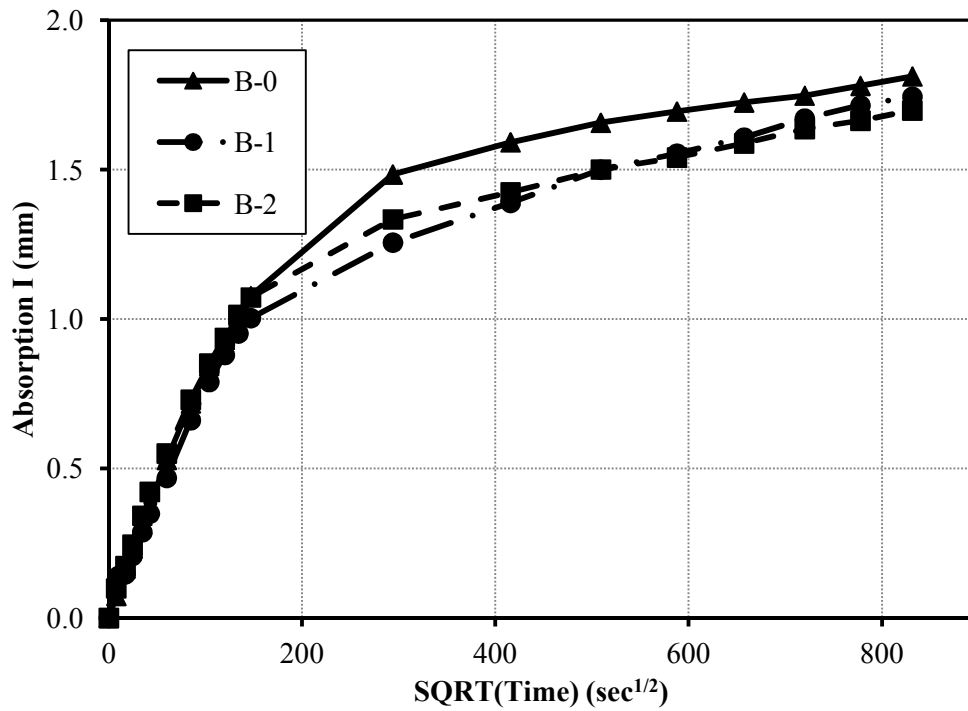
Figure 46 Absorption-time relationships for Group B specimens.

74

The previously presented results reveals that results of the water absorption test may be used to assess the concrete resistance to PSA. Results indicated notable correlation between the different absorption parameters and the surface damage caused by PSA measured in terms of mass loss. However, the significance of these correlations may be extensively binder dependent. Furthermore, comparing absorptions results of mixtures incorporating different types of binders should be performed with caution. For specimens including portland cement as a single binder (Group A), the damage caused by PSA was linearly related to the absorption parameters especially the total absorption and the secondary absorption rate. On the other hand, these relations were less significant for specimens including binary binder as cement and fly ash (Group B). This may attributed to the relatively coarse microstructure of these mixtures as well as the different transport properties of these mixtures which significantly affect the water absorption results for them. These observations may suggest that the absorption test can be a preliminary indication of concrete resistance to PSA. Compared to the duration and procedures of the PSA exposure testing, absorption testing can be a rapid, simple and reliable alternative that can be performed with limited technical skills and resources. However, the exact correlation between the two testing approaches as well as MIP testing should be further investigated and verified with additional statistical data and for different binders and exposures.
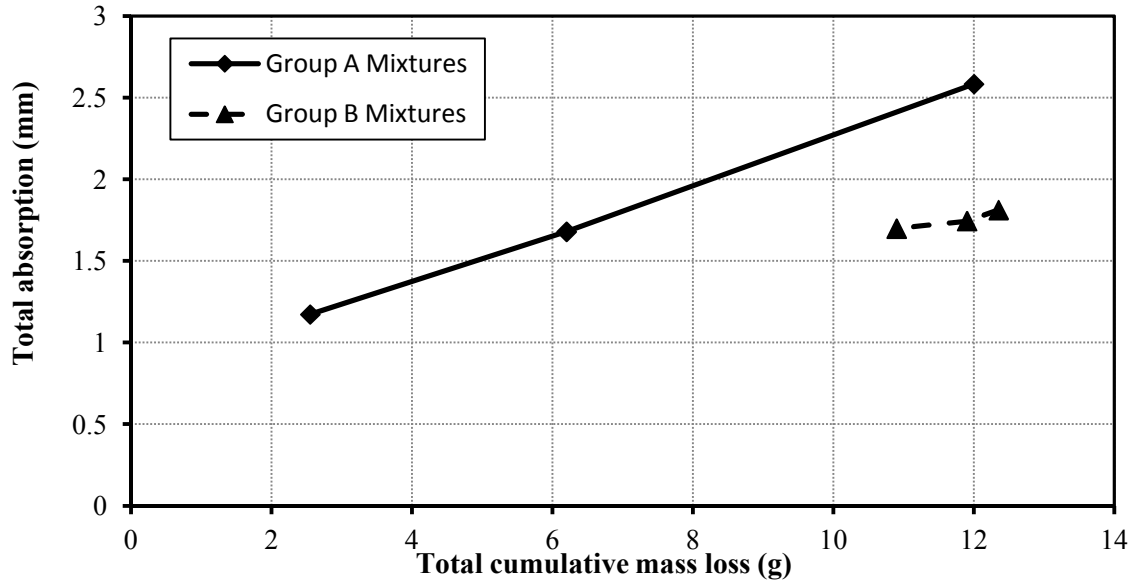
Figure 47 Total absorption related to the total mass loss due to PSA.
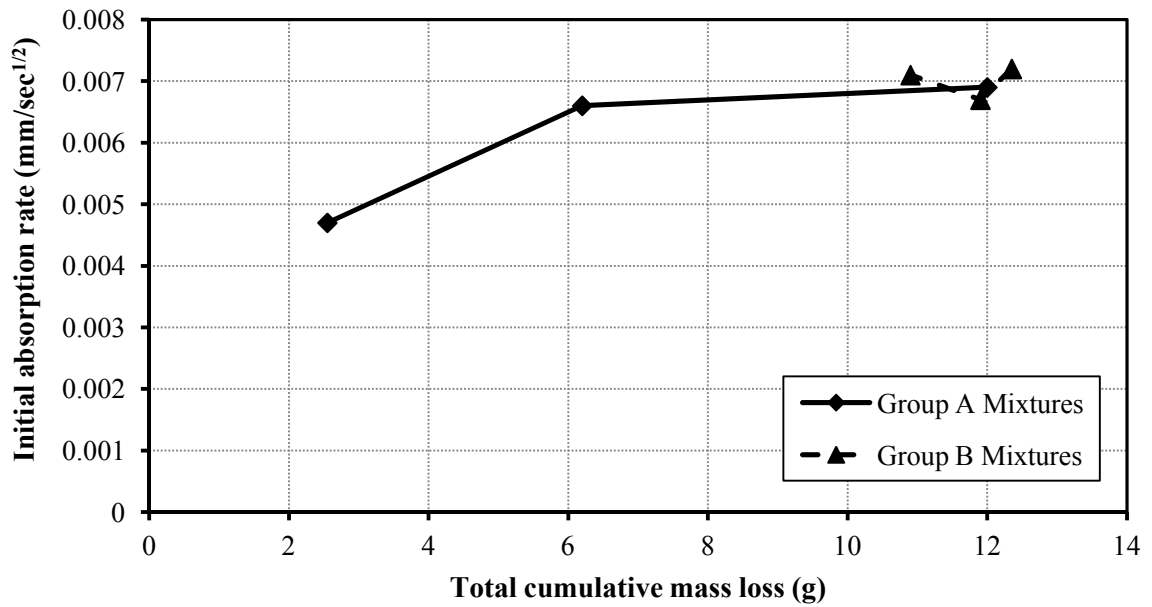
Figure 48 Initial absorption rate versus the total mass loss due to PSA.

76
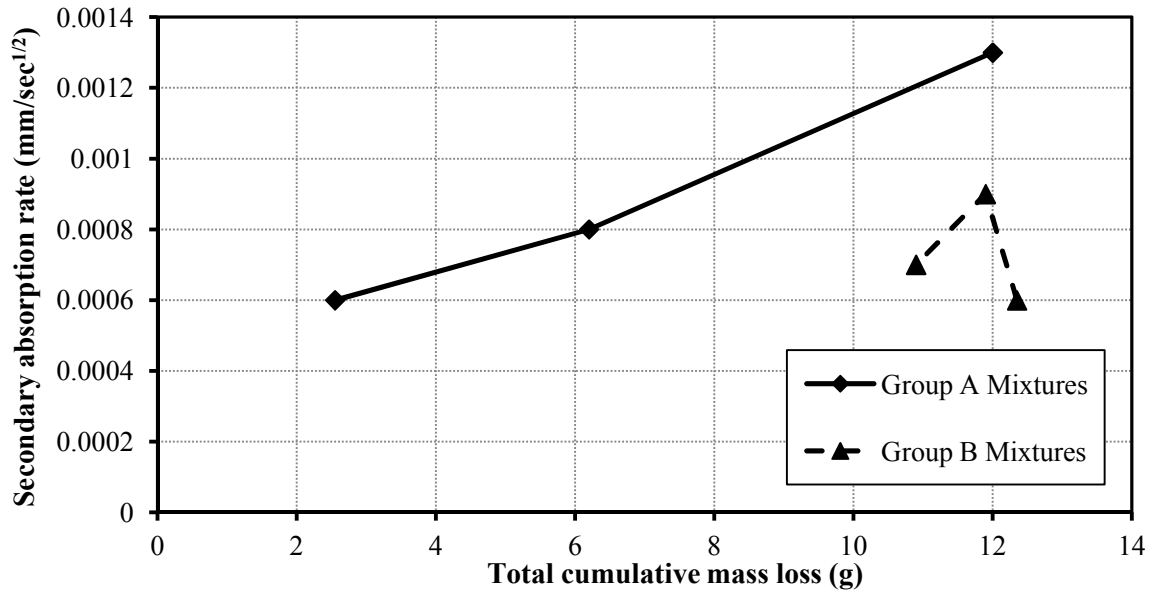
Figure 49 Secondary absorption rate versus the total mass loss due to PSA.

6.3.3 DME and tensile strength

Since the trends of RDME indicate the change in internal conditions of concrete specimens and the presence of cracking, the change in the DME was monitored during the exposure period. The initial DME (shown in Table 11) was measured for each specimen after 28 days of standard curing followed by 48 hours of air drying. The RDME was calculated over the testing period as previously described for Groups A and B as shown in Figures 50 and 51, respectively. For Group A specimens, most of the drop in RDME took place within the first 50 cycles of exposure, then almost constant values of DME were measured for the three mixtures. Conversely, rapid drop in RDME can be observed in Group B specimens within the first 25 cycles, followed by almost constant values afterward. The initial drop may be attributed partially to the change in moisture content in the specimen, knowing that the initial reading of DME was measured at air dry conditions as previously described. However, relating these drops to the initial rapid mass

77

loss (see Figures 40 and 41) may provide an interpretation of the trend and rate of damage caused by PSA. Combining the observations of the rates of damage in terms of mass loss and reduction of RDME, almost similar trends may be seen during the early period of the exposure. These results confirm that the faster rate of damage occurred during the first few cycles most likely due to the significantly higher rates of initial absorption for all the mixtures (see Table 10). Subsequently, the saturation level of the specimens reached steady conditions in which secondary rates of absorption were controlling the damage speed. Despite the severe scaling observed at the surface of some specimens, the change in RDME was not very significant in any of the tested specimens.

Generally, for all the specimens, the final values of RDME at the end of exposure were almost constant (around 60%) regardless the trend they followed during the exposure. These results indicate that the damage observed in the specimens as well as the mass loss had occurred mainly on the specimen's surface without extensive cracking or distress in the core of the specimen.

The splitting tensile strength was evaluated for the tested specimens at the end of exposure (112 cycles) as well as the strength of similar specimens which were kept in the standard curing tank during the exposure period. The relative tensile strength was calculated for each mixture as the mean strength of the specimen subjected to PSA attack divided by the mean strength of the specimens in the curing tank. Table 11 presents the calculated values of the relative tensile strength for the six mixtures after exposure. For all the mixtures, the strength of the specimens subjected to PSA exposure was lower than it for normally cured concrete. However, the values of the relative tensile strength had limited variation between the tested mixtures (ranged between 69% and 85%) which

78

contradicts with the observed damage and mass loss. Moreover, it is noteworthy that the excessive surface damage occurred on most of the specimen may led to stress concentration during the splitting tensile testing due to uneven surface. This may explain the irregularities between the relative tensile strength and the mass loss results.
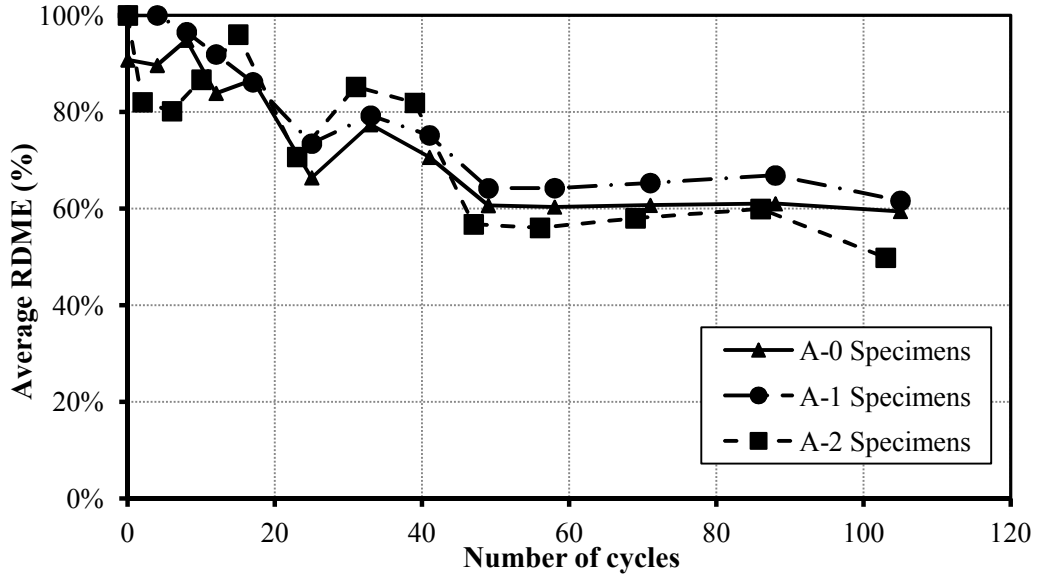
Figure 50 Average RDME for Group A specimens partially immersed in sodium sulfate.
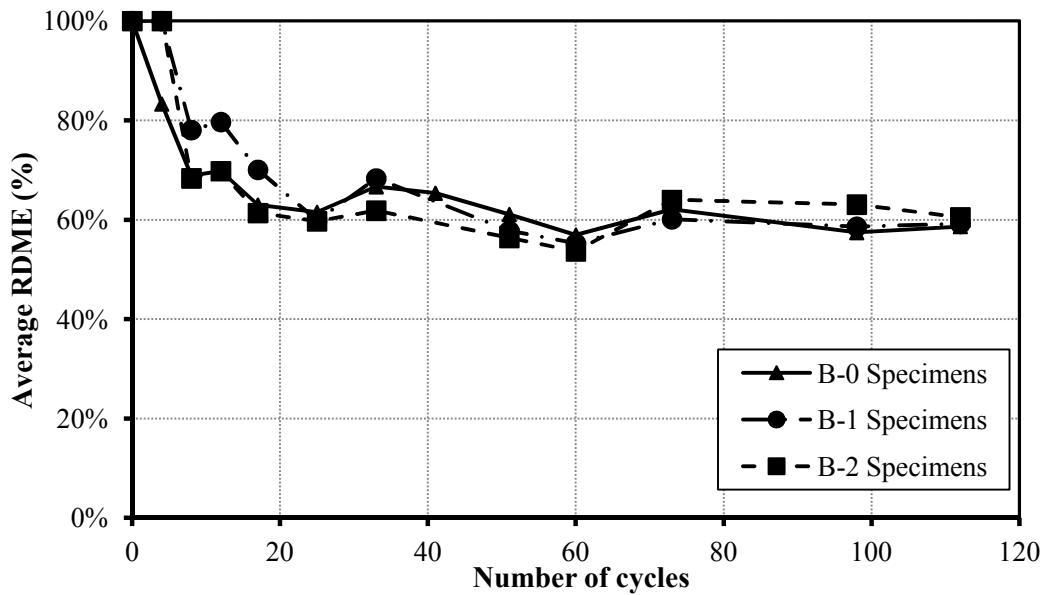
Figure 51 Average RDME for Group B specimens partially immersed in sodium sulfate.

79

Table 11 Initial DME and tensile strengths.

Mixture	Initial DME (GPa)	Splitting tensile strength at the end of exposure - standard curing conditions (psi)	Relative splitting tensile strength of specimens exposed to PSA (%)
A-0	8.85	1432	85.1%
A-1	10.51	1422	84.0%
A-2	13.21	1394	74.0%
B-0	6.60	1673	79.1%
B-1	8.41	1737	85.5%
B-2	10.38	1684	68.9%

6.3.4 XRD and SEM

XRD analysis was conducted on powder samples taken from the location having the most severe damage which was above the solution level and from the continuously immersed portions of the specimens. All the XRD diffractograms for the tested samples along with the Rietveld analysis are presented in the appendix. The summary of the Rietveld quantitative analysis of the XRD results are shown in Table 12. The predominant minerals recognized in the samples include minerals likely to exist as part of the aggregates (i.e. dolomite, calcite and quartz) or other minerals normally present in cement matrix as portlandite. Moreover, for all the samples, thenardite (anhydrous form of sodium sulfate) existed in different amounts. No traces of mirabilite (hydrous form of sodium sulfate) were identified in any of the samples. This was mainly because XRD

80

powder samples were taken from the portion of the specimens above the solution after the hot/dry period. Additionally, for the immersed samples, the time interval between extraction and preparation of the powder samples to the time of testing was sufficient to transform the salt to the anhydrous form in the lab ambient conditions (see Figure 29).

Table 12 Rietveld quantitative XRD analysis results for the tested specimens.

Mixture	Sample Location	Thenardite	Dolomite	Calcite	Quartz Low	Portlandite	Gypsum	Ettringite
A-0	Above Solution	7.26%	71.17%	12.56%	2.40%	3.28%	1.88%	1.42%
	Immersed in Solution	3.96%	72.30%	14.13%	2.91%	1.77%	1.54%	1.87%
A-1	Above Solution	9.02%	70.00%	14.59%	2.33%	2.08%	1.14%	0.85%
	Immersed in Solution	3.44%	73.12%	10.98%	3.64%	1.55%	3.34%	1.71%
A-2	Above Solution	16.03%	71.58%	5.20%	3.79%	0.82%	0.44%	0.24%
	Immersed in Solution	6.71%	66.87%	19.11%	3.08%	1.12%	1.12%	0.68%
B-0	Above Solution	8.85%	74.74%	8.31%	5.00%	0.91%	0.67%	1.51%
	Immersed in Solution	3.37%	69.27%	17.75%	3.96%	2.02%	1.78%	1.83%
B-1	Above Solution	15.39%	70.80%	8.44%	2.99%	1.00%	0.42%	0.95%
	Immersed in Solution	3.94%	80.61%	10.29%	3.32%	0.38%	0.83%	0.63%
B-2	Above Solution	23.38%	65.32%	7.45%	2.61%	0.52%	0.23%	0.48%
	Immersed in Solution	2.02%	77.09%	13.94%	5.18%	0.23%	0.90%	0.64%

XRD results indicated the presence of traces of other minerals including gypsum and ettringite which are usually generated as products of chemical sulfate attack to cement

81

matrix. However, the percentages of these minerals ranged between 0.23% and 3.34% by mass for all the samples either for those taken from the dry or the immersed portions of the specimen. These amounts were insufficient to be considered as a major cause of the observed distress. In addition, no trend could be detected that linked these amounts to the level of damage observed in the tested specimens. For instance, the maximum percentage of gypsum (3.34%) was detected in the immersed portion of specimen A-1 which experienced relatively low levels of mass loss (see Figure 40). Conversely, specimens B-2 containing the lowest percentage of gypsum above the solution level (0.23%) experienced significant damage as indicated by visual inspection and mass loss (see Figures 38 and 41).

As a general observation, significantly large amounts of thenardite existed in the samples taken from the dry portion of the specimens compared to the quantities identified in the immersed portions. For instance, sample taken from the dry potion of specimen B-2 included more than 10 times the percentage existed in the immersed sample of the same specimen. This observation emphasizes the effect of the repeated cycles of dry and wet ambient conditions as salt accumulates inside the pores close to the evaporation surface during the hot/dry period of the exposure cycle. In turn, this crystals accumulation caused a pressure build up inside the pores as cycles progressed. On the other hand, the concentrations of the salt in samples from the immersed portions were significantly lower than the dry portion for all the specimens. Generally, the quantities of salt in pores of the immersed portion are primarily governed by the solution concentration which was replaced periodically. This also may be confirmed by the approximately similar amounts of salt in the immersed portion of all the six mixtures.

Comparing the percentages of thenardite detected in the dry portions of the tested samples to the porosity parameters (Table 9), it is remarkable that larger amounts of thenardite could be found in specimens with finer pore structure (i.e. larger percentage of small pores). For instance, mixture B-1 and B-2 having the finest pore structure of the six mixtures included the highest percentages of thenardite in the dry portion of the specimen. This may highlight the effect of capillary action which increases with the pore refinement providing faster supply of solution through the immersed portion of the specimen. This conforms also to the excessive mass loss in specimens with the extra fine pore structure (B-1 and B-2), However, specimens A-1 and A-2 had relatively low levels of damage despite of the high salt concentrations which is attributed to their low total porosity as described earlier.

Fractured samples taken from the tested specimens from different locations at the end of exposure were tested using SEM-SEI, while the chemical composition of the crystals was detected using EDX technique. Samples taken from the both immersed and dry portions of specimens were carefully examined starting from the outer surface towards the center of the specimen. Crystals of thenardite, gypsum, and ettringite could be detected in most of the samples, especially in the regions closer to the surface of the specimen (around 15 mm from the surface). Figures 52 through 56 show typical micrographs and EDX spectra for samples taken from different locations of the tested specimens at the end of exposure.

Figure 52 SEM micrograph and EDX spectrum for sample taken from above the solution in specimen A-2: a) 500X magnification micrograph, and b) EDX spectrum for thenardite.

Figure 53 SEM micrographs and EDX spectra for a sample taken from the immersed portion of specimen A-2: a) 1000X magnification mirograph, b) 2000X magnification mirograph, c) EDX specturm for ettringite, and d) EDX specturm for thenardite.

84

For all of specimen, larger and denser crystals of thenardite could be detected in the samples taken from the dry portion of the specimens (above solution) which conforms with the findings of the XRD analysis (Table 12). These crystals could be seen usually accumulated with various sizes and shapes around air voids and fissures. For instance, Figure 52 shows different sizes of thenardite crystals in a sample taken from the dry portion of specimen A-2. Moreover, Figure 54 displays large amounts of thenardite crystals accumulated around an air void which may act as a pressure relief space for crystals generated inside small pores. This observation conforms to the significant damage observed in specimens of B-2 in terms of scaling and mass loss and gives an idea about the deleterious effect of this crystallization inside large percentage of micro-pores detected in B-2 (see Table 9). On the other hand, less thenardite crystals could be observed in samples taken from the immersed portions, besides that these crystals were accumulated as seen in dry portions. For example, less dense thenardite crystals can be seen in Figures 53 and 56 showing samples taken from immersed portions of specimen A-2 and B-2, respectively. This also confirms the lower quantities of thenardite identified using XRD analysis (Table 12) for samples taken from immersed portions.

Ettringite needle-shaped crystals were identified in samples taken from the immersed portions of the specimens particularly around large pores and air voids as shown in Figures 53 and 55. Also, ettringite was observed incidentally in samples taken from thy drying portions of specimens (see Figure 54). However, concentrations and sizes of these crystals does not appear to be a potential cause of damage since these crystals did not fill the air voids as may usually be observed in case of chemical sulfate attack on cement matrix (Brown and Hooton, 2002). For instance, Figure 53 showing a large air void in a

85

sample taken from the immersed potion of specimen A-2 indicates the formation of ettringite crystals on the wall of the void although these crystals are relatively small and scattered. Furthermore, similar observation may be seen in Figure 55 which shows a sample taken from the immersed potion of specimens A-0. Gypsum crystals were also detected in some of the immersed samples less frequently (see Figure 56).
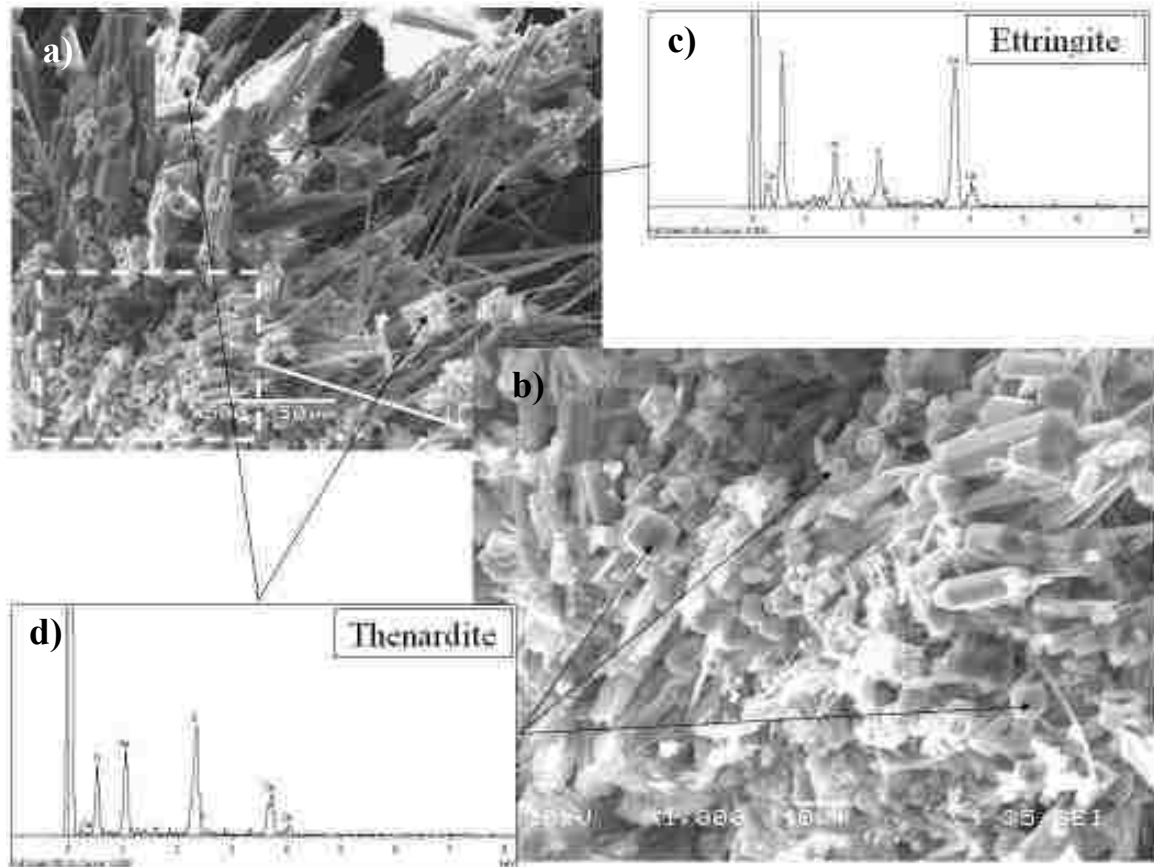
Figure 54 SEM micrographs and EDX spectrumfor a sample taken from above the solution in specimen B-2: a) 500X magnification micrograph, b) 1000X magnification micrograph, c) EDX spectrum for ettringite, and d) EDX spectrum for thenardite.

Evidences obtained from SEM along with XRD analysis confirms that crystallization of sodium sulfate is the main cause of deterioration observed in the tested specimens. This evidence also proves that chemical attack of sodium sulfate had a minor/insignificant role

in the damage observed in the tested specimens. This also conforms to the visual inspection of the specimens (Figures 34 through 39) which indicate no or inconsiderable damage at the immersed portions of the specimens although these parts are more vulnerable to the chemical attack.
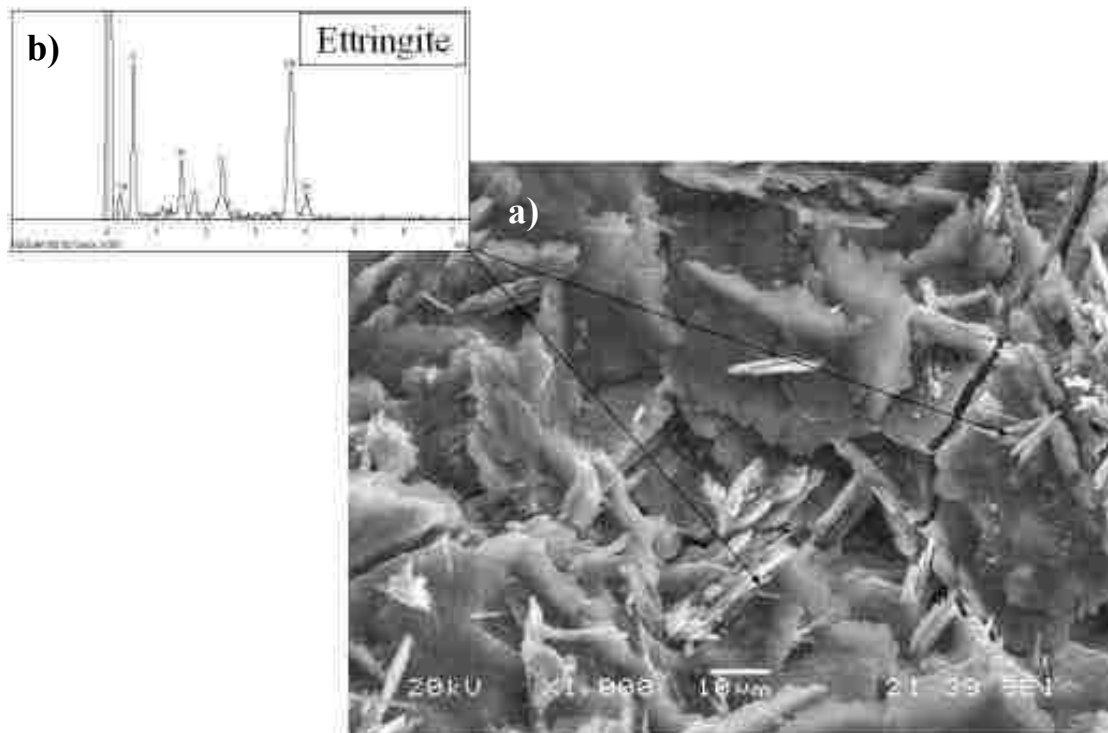
Figure 55 SEM micrograph and EDX spectrum for a sample taken from the immersed portion of specimen A-0: a) 1000X magnification mirograph, and b) EDX specturm for ettringite
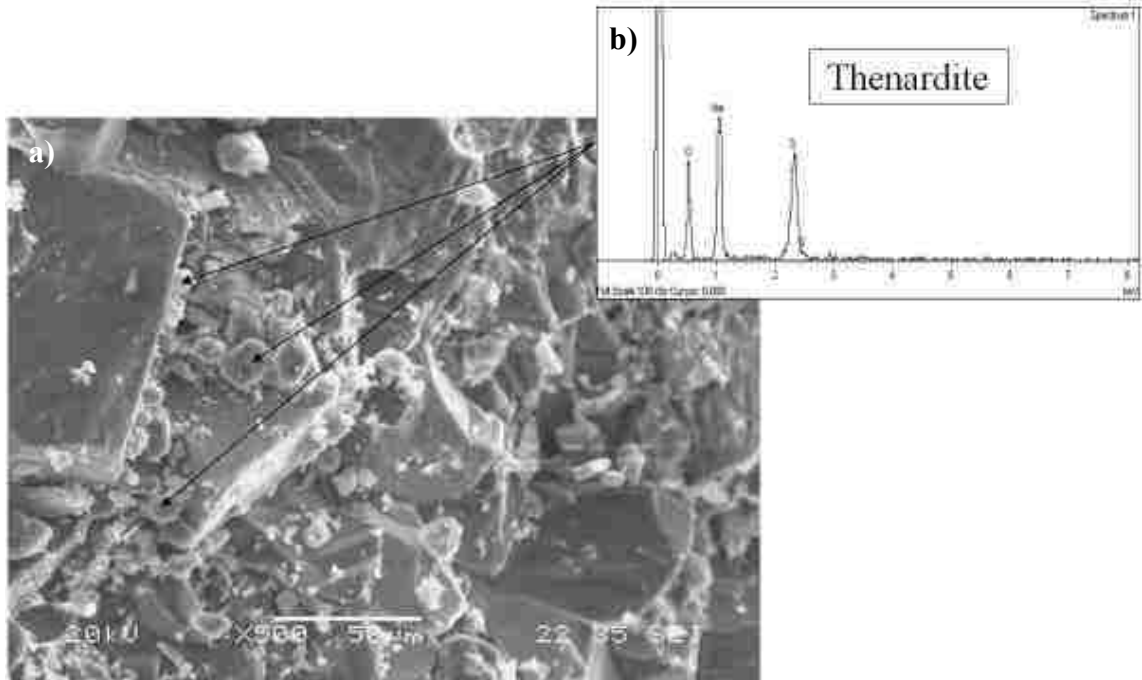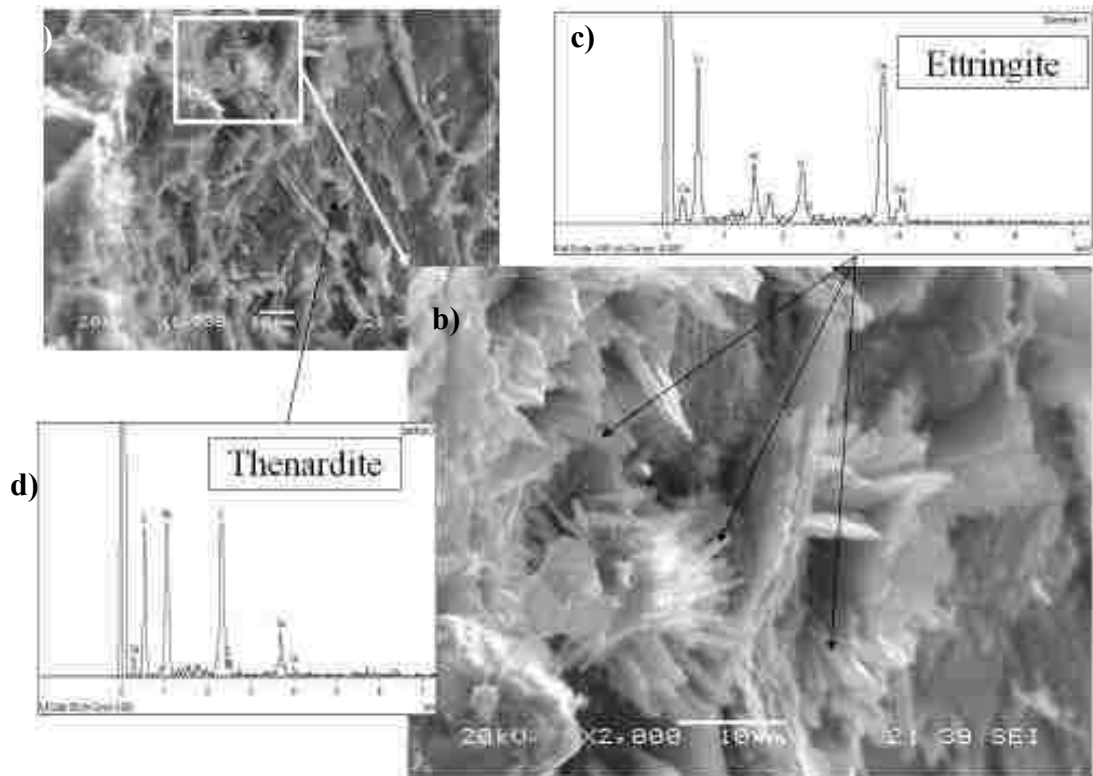
Figure 56 SEM micrograph and EDX spectra for a sample taken from the immersed portion of specimen B-2: a) 2000X magnification micrograph, b)EDX spectum for gypsum.

Chapter 7: Alkali-Silica Reaction

7.1 Introduction and Background

Unlike natural rocks, concrete is an alkaline material due to the presence of different hydroxides created during the hydration reaction of cement. This very alkaline medium promotes reactions between components of certain types of aggregates and cement hydration products. Generally, three main types of alkali-aggregate reactions (ARR) are believed to cause concrete cracking and deterioration. These reactions are known as (i) alkali-silicate, (ii) alkali-carbonate and (iii) alkali-silica reactions (Hobbs, 1988).

AAR, first observed in the United States during the 1920s, became a major focus of attention in terms of public awareness and research efforts since the 1970s, in various parts of the world. In the United States, Federal Highway Administration (FHWA) reported that different severity levels and types of this reaction were evident in 35 states (FHWA-RD-03-047, 2003). For the State of Nevada, cracking caused by AAR was identified in the Hoover dam, the world's largest concrete structure, located on the Colorado River (Hobbs, 1988). In addition, experimental studies showed that types of Nevada opal were found to be reactive (Wang and Gillott, 1993).

Alkali-silica reaction (ASR), which is considered to be the most common form of AAR, involves reactions between alkaline solutions in concrete pores and some forms of silica present in certain types of aggregates such as those found in volcanic glasses, tridymite, cristobalite, and opal (Hobbs 1988). This reaction is associated with the formation of expansive alkali-silica gel. In the presence of sufficient moisture, this gel expands within

89

pores and microcracks in concrete. This expansion develops swelling pressure which causes deterioration and even failure in severe cases. The extent of reaction and the rate of deterioration in concrete structures are affected mainly by three major factors; (i) concrete constituents (aggregates and cementitious materials), (ii) amount of moisture available, and (iii) temperature. Typically, cracks on concrete affected by ASR can be visualized after 5-15 years of construction but the reaction may progress continuously or intermittently for several decades (Blight and Alexander, 2011). It was found that the alkali-reactive aggregates are widespread in the United States, Eastern Canada, Australia and several countries in Europe and South Africa (Mehta and Monteiro, 2006).

Concerning long term performance, ASR can influence the strength, stiffness and durability of concrete structures. Mainly concrete pavements, bridges and parking garages are significantly affected by ASR as they are exposed to high moisture along with high temperatures in different seasons. Experimental studies performed on concrete members made with ASR reactive aggregates showed significant declination of mechanical behavior after various time periods and types of exposure (Swamy and Al-Asali, 1989, Fan and Hanson, 1998). Usually, the cracks generated by ASR can be identified by its random orientation with no preferred direction of strongest crack development (AASHTO SHRP C-315, 1991). Furthermore, in some cases, white staining caused by the leaching of silica gel out of these crack can be an evidence of the presence of ASR. This silica gel can also appear as whitish powder covering the crack surfaces during the prolonged dry seasons. A crack pattern associated with the development of ASR in highway pavement is commonly known as map-cracking or pattern-cracking which tends to be parallel to the direction of traffic.

Silica (SiO$_2$), which is the main component of the Earth's crust (Iler, 1979), exists in almost all types of aggregates. In addition, it exists at different ratios in cement and supplementary cementitious materials (SCMs) such as silica fume and fly ash. However, the presence of silica is not the key factor which activate the ASR but the form in which the silica exists in the aggregate. Typically, non-crystalline (amorphous) forms of silica present in some aggregates are the main reactive form of silica. Pessimum, which represents the maximum expansion caused by ASR, can occur with certain combinations of reactive silica in aggregate and specific types and content of cementitious materials. This combination should be studied carefully for each type of aggregate and/or supplementary cementitious materials in order to avoid ASR during concrete mixture design and proportioning.

Silica fume (micro-silica) has been widely investigated in terms of ASR mitigation. Generally, silica fume significantly reduces the expansions caused by ASR. Additionally, the alkalinity and of the pore solution is reduced in mortars incorporating silica fumes (Aquino et al., 2001; Rasheeduzzafar and Hussain, 1991; Canham et al., 1987: Thomas et al., 1999). However, other studies indicated that using silica fume in the granulated form may generate more expansive gel increasing the mortar-bar expansion (Pettersson, 1992).

For over 50 years, Class F fly ash has been effectively used for controlling the damage caused by ASR (Thomas et al., 2012). Fly ash, as a byproduct of coal consumption, is more environmentally friendly compared to cement (Haque et al., 1984). For the ASR mitigation efficiency, economic benefits and its environmental impact, several agencies included in its specification for concrete mixtures a minimum amount of fly ash to avoid or mitigate the effect of ASR (Malvar et al., 2002;ACI Committee 221, 1998). On the

91

other hand, reports had shown that the increase in demand of fly ash along with the limitation of its supplies, due to restriction on new coal power plants, may lead to shortage in suitable fly ash for concrete industry. Therefore, other waste or natural materials has been extensively investigated to be used as pozzolans in concrete and mortar. Metakaolin, calcined clay and different types of natural pozzolans have been investigated to mitigate ASR in concrete with various levels of reactivity and different types of reactive aggregates (Sabiret al., 2001; Ramlochanet al., 2000; Turanliet al., 2003).

7.2 Experimental Program

An experimental program was designed to investigate the effect of nano-silica, either solely or combined with different SCMs, on ASR. This effect will be investigated in terms of expansion, mechanical properties and microstructure of mortars and concrete made with a known ASR reactive aggregate. To achieve these goals, two types of specimens were used. The accelerated mortar-bar method was used to measure the expansion caused by ASR for different mixtures. Additionally, concrete cylinders were prepared to study the ASR effect on mechanical properties and microstructure.

For both mortar and concrete specimens, the cement used was type II/VI portland cement meeting ASTM C150 specifications. The main composition and properties of the cement are presented in Table 13. Also, the chemical and physical properties of Class F fly ash and metakaolin are listed in the same table. The same type of nano-silica described in chapter 2 was used for this study. Polycarboxylate based high range water reducing agent

92

(HRWRA) with specific gravity 1.068 and solids content of 40%was used at different dosages to achieve constant level of workability for some of the mixtures.

Table 13 Properties of cementitious materials and aggregate.

	Type II/VIPortland Cement	Class FFly Ash	Metakaolin	Aggregate Rock
SiO_2 (%)	20.6	58.3	51.7	63.0
Al_2O_3 (%)	3.4	16.6	43.2	11.4
Fe_2O_3 (%)	3.4	4.6	0.4	3.5
CaO (%)	63.5	10.2	-	6.9
MgO (%)	4.7	-	-	2.0
SO_3 (%)	2.4	0.8	-	-
Na_2O (%)	0.5	-	-	2.4
K_2O (%)	-	-	-	3.4
LOI (%)	-	-	-	6.5
Loss on Ignition	1.20	1.52	-	-
Specific Gravity	3.15	2.35	2.20	-
Fineness (m^2/kg)	376	290	-	-

Fine and coarse aggregates used in all the mixtures (concretes and mortars) were taken from the same quarry and had the same chemical and geological classification. This aggregates source was known to be reactive as expansion of the mortar bars exceeds the acceptable limits. The fine aggregates, used for the mortar and concrete mixtures, had specific gravity of 2.72, absorption of 3.75% and fineness modulus of 3.0. The coarse

93

aggregate specific gravity, absorption, and dry rodded unit weight were 2.70, 2.20% and 103 lb/ft^3 (1650 kg/m^3), respectively. The rock type, in which the aggregates were taken from, can be classified as dacite according to its geological nomenclature. Dacite rocks, possibly containing opal, tridymite, cristobalite, volcanic glass and beekite minerals, are known to be one of the ASR potentially reactive rocks (Tuthill, 1982 and Thomas et al., 2007). The chemical composition of the rocks from the used quarry is also shown in Table 13.

To study the expansion caused by ASR, the accelerated mortar bars test was used according to ASTM C1260 and ASTM C1567. Reactive fine aggregate was prepared and graded as specified by the previously mentioned ASTM standards. For the different cementitious materials combinations, mortar was prepared according to the standard with proportion of 1 part of cementitious materials to 2.25 part of graded aggregate by mass (dry materials) and with water-to-cement ratio of 0.47. Mortar bars of dimensions 1"×1"×11" were molded and compacted according to the ASTM standards. The molds were then kept in moisture cabinet with relative humidity not less than 90% for 24 hours. After unmolding, the bars were soaked in tap water and placed in an oven of temperature 80°C for 24 hours for conditioning. The zero reading of the bars length was then measured using length comparing device with accuracy of 0.0001 inch as shown in Figure 57. Immediately after the measurement, specimens were stored in 1 N sodium hydroxide (NaOH) solution in a convection oven of temperature 80°C ± 2°C. The expansion in the bars was measured and recoded every 3-4 days for the first 14 days after starting the exposure, and every 7-10 days after that. According to ASTM standards, the main reference expansion value was measured after 14 days of exposure. Furthermore,

for further understanding of ASR behavior at longer periods, the expansion was then monitored continuously for up to the age of 80 days.

Figure 57 Length comparator and mortar bar specimen.

In order to study the effect of nano-silica on ASR, different combinations of cementitious materials and nano-silica were used as binders for different mortar mixtures. Beside the control mixture (100% cement), seven different combinations of cementitious materials and nano-silica were used to prepare the mortar bars as previously described. It was confirmed through various studies as well as the practice that Class F fly ash and metakaolin are very efficient for ASR mitigation. Hence, this experimental study aims to compare the effect of these pozzolans to the effect of nano-silica on ASR. Additionally, combining these well-known mitigation pozzolans with nano-silica will be investigated.

Table 14 presents the cementitious material combinations used for the eight tested mortar mixtures. For all the mixtures, the same aggregates were used with the proportions and

95

gradations specified by the ASTM standards as described earlier. At least 3 mortar bars were prepared and tested for each of the eight mixtures. Due to the significant impact of using metakaolin on the workability of the mortar, HRWRA was needed to insure proper mixing for mixtures CM and CMN(which are two mixtures containing metakaolin) with the rate of 10.7 fl oz for every 100 lb of cementitious materials. This provided a consistent level of workability for all of the eight mixtures and consequently a similar level of compaction in the molds.

Table 14 Cementitious materials combinations for mortar mixtures.

Mixture	Type II/IV Cement	Class F Fly Ash	Metakaolin	Nano-Silica
C0	100%	0%	0%	0%
CN1	97%	0%	0%	3%
CN2	94%	0%	0%	6%
CF	70%	30%	0%	0%
CFN1	83%	14%	0%	3%
CFN2	68%	29%	0%	3%
CM	90%	0%	10%	0%
CMN	92%	0%	5%	3%

The second phase of this study was to investigate the effect of ASR on the mechanical properties of concrete made with different combination of cementitious materials. To achieve these goals, an accelerated exposure was used to study the compressive strength of concrete cylinders made with reactive aggregates. Based on the results from phase I of this study (mortar bars expansion), six concrete mixtures were selected to be tested in the second phase. Beside the control mixture having cement only as a binder, cement was combined with either fly ash or metakaolin in 2 of the concrete mixtures. Moreover,

96

nano-silica was combined with cement and each of the fly ash and metakaolin in the other 3 mixtures. For all mixtures, the w/c ratio was kept constant at 0.38 and the total cementitious materials content was 660 lb per cubic yard of concrete. Different dosages of HRWRA were used to achieve consistent level of workability (slump values between 3" and 6"). As expected, higher dosages were needed with mixtures containing nano-silica and/or metakaolin. Table 15 shows the proportions of the concrete mixtures used in the study.

Table 15 Proportions of concrete mixtures per cubic yard.

Mixture	Cement (lb/yd^3)	Fly Ash (lb/yd^3)	Metakaolin (lb/yd^3)	Colloidal Nano-SiO$_2$ (lb/yd^3)	Water* (lb/yd^3)	HRWRA (fl oz / 100 lb of Binder)	Coarse Aggregate (lb/yd^3)	Fine Aggregate (lb/yd^3)
CR-0	660	-	-	-	250	12	1788	1375
CR-N	620.4	-	-	79.2	210.4	36	1762	1358
CR-F	462	198	-	-	250	10	1755	1350
CR-FN	547	93	-	39.6	230.2	18	1765	1358
CR-M	594	-	66	-	250	40	1798	1385
CR-MN	607	-	33	39.6	230.2	32	1785	1375

* The content of mixing water was adjusted by the amount of water in the nano-silica solution.

Concrete cylinders were prepared from each mixture according to ASTM C39. The cylinders were 3" in diameter and 6" height. After 24 hours of mixing, specimens from

97

each mixture were unmolded and they were divided into 2 groups each containing 6 cylinders at least. The first group was kept in a standard curing tank, immersed in tap water at a temperature of 23°C ± 2°C till the time of testing. The second group of cylinders was immersed in 1N NaOH solution inside sealed plastic containers which were kept in an oven of temperature 80°C ± 2°C. Figure 58 shows the containers and the concrete cylinders inside the oven. After 28 and 180 days of mixing, 3 cylinders of each of the two groups were tested to evaluate the compressive strength. Sulfur capping was used for all the tested cylinders according to ASTM C617.

7.3 Results and Analysis

7.3.1 Accelerated mortar-bars

For the first phase of this study, the expansion in mortars bars immersed in NaOH solution at 80°C was monitored and the expansion ratios were calculated for approximately 80 days. The main expansion ratio readings taken at 14 days of exposure were compared to the limits recommended in the ASTM C1260 and C1567 standard appendix. These standards consider the aggregate and/or the cementitious materials combination to be indicative of innocuous ASR behavior if the expansion percentage is less than 0.10%. For expansions more than 0.20%, the standards recommends considering this case to be potentially deleterious, while for expansions between those two limits need further testing to define the causes of expansion. Table 16 presents the expansions at different ages of exposures including the reference 14 days expansion ratio. The values shown in the table represents the average expansion ratios of at least 3 bars for each mixture.

Figure 58 Containers and concrete cylinders inside the oven.

The expansion values presented in Table 16 indicates that the aggregates used in this study can be considered as potentially reactive. This can be basically revealed through the 14 days expansion value and the guidance limits recommended by the ASTM standards as previously described. Based on the 14 days expansion results, the efficiency of the different pozzolans dosage used can be judged by comparing it to the reference values. It can be noticed the 30% of Class F fly ash (mixture CF) or 10% of the metakaolin (mixture CM) could reduce the expansion values to nearly the acceptable limits. Also, 6% of nano-silica (mixture CN2) could achieve the same or slightly better performance in terms of ASR mitigation. However, the most efficient mitigation performance, measured in terms of reducing the 14 days expansion, was achieved by combining the classical mitigation pozzolans with 3% of nano-silica. This can be observed by means of the significantly lower expansion values for mixtures CFN2 and CMN.

The long term expansion caused by ASR was also investigated in this study as shown in Table 16 and Figure 59, which presents the relationship between the expansion in mortar bars and the exposure time up to 80 days. It should be noticed that this long exposure period combined with the accelerated conditions simulate a very long period of ASR in actual service conditions. This period might even exceed the design service life for most structures, therefore this very high expansion values may not be observed in practice.

Table 16 Expansion ratios in mortar bars.

Mixture	Average Expansion Ratio (%)		
	14 days	28 days	80 days
C0	0.335%	0.638%	1.055%
CN1	0.190%	0.381%	1.117%
CN2	0.094%	0.253%	0.903%
CF	0.103%	0.258%	0.882%
CFN1	0.108%	0.247%	0.788%
CFN2	0.036%	0.165%	0.496%
CM	0.107%	0.226%	0.750%
CMN	0.051%	0.167%	0.582%

The results of the long term expansion indicate that the rate of expansion was significantly reduced when supplementary cementitious materials were used. Generally, the control mixture (C0), containing only portland cement, represents the upper limit of the expansions at all ages of exposure except for mixture CN1 which had a slightly higher expansion at the end of the exposure period. For the control mixture, the rate of increase in expansion was higher during the first 30 days of the exposure, and starts gradually declining after 30 days and tends to reach a constant maximum value. For the

100

other seven mixtures, the expansion increase tended to follow almost a linear behavior after the first 14 days and up to the end of the exposure.
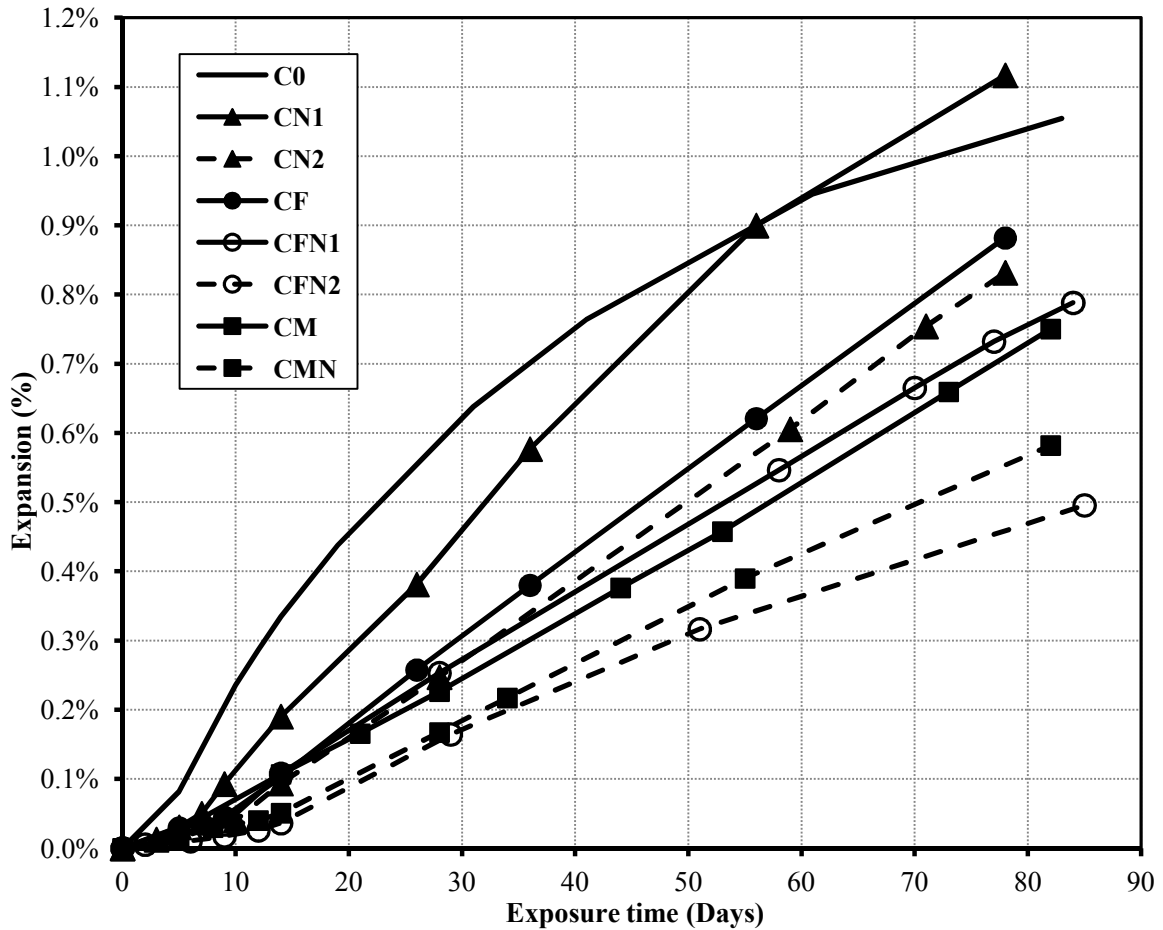
Figure 59 Expansion in mortar bars at different exposure ages.

After the exposure period, the mortar bars were left to cool down and air dry then they were visually inspected. Excessive cracking and deformation was observed in most of the bars at different levels after the relatively long period of accelerated ASR. Figure 60 shows examples for the different levels of damage in mortar bars at the end of exposure for three of the tested mixtures. This figure indicates the severe damage and the excessive cracking in the control mixture (C0) due to the ASR gel expansion. Significantly lower

101

level of cracking can be noticed in case of using 30% class F fly ash (mixture CF). On the other hand, mixtures CFN2 combining fly ash and nano-silica experienced very low level of cracking after exposure knowing that this mixture recorded the lowest percentage of expansion at the end of exposures (see Table 16). Generally, for all the mixtures, the extent of cracking observed was proportional to the expansion ratio measured at the end of exposure.

7.3.2 ASR effect on compressive strength

In the second phase of this study, the effect of ASR on the mechanical properties of concrete was investigated. The compressive strength of concrete cylinders was evaluated at 28 days and 180 days after mixing. Two groups of cylinders were tested for each mixture at these ages. The first group was kept in the standard curing conditions, while the second group was exposed to an accelerated ASR attack similar to the exposure of the mortar bars. The first group represents no ASR effect as these periods are insufficient to initiate ASR under normal curing conditions. Conversely, the other group immersed in NaOH solution at 80°C simulates an aggressive ASR effect.

102
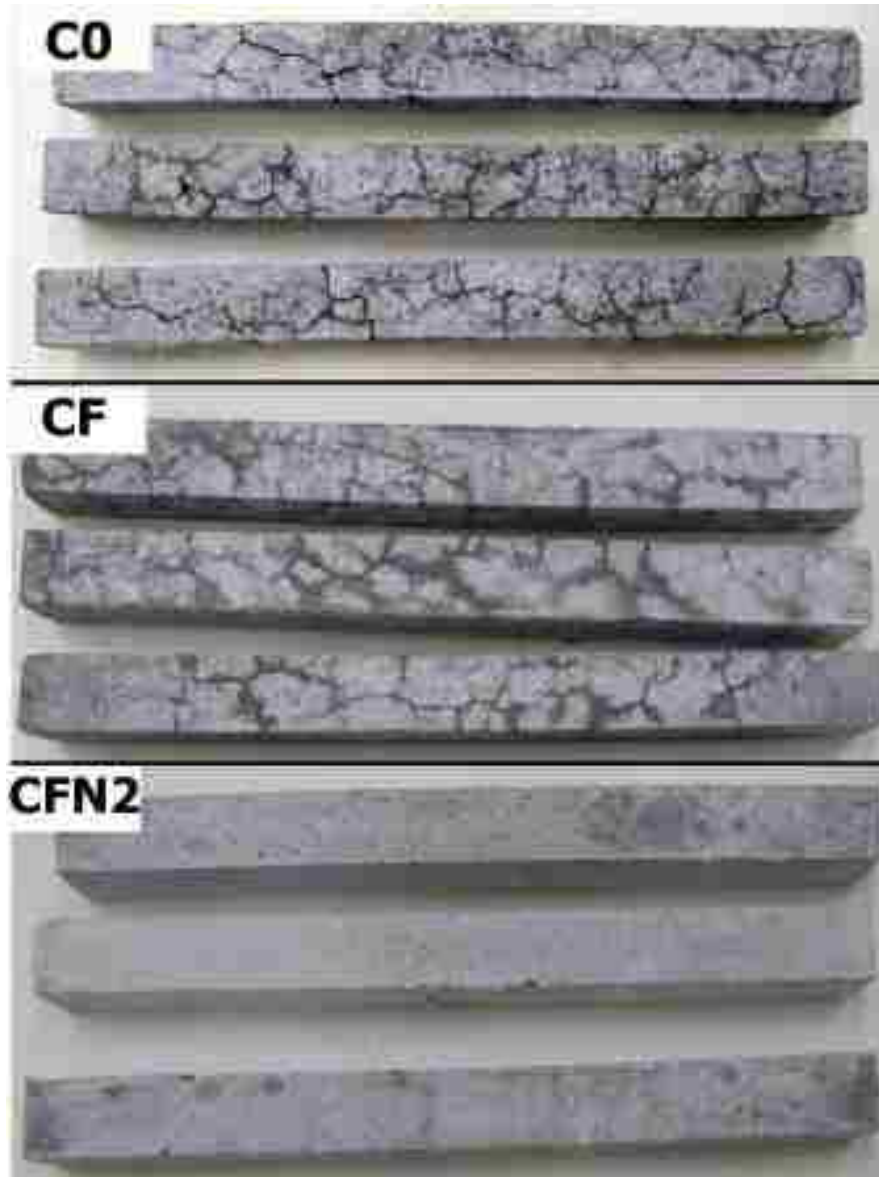
Figure 60 Mortar bars after exposure for mixture C0, CF and CFN2.

In order to monitor the change in the mechanical properties of concrete cylinders during the exposure period, the DME of the specimens was evaluated every 1-2 weeks during the first 3 months of exposure. The RDME was plotted against the exposure time as shown as an example plot in Figure 61 showing mixture CR-0 results. Despite some available literature reporting reduction of RDME due to ASR (Swamy and Al-Asali, 1988; Fan and Hanson, 1998; Rivard and Saint-Pierre, 2009), the results indicated

insignificant variation in the measured value for all the tested mixtures. This may be attributed to the accumulation of the silica gel within the cracks generated due to expansion. This accumulated gel provided a solid medium transferring the vibration through the crack without noticeable change in the measured resonance frequency.
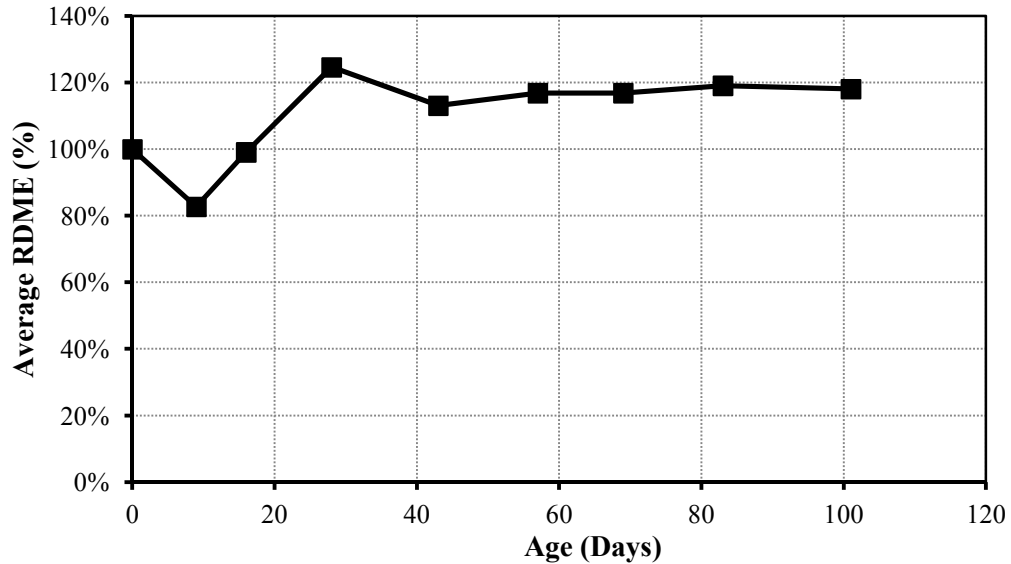
Figure 61 Change in RDME for CR-0 during exposure.

Unlike the mortar bars, no visible cracking or signs of deterioration were visible on any of the cylinders subject to the accelerated ASR exposure except for presence of white precipitation on the surface of the cylinders. Figure 62 shows three typical cylinder specimens at the end of the 180 days exposure period. This lack of visual damage may be attributed to the lower rate of reaction in case of concrete compared to the mortar mixtures. As the reaction takes place mainly on the surface of the aggregates, the large amounts of fine aggregates in mortars provided a larger surface area for the reaction and therefore more rapid ASR. Additionally, presence of coarse aggregate in concrete mixtures may provide some form of internal support limiting excessive cracking and expansion caused by ASR especially during the early ages (Zhang et al., 1999).

104

Figure 62 Concrete cylinders after 180 days of exposure.

For most of the mixtures, the strength of the cylinders subjected to the aggressive ASR accelerated exposure was lower than the strength of the corresponding specimens kept in the curing tank. This reduction in strength is believed to be the structural effect of the ASR, as the specimens in normal curing conditions are considered to experience no ASR reaction due to the short period, as previously discussed. Figures 63 and 64 illustrate the average compressive strength of the six concrete mixtures at 28 and 180 days, respectively. Also, Table 17 presents the percentage of reduction in compressive strength due to ASR at the two testing ages. This percentage was calculated for each age as the difference between the compressive strengths of the two tested groups (the standard curing and accelerated ASR condition) divided by the strength of the cylinders in standard curing conditions. Evaluating these reduction percentages was a main goal of the experimental program, rather than comparing the strength of the different mixtures.
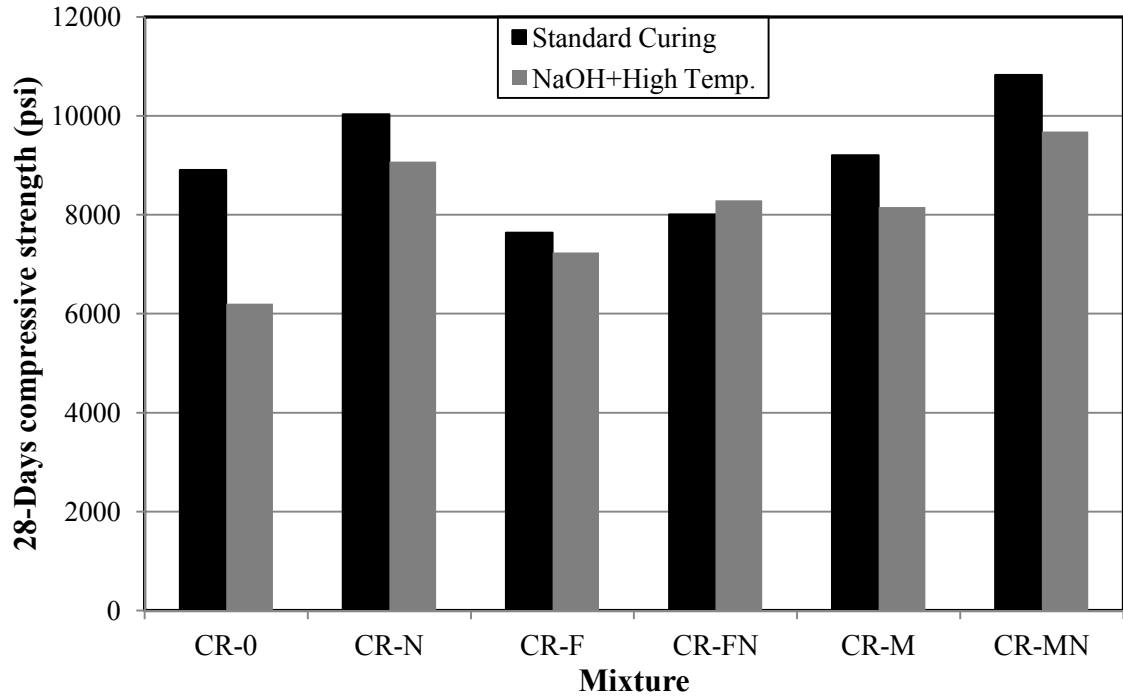
Figure 63 Compressive strength of concrete at 28 days.
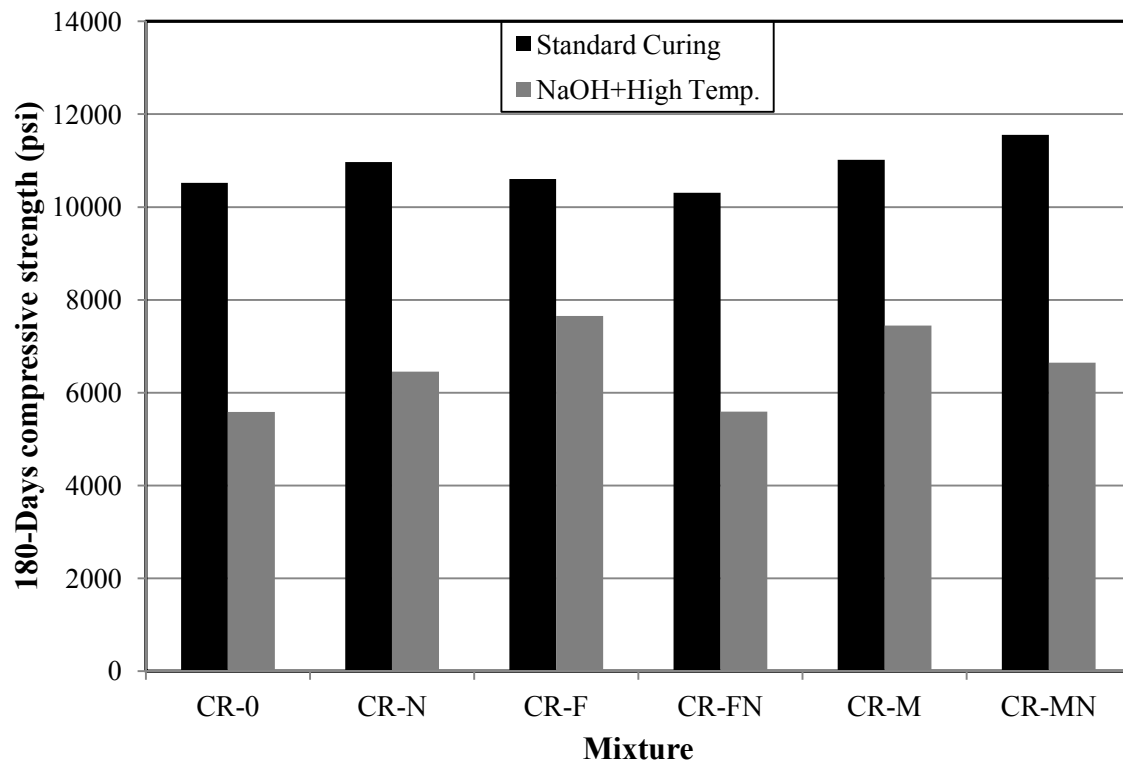
Figure 64 Compressive strength of concrete at 180 days.

106

Table 17 Percentage of reduction in strength due to ASR.

Mixture	Reduction in Compressive Strength (%)*	
	28 days	180 days
CR-0	30.4%	46.9%
CR-N	9.5%	41.2%
CR-F	5.3%	27.8%
CR-FN	-3.6%	45.8%
CR-M	11.4%	32.4%
CR-MN	10.6%	42.5%

* Postive values indicates reduction in strength.

As shown in Figures 63 and 64, as well as Table 17, the control mixture (C0) experienced the highest values of strength reduction at 28 and 180 days. Despite the extremely high temperature of the solution surrounding the specimens during exposure which should accelerate the hydration and pozzolanic reactions compared to curing tank conditions, a considerable drop of strength could still be observed. This drop in strength (approximately 30% and 47%) may have a significant effect on the performance of concrete structures having relatively long design service life. At 28 days, mixtures incorporating Class F fly ash (CR-F) or both fly ash and nano-silica (CR-FN) experienced very low levels of change in strength which fall around the normal variation in experimental results. These results, along with the expansion values, indicate that using Class F fly ash or combing it with nano-silica is an effective technique in terms of mitigation of ASR effect. In addition, using metakaolin, nano-silica or combining both of them caused significant improvement in terms of strength reduction at 28 days of exposure. The strength reduction for these mixtures was around 10% at 28 days which may not be considered a critical value for the structural performance. After 180 days of exposure, most mixtures had significant strength reduction. It should be noted that the

107

180 days of accelerated exposure is an extremely aggressive testing regime which may not exist in the service life of a structure. However, all of the mitigation techniques used showed better performance than the control mixture at different degrees.

7.4 ASR Testing Conclusions

As a relatively new material, there was insufficient experimental data about the effect of nano-silica on ASR. One of the main objectives of this study was to investigate the effect nano-silica on ASR mitigation. Based on the results of this study, incorporating nano-silica in concrete or mortar mixtures generally did not intensify the effect of ASR. Moreover, using relatively high dosages of nano-silica slowed down the reaction and suppressed its effect on concrete. This may be attributed to the improvement of the microstructure of the cement matrix and increase of its strength as described in chapter 3 and 5 of this study.

This study indicates that ternary cementitious blends incorporating nano silica performed significantly better than the binary blends containing cement and pozzolans only. In terms of reducing expansion and strength loss caused by ASR, the best results were achieved in cases of using fly ash or metakaolin combined with nano-silica. This phenomenon may be explained by the rapid acceleration of the pozzolanic reaction in presence of nano silica particles as confirmed by the results of the thermogravimetric analysis presented in chapter 5 and the higher strength gain rate shown in chapter 3. This rapid pozzolanic reaction helps consuming large amount of portlandite (calcium hydroxide), which reduces the alkalinity inside the pores of the hardened cement matrix (Thomas at al., 1999 and Thomas et al., 2012). The reduction of alkalinity of the pore

108

solution may retard the reaction between the alkalis and the amorphous silica in aggregates which is responsible for the formation of the expansive gel.

Generally, the effect of nano-silica conforms to the literature about using silica fume for ASR mitigation. However, relatively very low dosages of nano-silica (as low as 3% of cementitious materials) were effective in terms of ASR mitigation compared to higher addition rates normally used for micro-silica. In addition, the adequate dispersion of the colloidal nano-silica prevent some problems of excessive expansions that may be observed in some case of using granulated silica fume as reported in literature (Pettersson, 1992).

Chapter 8: Conclusions and Recommendations

The study addressed a broad research program involving different aspects of nano-silica use in concrete. Further understanding of the effect of this new material on the macro- and micro- scale characteristics of concrete was provided. The results presented in this study show that various aspects of concrete performance may be controlled through the addition of low dosages of nano-silica. This new material, which may be considered as a breakthrough in concrete industry, enables the development of high performance concrete at considerably lower cost and with improved ecological carbon footprint.

8.1 Summary and Conclusions

Considering the materials, mixture designs, and testing methods implemented in the present study, the following conclusions can be drawn:

- The overall performance of concrete, with or without fly ash, was significantly improved with the addition of variable dosages of nano-silica.

- For mixtures incorporating nano-silica, the increase in the peak temperature recorded within 15 hours after mixing indicated that the ultrafine nature of nano-silica was responsible for speeding up the kinetics of hydration reactions.

- At all curing ages, the strength generally increased with the addition of nano-silica up to 6%. In particular, at 28 days, the compressive strength was considerably improved for mixtures incorporating 30% Class F fly ash and nano-silica, which indicates that

110

the inherently slower rate of strength development of concrete containing Class F fly ash can be controlled by the addition of small dosages of nano-silica.

- The concrete resistance to abrasion was improved with the addition of nano-silica especially for the mixture including portland cement as a single binder. The abraded volume was reduced by around 23% with the addition of 3% of nano-silica, while adding 6% nano-silica resulted in 36% lower volume of abrasion. This improvement agreed with the mechanical properties indicating significant enhancement of concrete microstructure which was confirmed by the MIP and SEM results.

- The RCPT results showed that the passing charges and physical chloride ion penetration depths significantly decreased with the addition of nano-silica. This suggested that the incorporation of small dosages of nano-silica has a pronounced effect on reducing the conductivity and refining the pore structure of the cementitious matrix.

- MIP results showed that the total porosity and the threshold pore diameter were significantly lower for mixtures containing nano-silica. More refinement of the pore structure was achieved with increasing the nano-silica dosage up to 6%.

- TG results indicated that the addition of nano-silica led to significant consumption of portlandite (CH) in the pozzolanic reaction. However, increasing the dosage of nano-silica from 3% to 6% did not increase the consumption of CH, which suggests that the general improvement in performance associated with the increase of the nano-silica addition from 3% to 6% may be mainly attributed to the physical filler effect in the cementitious matrix. BSEM analysis showed notable densification in the ITZ for

111

specimens containing nano-silica. Also, for specimens containing Class F fly ash and nano-silica, BSEM showed higher degree of hydration at 28 days relative the control mixture containing only Class F fly ash. This suggests that the delay in microstructure development and durability improvement of concrete comprising Class F fly ash can be mitigated by the addition of small dosages of nano-silica.

- Damage caused by crystallization of salt in concrete pores should be considered as an important cause of damage in areas with salt-rich soils. This type of environmental attack should be taken into account during the concrete mixture design especially in regions with hot and dry seasons.

- PSA damage could be observed in form of surface deterioration which can be mainly measured in lab as the mass loss of specimens. Generally, mixtures including portland cement as a single binder showed higher resistance to PSA. Addition of different dosages of nano-silica significantly improved PSA resistance expressed in terms of mass loss during testing. However, for mixtures incorporating fly ash, the nano-silica addition was not effective in enhancing PSA resistance.

- The porosity of concrete as well as the pore size distribution may affect the surface damage caused by PSA. The total porosity may play a significant role in determining PSA resistance particularly for mixtures with single binder (OPC). Experimental results indicate that excessive pore refinement may increase the vulnerability of damage caused by PSA especially for mixtures having relatively high total porosity.

- Water absorption test may be used as an effective and rapid tool to asses/compare the ability of concrete to resist PSA. However, experimental results indicate that this test

112

may be binder dependent when related to the PSA resistance. The total absorption as well as the secondary absorption rate measured during absorption test was remarkably related to the mass loss caused by PSA for mixtures with portland cement as a single binder. On the other hand, these correlations were less accurate for mixtures with fly ash

- Nano-silica could mitigate the effect of ASR on concrete and mortar expansion. However, combining nano-silica with other pozzolanic materials like fly ash or metakaolin showed the best performance in terms of reducing expansion or preventing strength reduction due to ASR. This is attributed to the accelerated pozzolanic reaction caused by the nano-silica which help reducing the alkalinity of concrete pores solution and improving microstructure. This was also confirmed by the TG and MIP results.

8.2 Recommendations and Future Research

Nanotechnology can be the next big move in concrete industry due to the potential in terms of controlling concrete performance either on the micro or macro level. Materials of nano –sized particle had shown significant different behavior than materials having the same chemical compositions with larger particle size. Therefore, different materials should be investigated in the nano particle arena as concrete additives.

Nano-silica can be of economical and ecological value if used to control the strength gain rate and durability of concrete. Using this new material can be the clean and economic alternative of increasing the cementitious materials content. In applications like pavements and overlay repairs, significantly high cement content is usually used for the

113

sole purpose of achieving very high strength to open roads for traffic. Nano-silica may reduce the amounts of the cement needed in these cases as it can control strength gain rate by controlling the added dosages.

The next step for the research of nano-silica in concrete should be testing nano-particles with the different types of pozzolans including those types known to have problems with performance or strength gain rate or durability. In addition, nano-silica may also be investigated when used with materials having ASR issues including recycled concrete and Class C fly ash.

Appendix

Specimen A-0 (above solution):

Legend:
- Thenardite 7.26 %
- Dolomite 71.17 %
- Calcite 12.59 %
- Quartz low 2.40 %
- Portlandite 3.28 %
- Gypsum 1.88 %
- Ettringite 1.42 %

— Sample 1 D 5-90 10-06-12.raw_1

X-axis: 2Th Degrees
Y-axis: Sqrt(Counts)
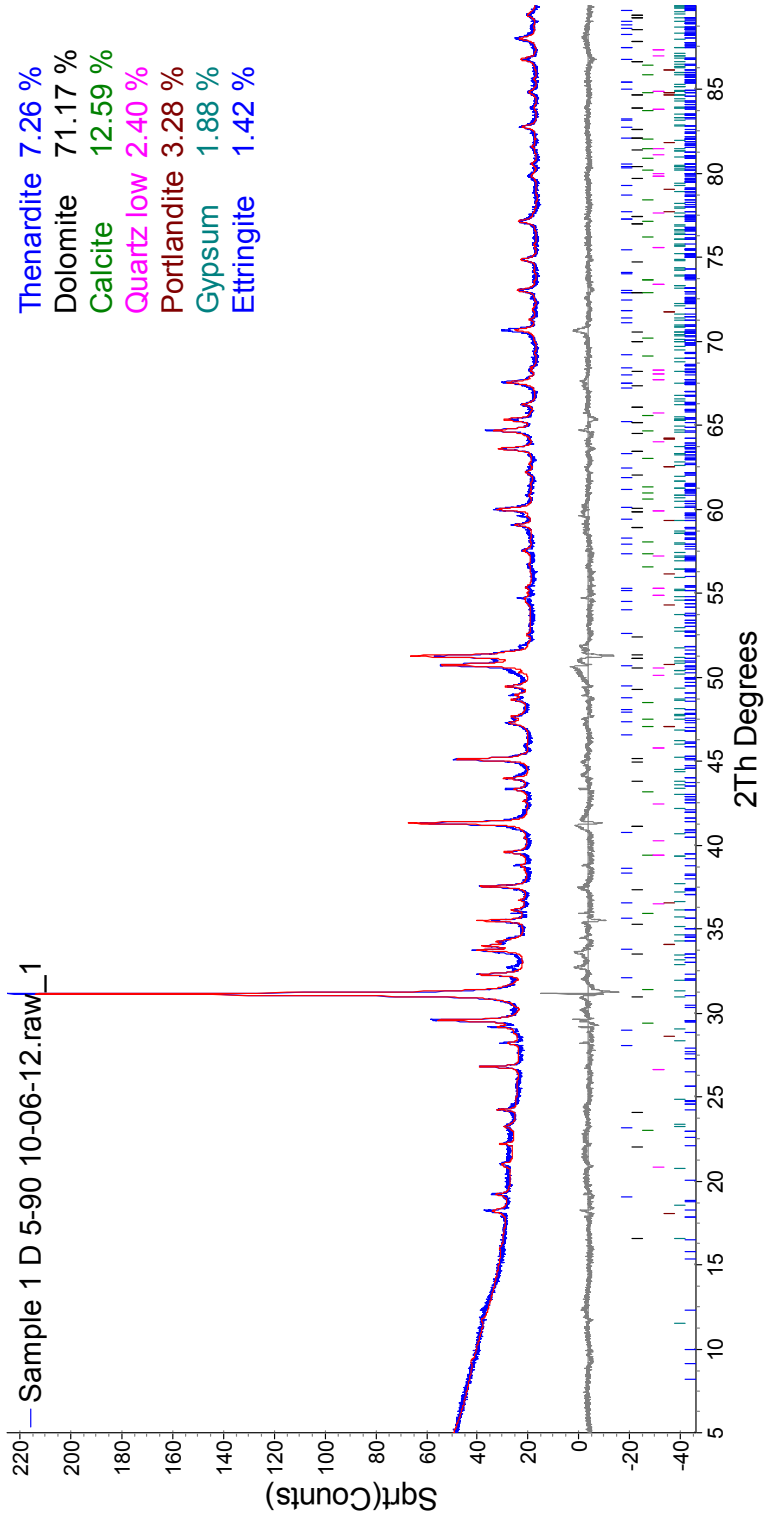
Specimen A-0 (immersed in solution):

Thenardite	3.96 %
Dolomite	72.30 %
Calcite	14.13 %
Quartz low	2.91 %
Portlandite	1.77 %
Na2S2O6x2H2O	1.52 %
Gypsum	1.54 %
Ettringite	1.87 %

116
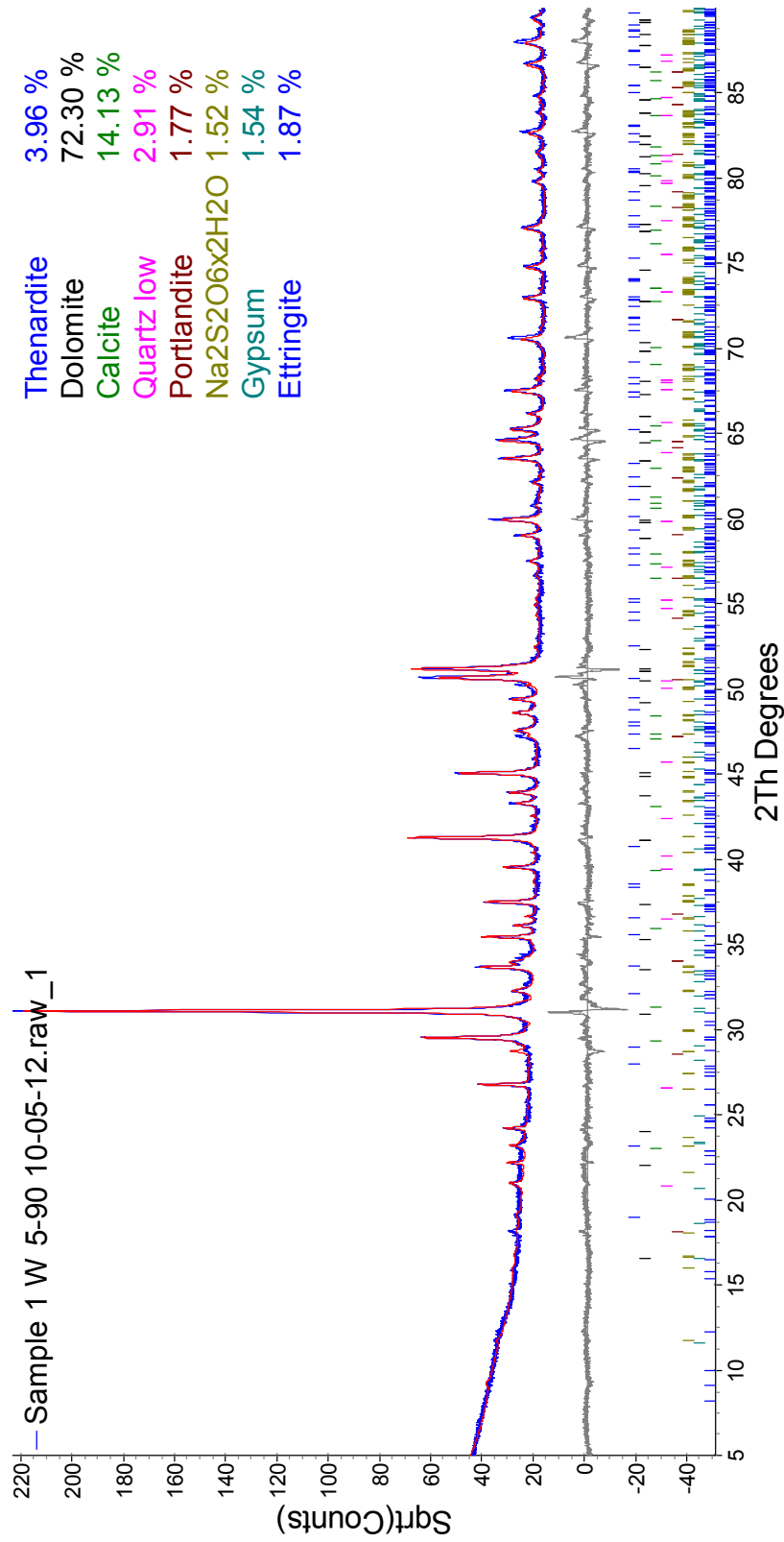
Specimen A-1 (above solution):
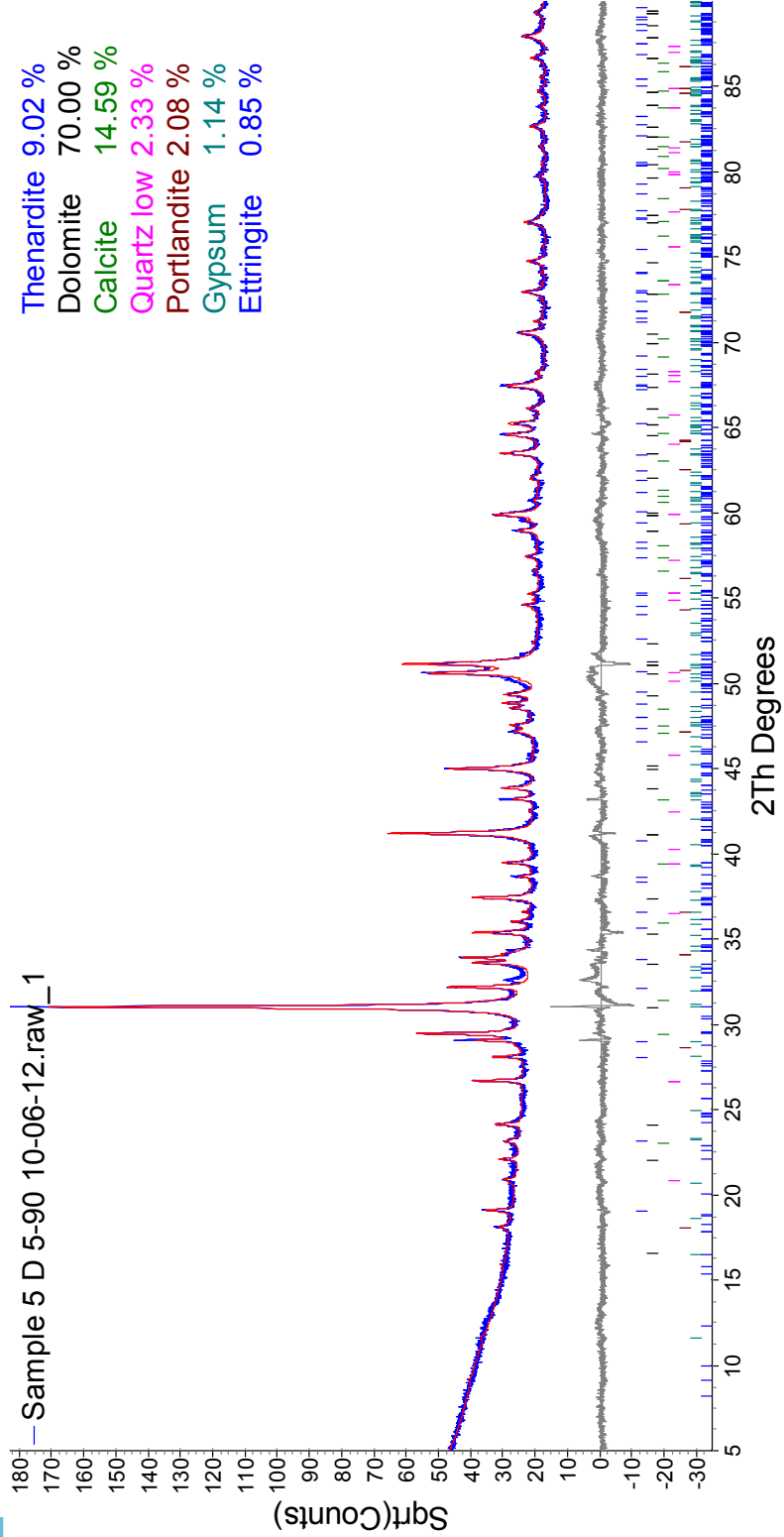
Specimen A-1 (immersed in solution):

Thenardite 3.44 %
Dolomite 73.12 %
Calcite 10.98 %
Quartz low 3.64 %
Portlandite 1.55 %
Na2S2O6x2H2O Pnma 2.24 %
Gypsum 3.34 %
Ettringite 1.71 %

118
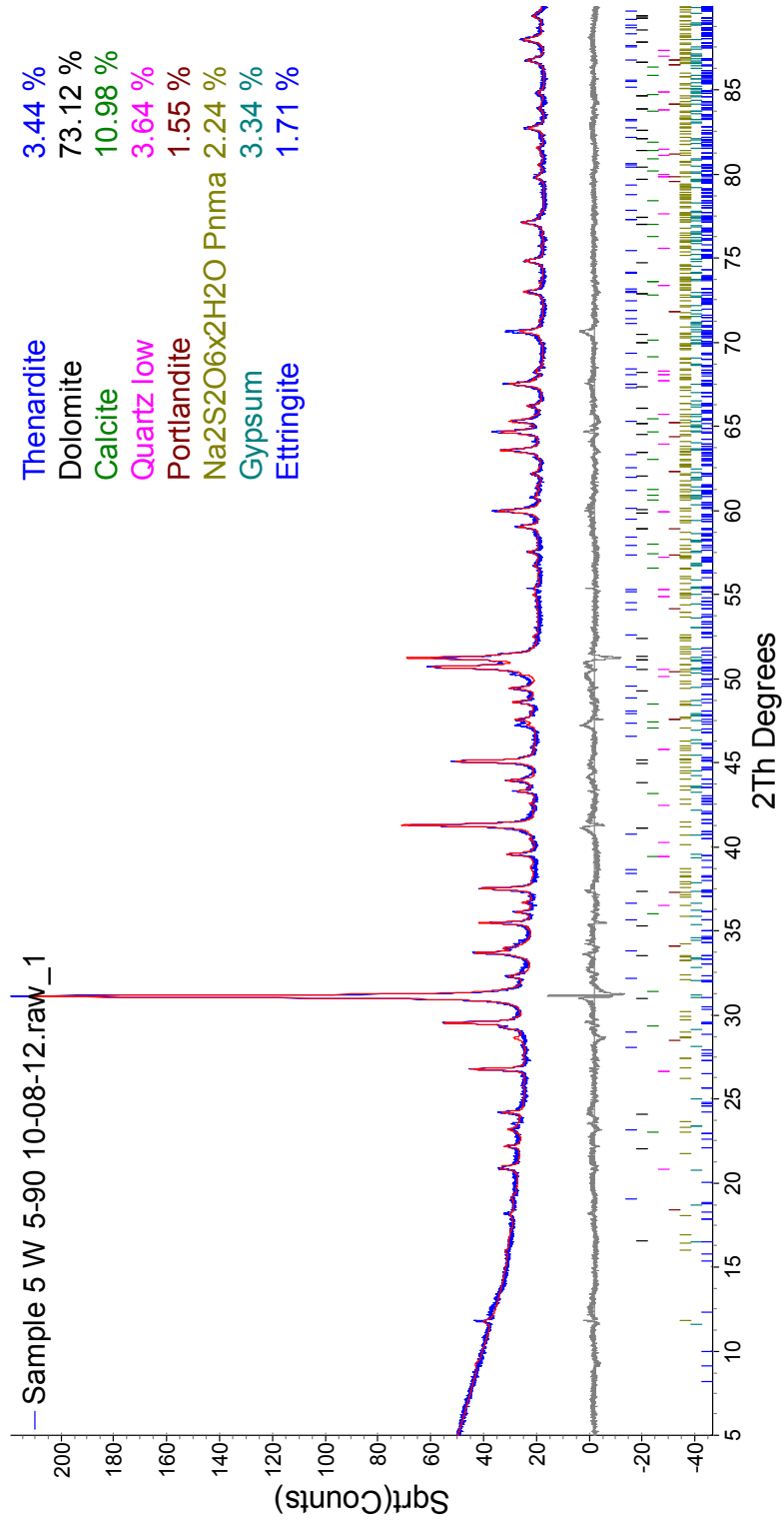
Specimen A-2 (above solution):

Thenardite	16.03 %
Dolomite	71.58 %
Calcite	5.20 %
Quartz low	3.79 %
Portlandite	0.82 %
Na2S2O6x2H2O Pnma	1.90 %
Gypsum	0.44 %
Ettringite	0.24 %

119
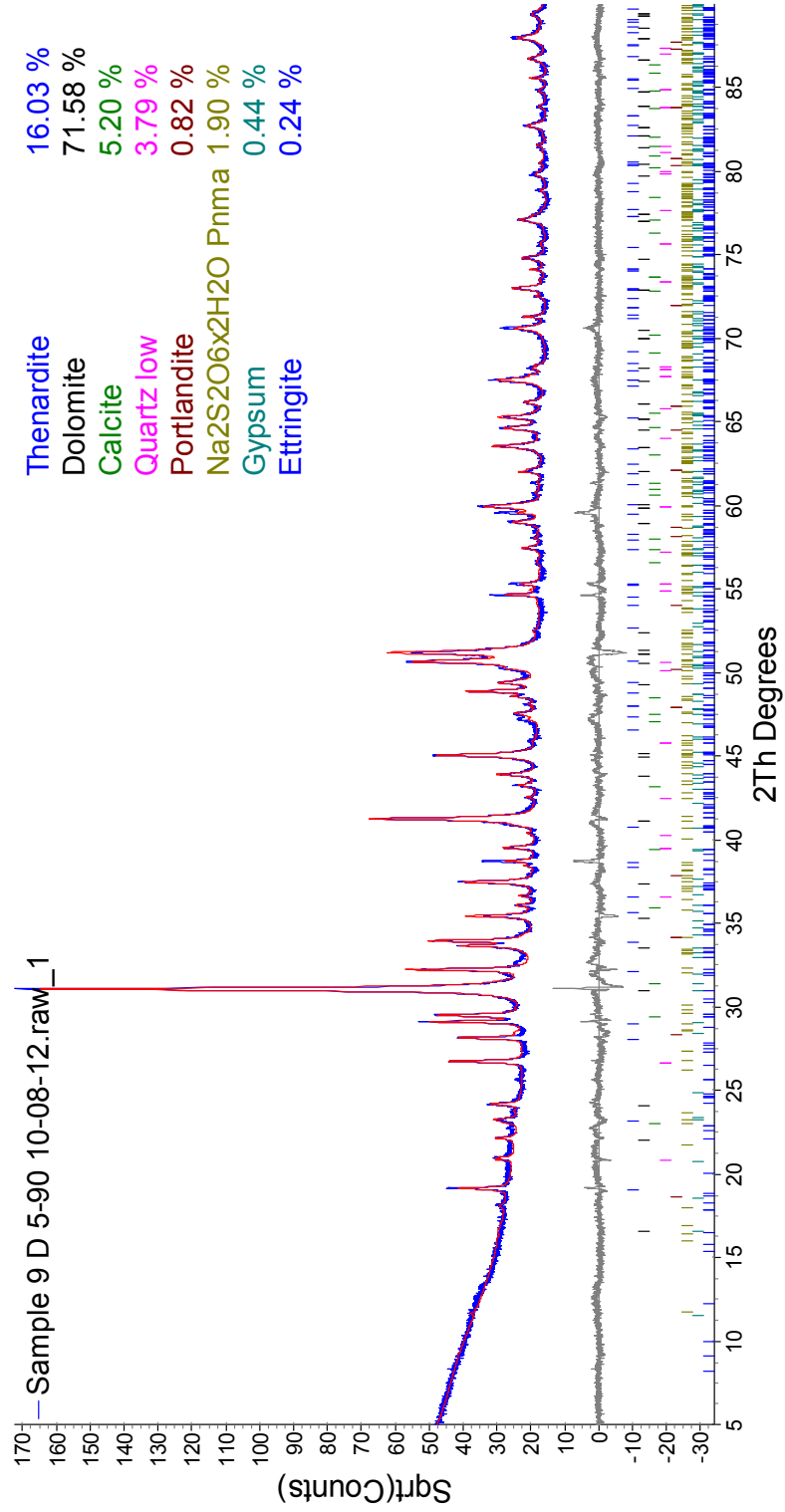
Specimen A-2 (immersed in solution):

Thenardite 6.71 %
Dolomite 66.87 %
Calcite 19.11 %
Quartz low 3.08 %
Portlandite 1.12 %
Na2S2O6x2H2O Pnma 1.31 %
Gypsum 1.12 %
Ettringite 0.68 %

120
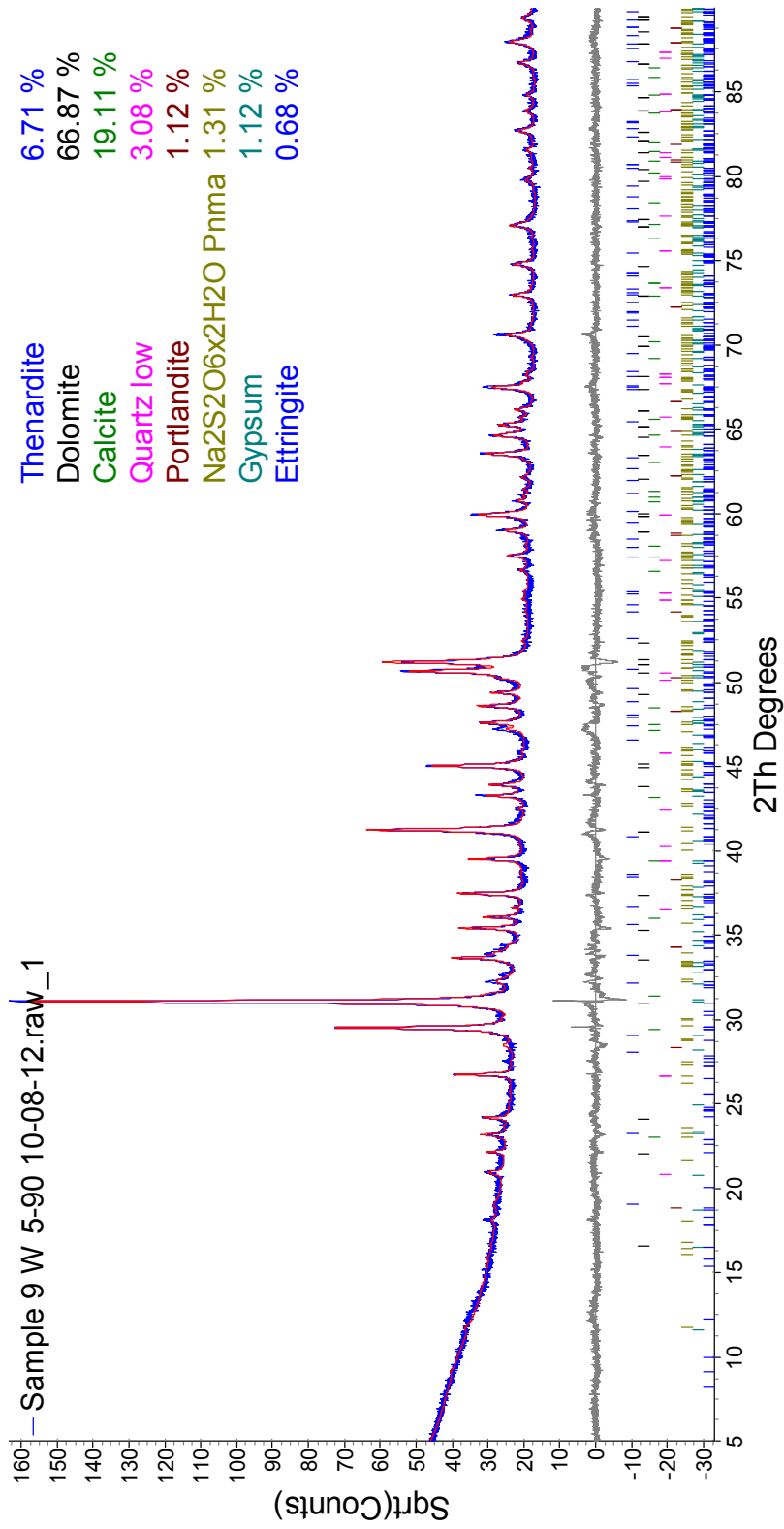
Specimen B-0 (above solution):

Thenardite	8.85 %
Dolomite	74.74 %
Calcite	8.31 %
Quartz low	5.00 %
Portlandite	0.91 %
Gypsum	0.67 %
Ettringite	1.51 %

121
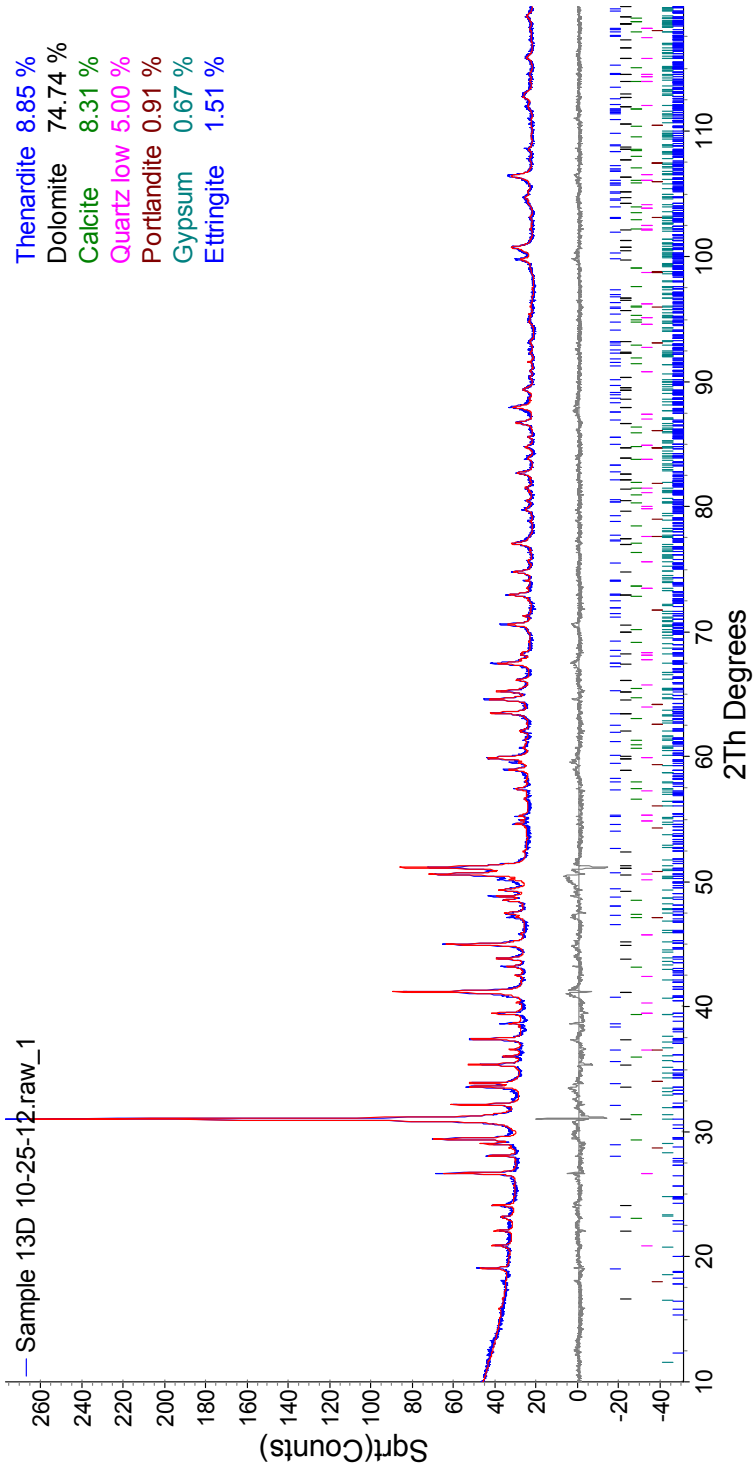
Specimen B-0 (immersed in solution):

Dolomite 69.27 %
Calcite 17.75 %
Quartz low 3.96 %
Portlandite 2.02 %
Gypsum 1.78 %
Ettringite 1.83 %
Thenardite 3.37 %

Sample 13W 10-25-12.raw_1

2Th Degrees

Sqrt(Counts)

122
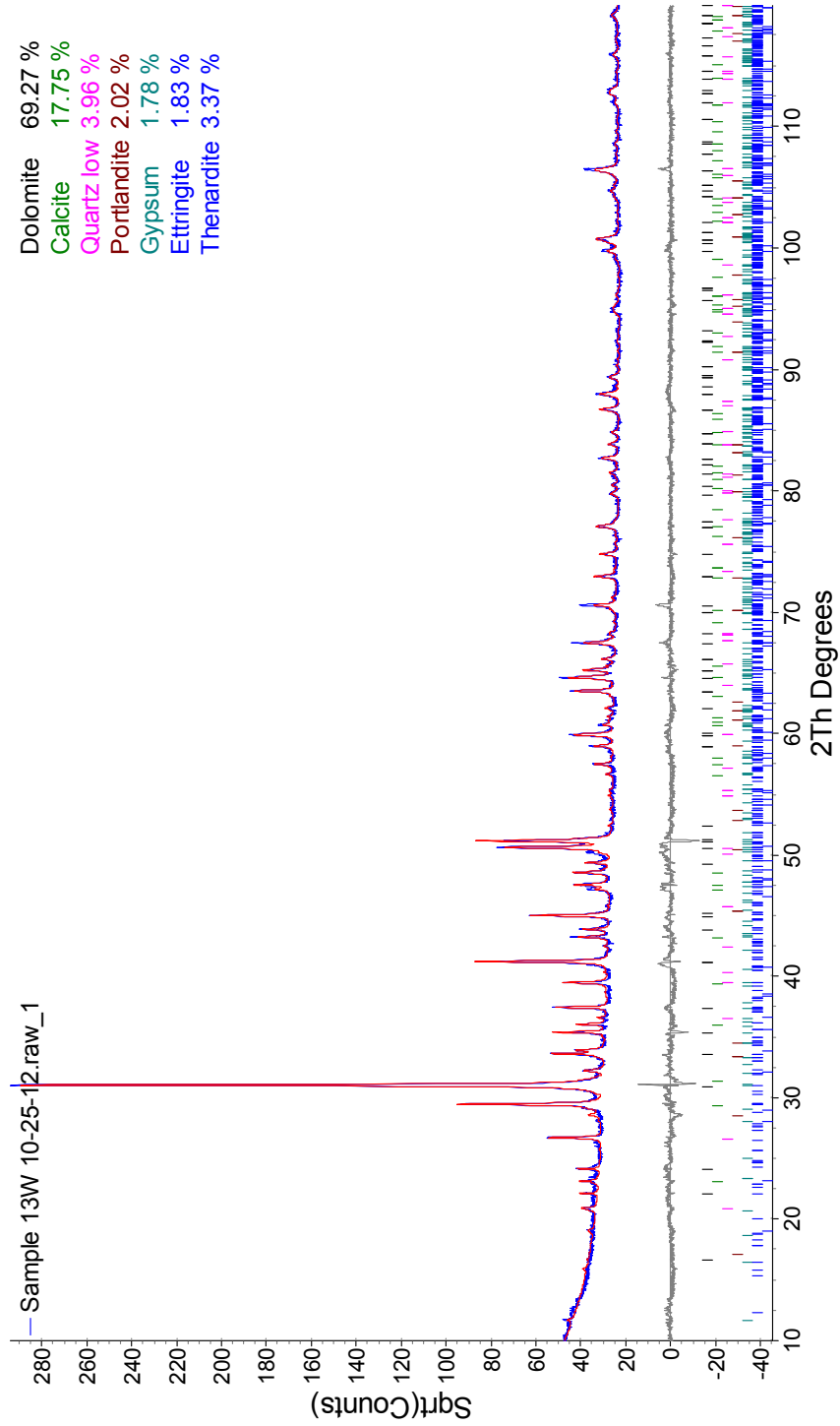
Specimen B-1 (above solution):

Dolomite	70.80 %
Calcite	8.44 %
Quartz low	2.99 %
Portlandite	1.00 %
Gypsum	0.42 %
Ettringite	0.95 %
Thenardite	15.39 %

Sample 17D 10-31-12.raw_1

123
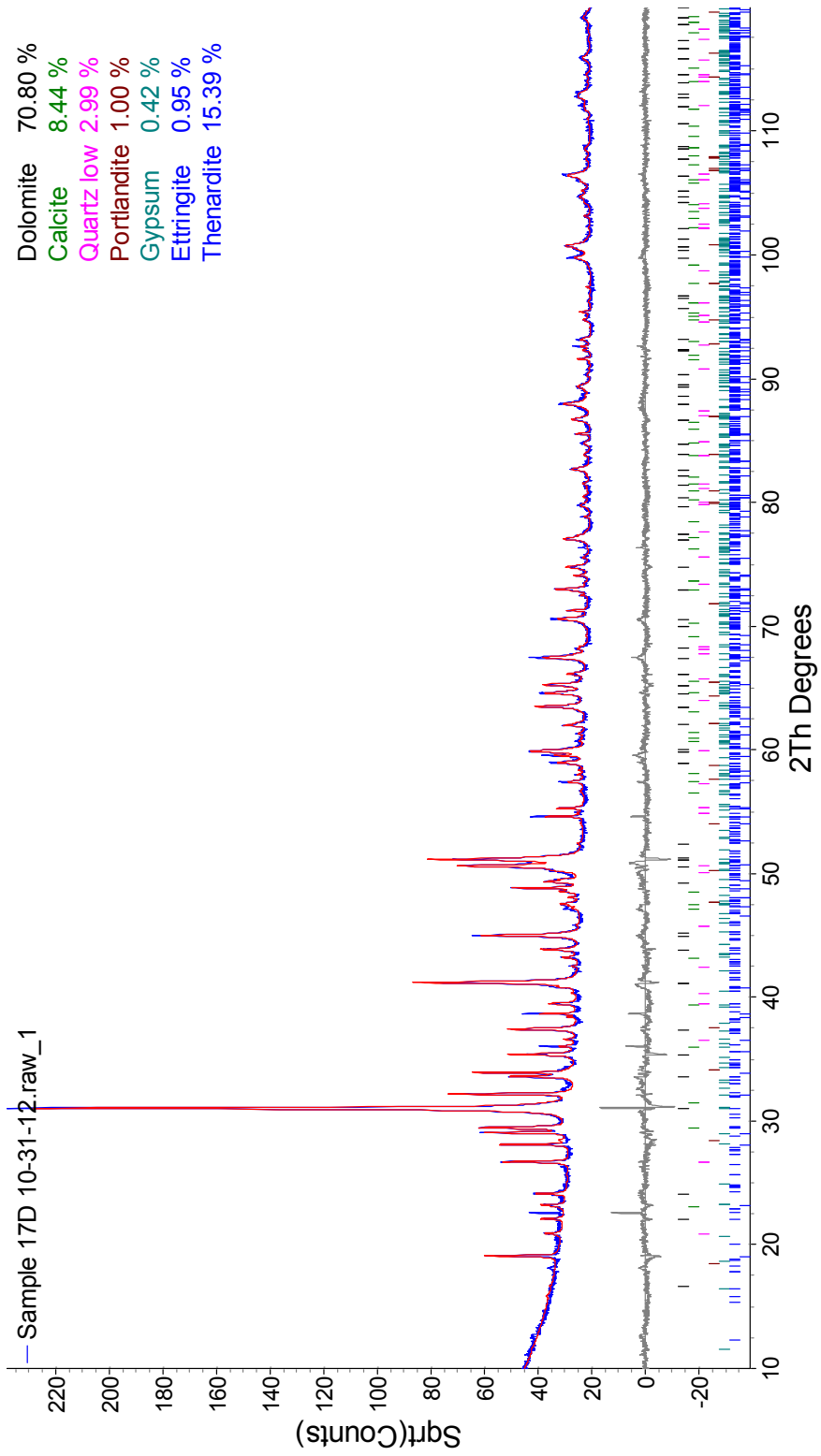
Specimen B-1 (immersed in solution):

Dolomite   80.61 %
Calcite   10.29 %
Quartz low 3.32 %
Portlandite 0.38 %
Gypsum   0.83 %
Ettringite   0.63 %
Thenardite   3.94 %

— Sample 17W 11-01-12.raw_1

2Th Degrees

Sqrt(Counts)
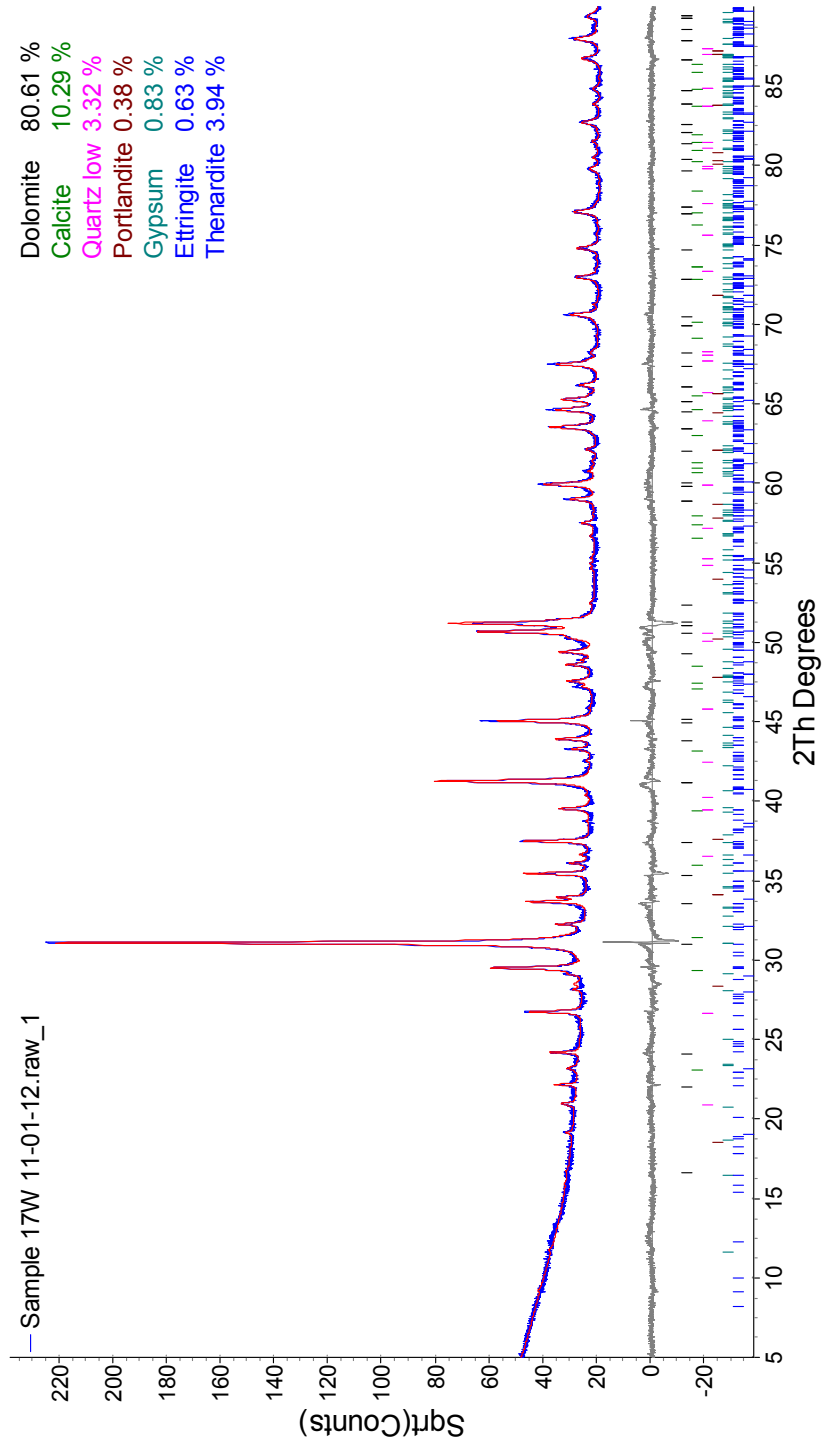
Specimen B-2 (above solution):

Dolomite 65.44 %
Calcite 7.49 %
Quartz low 2.65 %
Gypsum 0.23 %
Ettringite 0.48 %
Thenardite 23.70 %

— Sample 21 D 11-01-12.raw_1

2Th Degrees

Sqrt(Counts)

125
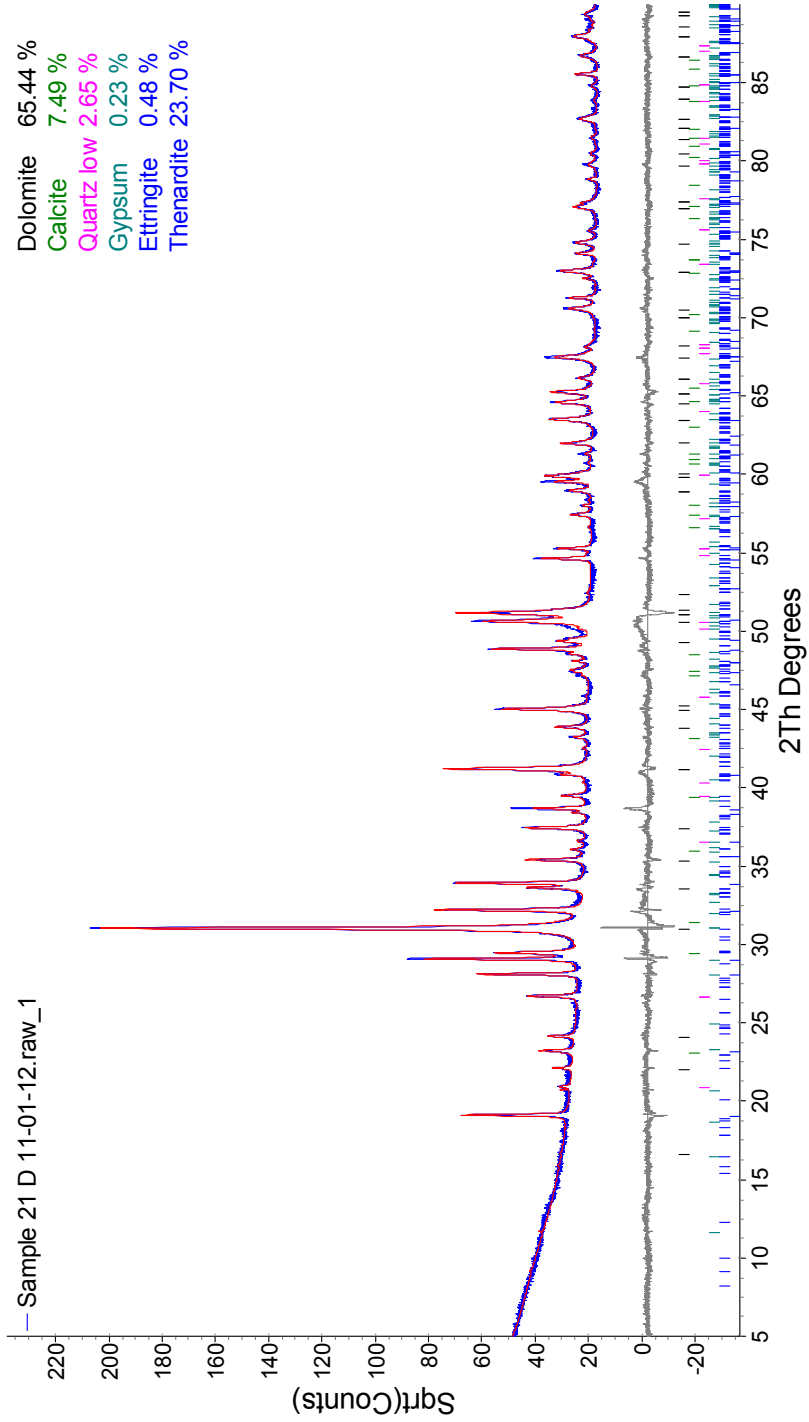
Specimen B-2 (immersed in solution):

Dolomite	77.09 %
Calcite	13.94 %
Quartz low	5.18 %
Portlandite	0.23 %
Gypsum	0.90 %
Ettringite	0.64 %
Thenardite	2.02 %

Sample 21 W 11-02-12.raw_1

Sqrt(Counts)

2Th Degrees

126
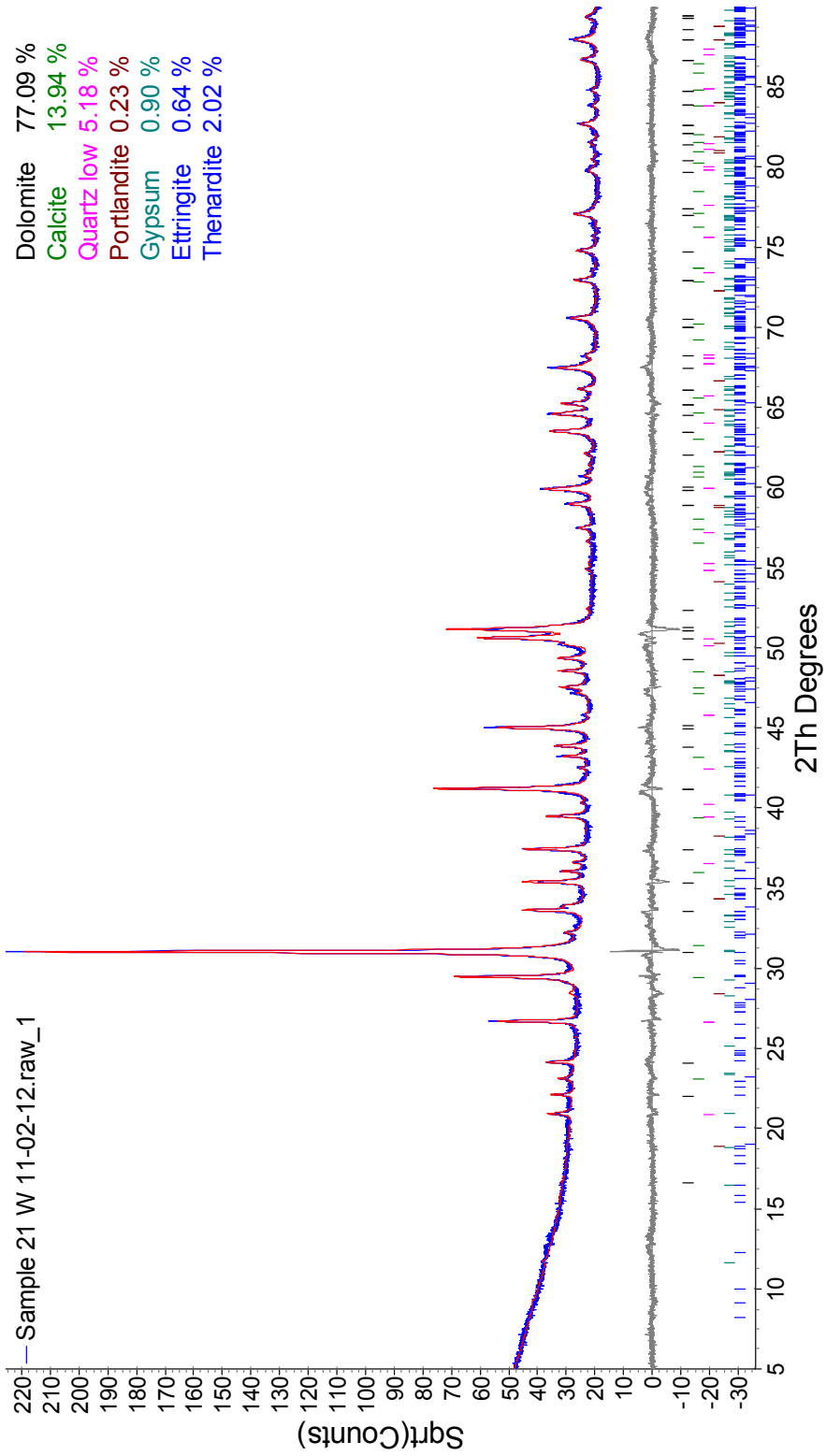
References

ACI Committee 221, 1998, "State-of-the-Art Report on Alkali-Aggregate Reactivity (221.1R-98)," American Concrete Institute, Farmington Hills, Mich., 31 pp.

Alasali M.M. and Malhotra V.M. (1991), "Role Concrete Incorporating High Volumes of Fly Ash in Controlling Expansion due to Alkali-Aggregate Reaction," *ACI Materials Journal*, V.88, No.2, pp. 159-163.

American Association of State Highway and Transportation Officials, AASHTO, "Handbook for the Identification of Alkali-Silica Reactivity in Highway Structures (SHRPC-315)", 1991.

American Society for Testing and Materials, ASTM C39, "Standard Test Method for Compressive Strength of Cylindrical Concrete Specimens", Annual Book of ASTM Standards, V.04.02, 2008.

American Society for Testing and Materials, ASTM C78, "Standard Test Method for Flexural Strength of Concrete (Using Simple Beam with Third-Point Loading)", Annual Book of ASTM Standards, V.04.02, 2007.

American Society for Testing and Materials, ASTM C143, "Standard Test Method for Slump of Hydraulic-Cement Concrete", Annual Book of ASTM Standards, V.04.02, 2010.

American Society for Testing and Materials, ASTM C150, "Standard Specification for Portland Cement", Annual Book of ASTM Standards, V.04.01, 2007.

American Society for Testing and Materials, ASTM C191, "Standard Test Methods for Time of Setting of Hydraulic Cement by Vicat Needle", Annual Book of ASTM Standards, V.04.01, 2008.

American Society for Testing and Materials, ASTM C192, "Standard Practice for Making and Curing Concrete Test Specimens in the Laboratory", Annual Book of ASTM Standards, V.04.02, 2005.

American Society for Testing and Materials, ASTM C215, "Standard Test Method for Fundamental Transverse, Longitudinal, and Torsional Frequencies of Concrete Specimens", Annual Book of ASTM Standards, V.04.02, 2008.

American Society for Testing and Materials, ASTM C231, "Standard Test Method for Air Content of Freshly Mixed Concrete by the Pressure Method", Annual Book of ASTM Standards, V.04.02, 2010.

American Society for Testing and Materials, ASTM C418, "Standard Test Method for Abrasion Resistance of Concrete by Sandblasting", Annual Book of ASTM Standards, V.04.02, 2005.

American Society for Testing and Materials, ASTM C494, "Standard Specification for Chemical Admixtures for Concrete", Annual Book of ASTM Standards, V.04.02, 2008.

American Society for Testing and Materials, ASTM C496, "Standard Test Method for Splitting Tensile Strength of Cylindrical Concrete Specimens", Annual Book of ASTM Standards, V.04.02, 2008.

American Society for Testing and Materials, ASTM C617, "Standard Practice for Capping Cylindrical Concrete Specimens", Annual Book of ASTM Standards, V.04.02, 2011.

American Society for Testing and Materials, ASTM C672, "Standard Test Method for Scaling Resistance of Concrete Surfaces Exposed to Deicing Chemicals", Annual Book of ASTM Standards, V.04.02, 2003.

American Society for Testing and Materials, ASTM C1064, "Standard Test Method for Temperature of Freshly Mixed Portland Cement Concrete", Annual Book of ASTM Standards, V.04.02, 2008.

American Society for Testing and Materials, ASTM C1202, "Standard Test Method for Electrical Indication of Concrete's Ability to Resist Chloride Ion Penetration", Annual Book of ASTM Standards, V.04.02, 2008.

American Society for Testing and Materials, ASTM C1231, "Standard Practice for Use of Unbonded Caps in Determination of Compressive Strength of Hardened Concrete Cylinders", Annual Book of ASTM Standards, V.04.02, 2010.

American Society for Testing and Materials, ASTM C1260, "Standard Test Method for Potential Alkali Reactivity of Aggregates (Mortar-Bar Method)", Annual Book of ASTM Standards, V.04.02, 2001.

American Society for Testing and Materials, ASTM C1567, "Determining the Potential Alkali-Silica Reactivity of Combinations of Cementitious Materials and Aggregate (Accelerated Mortar-Bar Method)", Annual Book of ASTM Standards, V.04.02, 2008.

American Society for Testing and Materials, ASTM C1585, "Measurement of Rate of Absorption of Water by Hydraulic-Cement Concretes", Annual Book of ASTM Standards, V.04.02, 2004.

Aquino W., Lange D.A., and Olek J. (2001), "The Influence of Metakaolin and Silica Fume on the Chemistry of Alkali-Silica Reaction Products", *Cement and Concrete Composites*, V.23, No. 6, pp. 485-493.

Balaguru, P. and Chong, K. (2008), "Nanotechnology and Concrete: Research Opportunities", *ACI Special Publication SP-254*, pp. 15-28.

Barker D.J., Turner S.A., Napier-Moore P.A., Clark M. and Davison J.E. (2009), "CO_2 Capture in the Cement Industry", *Greenhouse Gas Control Technologies 9*, Washington DC, pp. 87-94.

Bartos P.J.M. (2008), "Nanotechnology in Construction: A Roadmap for Development", *ACI Special Publication SP-254*, pp. 1-14.

Bassuoni M.T., Nehdi M.L. and Greenough T.R. (2006), "Enhancing the Reliability of Evaluating Chloride Ingress in Concrete Using the ASTM C 1202 Rapid Chloride Penetrability Test", *Journal of ASTM International*, V.3, No.3.

Bassuoni M.T., and Nehdi M.L (2009), "Durability of Self-Consolidating Concrete to Different Exposure Regimes of Sodium Sulfate Attack", *Materials and Structures,* V.42, No.8, pp. 1039-1057.

Belkowitz J. and Armentrout D.L. (2009), "The Investigation of Nano Silica in the

Cement Hydration Process", *ACI Special Publication SP-267*, pp. 87-100.

Bergemann C., Müller-Schulte D., Oster J.A., andLübbe A.S. (1999), "Magnetic Ion-Exchange Nano-and Microparticles for Medical, Biochemical and Molecular Biological Applications", *Journal of magnetism and magnetic materials*, V.194, No.1, pp. 45-52.

Berndt M.L. (2009). "Properties of Sustainable Concrete Containing Fly Ash, Slag and Recycled Concrete Aggregate", *Construction and Building Materials*, V.23, No.7, pp. 2606-2613.

Blight G.E., and Alexander M.G. (2011), "Alkali-Aggregate Reaction and Structural Damage to Concrete: Engineering Assessment, Repair and Management," Taylor and Francis.

Brown P., and Hooton R.D. (2002). "Ettringite and Thaumasite formation in laboratory Concretes Prepared Using Sulfate-Resisting Cements", *Cement and Concrete Composites* V.24, No.3, pp. 361-370.

Campillo I., Dolado J.S. and Porro A. (2003), "High-Performance Nanostructured Materials for Construction", *The Proceeding of the first International Symposium on Nanotechnology in Construction (NICOM1)*, Paisley, Scotland, UK, pp. 215-225.

Canham I., PageC.L., and Nixon P.J. (1987), "Aspects of the Pore Solution Chemistry of Blended Cements related to the Control of Alkali Silica Reaction", *Cement and Concrete Research*, V.17, No.5, pp. 839-844.

131

Carette G., Bilodeau A., Chevrier R.L., and Malhotra, V.M. (1993), "Mechanical Properties of Concrete Incorporating High Volumes of Fly Ash from Sources in the US", *ACI Materials Journal*, V.90, No.6, pp. 535-544.

Chatterji S. (2005), "Aspects of Generation of Destructive Crystal Growth Pressure," *Journal of Crystal Growth,* V.277, No.41–4, pp. 566-577.

Cohen M.D. and Mather B. (1991), "Sulfate Attack on Concrete - Research Needs", *ACI Materials Journal*, V.88, No.1 pp. 62-69.

Correns C.W. (1949), "Growth and Dissolution of Crystals under Linear Pressure", *Discussions of the Faraday Society*, No.5 pp. 267-271.

Damtoft J.S., Lukasik J., Herfort D., Sorrentino D. and Gartner E.M. (2008), "Sustainable Development and Climate Change Initiatives", *Cement and Concrete Research*, V.38, No.2, pp. 115-127.

Deja J., Uliasz-Bochenczyk A. and Mokrzycki E. (2010), "CO_2 Emissions from Polish Cement Industry", *International Journal of Greenhouse Gas Control*, V.4, No.4, pp. 583-588.

Detwiler R.J., Dalgleish B.J. and Brady R. (1989), "Assessing the Durability of Concrete in Freezing and Thawing", *ACI Materials Journal*, V.86, No.1, pp. 29-35.

Drexler K.E., Peterson C, Pergamit G. (1991), "Unbounding the Future: the Nanotechnology Revolution," New York: William Morrow.

132

Flatt R.J. (2002), "Salt Damage in Porous Materials: How High Supersaturations are Generated," *Journal of Crystal Growth,* V. 242, No.3–4, pp. 435-454.

Fan S., and Hanson J. M. (1998), "Effect of Alkali Silica Reaction Expansion and Cracking on Structural Behavior of Reinforced Concrete Beams," *ACI Structural Journal,* V.95, No.5, pp. 498-505.

Federal Highway Administration, "Guidelines for the use of Lithium to Mitigate or Prevent Alkali-Silica Reaction (ASR)," Publication No.FHWA-RD-03-047, 2003.

Gartner E.M. (2004), "Industrially Interesting Approaches to Low-CO_2 Cements", *Cement and Concrete Research*, V.34, No.9, pp. 1489-1498.

Ghasemi A.M.R., Parhizkar T. and Ramezanianpour A.A. (2010), "Influence of Colloidal Nano-SiO_2 Addition as Silica Fume Replacement Material in Properties of Concrete", *Proceeding of the Second International Conference on Sustainable Construction Materials and Technologies*, Ancona, Italy.

Gopalakrishnan K., Birgisson B., Taylor P., and Attoh-Okine N.O. (2011), "Nanotechnology in Civil Infrastructure: a Paradigm Shift.", Springer.

Goudie A. and Viles H. (1997), "Salt Weathering Hazards," John Wiley and Sons, Chichester.

Haque M.N., Langan B.W., and Ward M.A. (1984), "High Fly Ash Concretes", *ACI Journal Proceedings*, V.81, No.1, pp. 54-60.

Hartell J.A., Boyd A.J. and Ferraro C.C. (2011), "Sulfate Attack on Concrete: Effect of

Partial Immersion" *Journal of Materials in Civil Engineering,* V.23, No.5, pp. 572-579.

Haynes H. (2002), "Sulfate Attack on Concrete: Laboratory vs. Field Experience", *Concrete International*, V.24, No.7, pp. 64-70.

Haynes H. (2006), "A Mechanism of Distress to Concrete during Crystallization of Mirabilite," *Seventh CANMET/ACI International Conference of Durability of Concrete*, Supplementary Volume, Montreal, QC, Canada, pp. 1-16.

Haynes H. and Bassuoni M.T. (2011), "Physical Salt Attack on Concrete", *Concrete International*, V.33, No.11, pp. 38-42.

Haynes H., O'Neill R. and Mehta P.K. (1996), "Concrete Deterioration from Physical Attack by Salts", *Concrete International*, V.18, No.1, pp. 63-68.

Haynes H., O'Neill R., Neff M. and Mehta P.K. (2008), "Salt Weathering Distress on Concrete Exposed to Sodium Sulfate Environment", *ACI Materials Journal*, V.105, No.1, pp. 35-43.

Haynes H., O'Neill R., Neff M., and Mehta R.K. (2010), "Salt Weathering of Concrete by Sodium Carbonate and Sodium Chloride," *ACI Materials Journal*, V.107, No.3, pp. 258-266.

Hime W.G., Martinek R.A., Backus L.A., and Marusin S.L. (2001), "Salt hydration distress," *Concrete International*, V.23, No.10, pp. 43-50.

Hobbs D.W. (1988), "Alkali-silica reaction in concrete," Telford, London.

134

Iler R.K. (1979) "The Chemistry of Silica: Solubility, Polymerization, Colloid and Surface Properties and Biochemistry of Silica" New York: John Willy and Sons.

Kumar R. and Bhattacharjee B. (2003), "Study on Some Factors Affecting the Results in the Use of MIP Method in Concrete Research", *Cement and Concrete Research*, V.33, No.3, pp. 417-424.

Laplante P., Aiticin P.C., and Vezina D. (1991), "Abrasion Resistance of Concrete", *Journal of Materials in Civil Engineering*, V.3, No.1, pp. 19-28.

Lee B.Y., Thomas J.J., Treager M., and Kurtis K.E. (2009), "Influence of TiO2 Nanoparticles on Early C3S Hydration", *ACI Special Publication SP-267*, pp. 35-44.

Li, H., Xiao, H., Yuan, J., and Ou, J. (2004), "Microstructure of Cement Mortar with Nano-Particles", *Composites Part B: Engineering*, V.35, No.2, pp. 185-189.

Liu H. and Kuo C. (1996), "Quantitative Multiphase Determination using the Rietveld Method with High Accuracy", Materials Letters, V.26, No.3, pp. 171-175.

Malin M.C. (1974), "Salt Weathering on Mars," *Journal of Geophysical Research*, V.79, No.26, pp. 3888-3894.

Malvar L.J., Clie G.D., Burke D.F., Rollings R., Sherman T.W. and Greene J.L. (2002), "Alkali-Silica Reaction Mitigation: State of the Art and Recommendations", *ACI Materials Journal*, V.99, No.5, pp. 480-489.

Mehta P.K. (2000), "Sulfate Attack on Concrete: Separating Myths from Reality", *Concrete International*, V.22, No.8, pp. 57-61.

135

Mehta P.K. (2002), "Greeningof the Concrete Industry for Sustainable Development", *Concrete International*, V.24, No.7, pp. 23-28.

Mehta P.K., Monteiro P.J.M., (2006), "Concrete: Microstructure, Properties, and Materials," New York: McGraw-Hill.

Montgomery D.C. (2001), "Design and analysis of experiments," New York: John Wiley & Sons.

Naik T.R., and Ramme B.W. (1989), "High Early Strength Concrete Containing Large Quantities of Fly Ash",. *ACI Materials Journal,* V.86, No.2, pp. 111-116.

Naik T.R., Singh S.S., and Hossain M.M. (1995), "Abrasion Resistance of High-Strength Concrete made with Class C Fly Ash", *ACI Materials Journal*, V.92, No.6, pp. 649-659.

Naik T.R., Singh S.S., and Ramme B.W. (1998), "Mechanical Properties and Durability of Concrete made with Blended Fly Ash", *ACI Materials Journal*, V.95, No.4, pp. 454-462.

Pettersson K. (1992), "Effects of Silica Fume on Alkali-Silica Expansion in Mortar Specimens" *Cement and Concrete Research,* V.22, No.1, pp. 15-22.

Porro, A. (2005), "Nanoscience and Nanotechnology in Construction Materials", *Proceedings of the 2nd International Symposium on Nanotechnology in Construction (NICOM2),* RILEM PRO 45, Bilbao, Spain, pp. 3-8.

Ramlochan T., Michael T., and Gruber K.A. (2000), "The Effect of Metakaolin on Alkali-Silica Reaction in Concrete," *Cement and Concrete Research,* V.30, No.3, pp. 339-344.

Rasheeduzzafar and Hussain S.E. (1991), "Effect of Microsilica and Blast Furnace Slag on Pore Solution Composition and Alkali-Silica Reaction", *Cement and Concrete Composites*, V.13, No.3, pp. 219-225.

Reading T.J. (1982), "Physical Aspects of Sodium Sulfate Attack on Concrete," *ACI Special Publication SP-77*, pp. 75-81.

Rivard P., and Saint-Pierre F. (2009). "Assessing Alkali-Silica Reaction Damage to Concrete with Non-Destructive Methods: From the Lab to the Field", *Construction and Building Materials*, V.23, No.2, pp.902-909.

Rodriguez-Navarro C., Doehne E., and Sebastian E. (2000), "How Does Sodium Sulfate Crystallize? Implications for the Decay and Testing of Building Materials," *Cement and Concrete Research,* V.30, No.10, pp. 1527-1534.

Sabir B.B., Wild S., and Bai J. (2001), "Metakaolin and Calcined Clays as Pozzolans for Concrete: a Review," *Cement and Concrete Composites,* V.23, No.6, pp. 441-454.

Sahin R., Tasdemir M. A., Gul R.and Celik C. (2010). "Determination of the Optimum Conditions for De-icing Salt Scaling Resistance of Concrete by Visual Examination and Surface Scaling", *Construction and Building Materials*, V.24, No.3, pp. 353-360.

137

Scherer G.W., (1999), "Crystallization in Pores," *Cement and Concrete Research*, V.29, No.8, pp. 1347-1358.

Shi C., (1998),"Pozzolanic Reaction and Microstructure of Chemical Activated Lime-Fly Ash Pastes", *ACI Materials Journal*,V.95, No.5, pp. 537-545.

Shi D. and Winslow, D. N. (1985)."Contact angle and Damage during Mercury Intrusion into Cement Paste", *Cement and Concrete Research,* V.15, No.4, pp.645-654.

Snell L.M. and Snell B.G. (2002), "Oldest Concrete Street in the United States," *Concrete International*, V.24, No.3, pp. 72-74.

Sobolev K., Flores I., Torres-Martinez L.M., Valdez P.L., Zarazua E., and Cullar E.L. (2009), "Engineering of SiO_2 Nano-Particles for optimal Performance in Nano Cement-Based Materials", *Proceedings of the3rdInternational Symposium on Nanotechnology in Construction (NICOM3)*, Prague, Czech Republic, pp. 139-148.

Sperling C.H., and Cooke, R.U. (1985), "Laboratory Simulation of Rock Weathering by Salt Crystallization and Hydration Processes in Hot, Arid Environments," *Earth Surfaces Processes and Landforms*, V.10, No.6, pp. 541-555.

Swamy R.N., and Al-Asali M. (1988), "Engineering Properties of Concrete affected by Alkali-Silica Reaction,"*ACI Materials Journal,* V.85, No.5, pp. 367-374.

Swamy R.N., and Al-Asali M., (1989), "Effect of Alkali-Silica Reaction on the Structural Behavior of Reinforced Concrete Beams,"*ACI Structural Journal,* V.86, No.4, pp. 451-459.

Thaulow N. and Sahu S. (2004), "Mechanism of Concrete Deterioration due to Salt Crystallization," *Materials Characterization*, V.53, No.2–4, pp. 123-127.

Thomas M., ShehataM.H., Shashiprakash S.G., Hopkins D.S., and Cail K. (1999), "Use of Ternary Cementitious Systems containing Silica Fume and Fly Ash in Concrete", *Cement and Concrete Research*, V.29, No.8, pp. 1207-1214.

Thomas M.D.A., Fournier B., Folliard K.J., Ideker J.H., and Resendez Y. (2007), "The use of Lithium to Prevent or Mitigate Alkali-Silica Reaction in Concrete Pavements and Structures," U.S. Department of Transportation, Federal Highway Administration, FHWA-HRT-06-133, 47 pp.

Thomas M., Hooton R.D., Rogers C., and Fournier B. (2012), "50 Years Old and Still going Strong," *Concrete International*, V.34, No.1, pp. 35-40.

Turanli L., Bektas F., and Monteiro P.J.M. (2003), "Use of Ground Clay Brick as a Pozzolanic Material to Reduce the Alkali–Silica Reaction," *Cement and Concrete Research,* V.33, No.10, pp. 1539-1542.

Tuthill L.H. (1982), "Alkali-Silica Reaction-40 Years Later," *Concrete International*, V.4, No.4, pp. 32-36.

US Geological Survey, USGS (2010)."Minerals Commodity Summary - Cement - 2010", http://minerals.usgs.gov/minerals/pubs/commodity/cement/mcs-2010-cemen.pdf.Retrieved on 10-31-2010.

Wang H., and Gillott J.E. (1993), "Effect of Three Zeolite-Containing Natural Pozzolanic Materials on Alkali-Silica Reaction*", Cement, Concrete and Aggregates*, V.15, No.1, pp. 24-30.

World Business Council for Sustainable Development WBCSD (2002), "The Cement Sustainability Initiative: Our agenda for action", Geneva, Switzerland , July 2002.

Zhang C., Wang A., Tang M., Wu B., and Zhang N. (1999), "Influence of Aggregate Size and Aggregate Size Grading on ASR Expansion," *Cement and Concrete Research,* V.29, No.9, pp. 1393-1396.

CV

MOHAMED S. ZEIDAN

E-mail: sabry.m.z@gmail.com

EDUCATION

- **University of Nevada, Las Vegas**   Las Vegas, NV
  Doctor of Philosophy in Civil Engineering (Graduation: Jan. 2013, *GPA:* 3.81)
- **Alexandria University**   Alexandria, Egypt
  Master's of Science in Structural Engineering   (November 2006, GPA: 3.70)
  Bachelor's of Science in Civil Engineering   (June 2000, GPA: 3.85)

PROFESSIONAL CERTIFICATIONS

- **Civil Engineer Intern** (April 2011- Present)
  Nevada State Board of Professional Engineers and Land Surveyors.
- **Professional Engineer Exam** (Planned April 2013)
  Nevada State Board of Professional Engineers and Land Surveyors.
- **Licensed Civil Engineer** (August 2000 - Present)
  The Egyptian Engineering Syndicate.

PROFESSIONAL EXPERIENCE

Graduate Assistant   (Jan. 2009-Present)
Civil and Environmental Engineering Department, **University of Nevada, Las Vegas.**

Demonstrator/Assistant Lecturer   (Feb. 2001-Dec. 2008)
Structural Engineering Department, **Alexandria University**.

Structural Design Team Leader (Part-time)   (Sep. 2005 - Dec 2008)
Allam Engineering Design and Consulting Office.   Alexandria, Egypt

Structural Design Engineer (Part-time)   (Aug 2000 - May 2003)
Mahmoud Helmy's Consulting Office.   Alexandria, Egypt

TRAINING AND WORKSHOPS

- **Designing Effective Research Assignments**
  University Libraries - UNLV (Oct. 2011).
- **Thinking Skills (P1)**

141

Faculty and Leadership Development Project - Alexandria University (March 2007).

- **Effective Teaching (T1)**
Faculty and Leadership Development Project - Alexandria University (Feb. 2007).
- **Research Methodology (R1)**
Faculty and Leadership Development Project - Alexandria University (Jan. 2007).
- **New Trends in Teaching (T2)**
Faculty and Leadership Development Project - Alexandria University (Nov. 2006).

ACTIVITIES & REWARDS
- Attending the ACI 2009 fall convention, New Orleans, LA.
- Awarded Graduate & Professional Students Association travel grant, GPSA-UNLV (2009).
- Honorable mention at GPSA –UNLV research forum (2010).
- Attending Nevada Infrastructure Concrete Conferences - NICC (2009 & 2011).
- Attending the ASCE Structural Congress 2011, Las Vegas, NV.
- Best Dissertation Award (2nd place), UNLV College of Engineering Graduate Celebration (April 2012).

PUPLICATIONS
- Barakat M.A., Mahmoud Z.I. and Khalifa A.M., **Zeidan M.S.,** (2007) "Shear Strength of Concrete Beams Reinforced with FRP Longitudinal Bars" *Proceeding of the Sixth International Alexandria Conference on structural and Geotechnical Engineering*, Alexandria, Egypt.
- Said A.M. and **Zeidan M.S.** (2009), "Enhancing the Reactivity of Normal and Fly Ash Concrete Using Colloidal Nano-Silica", *ACI Special Publication* SP267-07, pp. 75-86.
- **Zeidan M.S.**, Barakat M.A., Mahmoud Z.I. and Khalifa A.M., (2011) "Evaluation of Concrete Shear Strength for FRP Reinforced Beams" *Proceeding of the 2011 ASCE Structural Congress*, Las Vegas, NV.
- Said A.M., **Zeidan M.S.**, Bassuoni M.T. and Tian Y. (2012), "Properties of Concrete Incorporating Nano-Silica", *Construction and Building Materials,*Vol.36, November 2012, pp. 838-844.
- Said A.M. and **Zeidan M.S.**, "ASR Mitigation using Nano-Silica", *Transportation Research Record: Journal of the Transportation Research Board*. (In preparation)
- Said A.M., **Zeidan M.S.** and Bassuoni M. T., "Physical Salt Attack Resistance of Concrete Incorporating Nano-Silica" (In preparation).